

Representations of celestial coordinates in FITS

M. R. Calabretta¹ and E. W. Greisen²

¹ Australia Telescope National Facility, PO Box 76, Epping, NSW 1710, Australia

² National Radio Astronomy Observatory, PO Box O, Socorro, NM 87801-0387, USA

Received 24 July 2002 / Accepted 9 September 2002

Abstract. In Paper I, Greisen & Calabretta (2002) describe a generalized method for assigning physical coordinates to FITS image pixels. This paper implements this method for all spherical map projections likely to be of interest in astronomy. The new methods encompass existing informal FITS spherical coordinate conventions and translations from them are described. Detailed examples of header interpretation and construction are given.

Key words. methods: data analysis – techniques: image processing – astronomical data bases: miscellaneous – astrometry

1. Introduction

This paper is the second in a series which establishes conventions by which world coordinates may be associated with FITS (Hanisch et al. 2001) image, random groups, and table data. Paper I (Greisen & Calabretta 2002) lays the groundwork by developing general constructs and related FITS header keywords and the rules for their usage in recording coordinate information. In Paper III, Greisen et al. (2002) apply these methods to spectral coordinates. Paper IV (Calabretta et al. 2002) extends the formalism to deal with general distortions of the coordinate grid. This paper, Paper II, addresses the specific problem of describing celestial coordinates in a two-dimensional projection of the sky. As such it generalizes the informal but widely used conventions established by Greisen (1983, 1986) for the Astronomical Image Processing System, hereinafter referred to as the *AIPS convention*.

Paper I describes the computation of world coordinates as a multi-step process. Pixel coordinates are linearly transformed to intermediate world coordinates that in the final step are transformed into the required world coordinates.

In this paper we associate particular elements of the intermediate world coordinates with Cartesian coordinates in the plane of the spherical projection. Figure 1, by analogy with Fig. 1 of Paper I, focuses on the transformation as it applies to these projection plane coordinates. The final step is here divided into two sub-steps, a spherical projection defined in terms of a convenient coordinate system which we refer to as *native spherical coordinates*, followed by a spherical rotation of these native coordinates to the required celestial coordinate system.

Send offprint requests to: M. Calabretta,
 e-mail: mcalabre@atnf.csiro.au

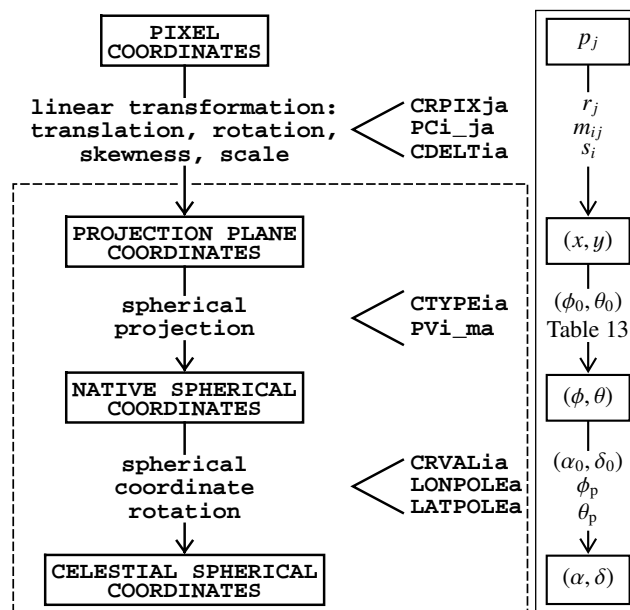


Fig. 1. Conversion of pixel coordinates to celestial coordinates. The INTERMEDIATE WORLD COORDINATES of Paper I, Fig. 1 are here interpreted as PROJECTION PLANE COORDINATES, i.e. Cartesian coordinates in the plane of projection, and the multiple steps required to produce them have been condensed into one. This paper is concerned in particular with the steps enclosed in the dotted box. For later reference, the mathematical symbols associated with each step are shown in the box at right (see also Tables 1 and 13).

The original FITS paper by Wells et al. (1981) introduced the $CRPIX\ ja^1$ keyword to define the pixel coordinates (r_1, r_2, r_3, \dots) of a *coordinate reference point*. Paper I retains

¹ The single-character alternate version code “a” on the various FITS keywords was introduced in Paper I. It has values blank and A through Z.

this but replaces the coordinate rotation keywords CROTA*i* with a linear transformation matrix. Thus, the transformation of *pixel coordinates* (p_1, p_2, p_3, \dots) to *intermediate world coordinates* (x_1, x_2, x_3, \dots) becomes

$$\begin{aligned} x_i &= s_i \sum_{j=1}^N m_{ij}(p_j - r_j), \\ &= \sum_{j=1}^N (s_i m_{ij})(p_j - r_j), \end{aligned} \quad (1)$$

where N is the number of axes given by the MAXIS keyword. As suggested by the two forms of the equation, the scales s_i , and matrix elements m_{ij} may be represented either separately or in combination. In the first form s_i is given by CDELTA*ia* and m_{ij} by PC*i_ja*; in the second, the product $s_i m_{ij}$ is given by CD*i_ja*. The two forms may not coexist in one coordinate representation.

Equation (1) establishes that the reference point is the origin of intermediate world coordinates. We require that the linear transformation be constructed so that the plane of projection is defined by two axes of the x_i coordinate space. We will refer to intermediate world coordinates in this plane as *projection plane coordinates*, (x, y) , thus with reference point at $(x, y) = (0, 0)$. Note that this does not necessarily correspond to any plane defined by the p_j axes since the linear transformation matrix may introduce rotation and/or skew.

Wells et al. (1981) established that all angles in FITS were to be measured in degrees and this has been entrenched by the AIPS convention and confirmed in the IAU-endorsed FITS standard (Hanisch et al. 2001). Paper I introduced the CUNIT*ia* keyword to define the units of CRVAL*ia* and CDELTA*ia*. Accordingly, we require CUNIT*ia* = 'deg' for the celestial CRVAL*ia* and CDELTA*ia*, whether given explicitly or not. Consequently, the (x, y) coordinates in the plane of projection are measured in degrees. For consistency, we use degree measure for native and celestial spherical coordinates and for all other angular measures in this paper.

For linear coordinate systems Wells et al. (1981) prescribed that world coordinates should be computed simply by adding the relative world coordinates, x_i , to the coordinate value at the reference point given by CRVAL*ia*. Paper I extends this by providing that particular values of CTYPE*ia* may be established by convention to denote non-linear transformations involving predefined functions of the x_i parameterized by the CRVAL*ia* keyword values and possibly other parameters.

In Sects. 2, 3 and 5 of this paper we will define the functions for the transformation from (x, y) coordinates in the plane of projection to celestial spherical coordinates for all spherical map projections likely to be of use in astronomy.

The FITS header keywords discussed within the main body of this paper apply to the primary image header and image extension headers. Image fragments within binary tables extensions defined by Cotton et al. (1995) have additional nomenclature requirements, a solution for which was proposed in Paper I. Coordinate descriptions may also be associated with the random groups data format defined by Greisen & Harten (1981). These issues will be expanded upon in Sect. 4.

Section 6 considers the translation of older AIPS convention FITS headers to the new system and provisions that may be made to support older FITS-reading programs. Section 7 discusses the concepts presented here, including worked examples of header interpretation and construction.

2. Basic concepts

2.1. Spherical projection

As indicated in Fig. 1, the first step in transforming (x, y) coordinates in the plane of projection to celestial coordinates is to convert them to native longitude and latitude, (ϕ, θ) . The equations for the transformation depend on the particular projection and this will be specified via the CTYPE*ia* keyword. Paper I defined “4–3” form for such purposes; the rightmost three characters are used as an *algorithm code* that in this paper will specify the projection. For example, the stereographic projection will be coded as STG. Some projections require additional parameters that will be specified by the FITS keywords PVI*ma* for $m = 0, 1, 2, \dots$, also introduced in Paper I. These parameters may be associated with the longitude and/or latitude coordinate as specified for each projection. However, definition of the three-letter codes for the projections and the equations, their inverses and the parameters which define them, form a large part of this work and will be discussed in Sect. 5. The leftmost four characters of CTYPE*ia* are used to identify the celestial coordinate system and will be discussed in Sect. 3.

2.2. Reference point of the projection

The last step in the chain of transformations shown in Fig. 1 is the spherical rotation from native coordinates, (ϕ, θ) , to celestial² coordinates (α, δ) . Since a spherical rotation is completely specified by three Euler angles it remains only to define them.

In principle, specifying the celestial coordinates of any particular native coordinate pair provides two of the Euler angles (either directly or indirectly). In the AIPS convention, the CRVAL*ia* keyword values for the celestial axes³ specify the celestial coordinates of the reference point and this in turn is associated with a particular point on the projection. For zenithal projections that point is the sphere's point of tangency to the plane of projection and this is the pole of the native coordinate system. Thus the AIPS convention links a celestial coordinate pair to a native coordinate pair via the reference point. Note that this association via the reference point is purely conventional; it has benefits which are discussed in Sect. 5 but in principle any other point could have been chosen.

Section 5 presents the projection equations for the transformation of (x, y) to (ϕ, θ) . The native coordinates of the reference point would therefore be those obtained for $(x, y) = (0, 0)$. However, it may happen that this point lies outside the boundary of the projection, for example as for the ZPN projection of

² Usage here of the conventional symbols for right ascension and declination for celestial coordinates is meant only as a mnemonic. It does not preclude other celestial systems.

³ We will refer to these simply as “the CRVAL*ia*”, and likewise for the other keyword values.

Table 1. Summary of important variable names and other symbols used throughout the paper.

| Variable(s) | Meaning | Related FITS keywords (if any) |
|------------------------|---|--|
| i | Index variable for world coordinates | |
| j | Index variable for pixel coordinates | |
| a | Alternate version code, blank or A to Z | |
| p_j | Pixel coordinates | |
| r_j | Reference pixel coordinates | CRPIX ja |
| m_{ij} | Linear transformation matrix | CD i_ja or PC i_ja |
| s_i | Coordinate scales | CDEL Tia |
| x_i | Intermediate world coordinates (in general) | |
| (x, y) | Projection plane coordinates | |
| (ϕ, θ) | Native longitude and latitude | |
| (α, δ) | Celestial longitude and latitude | |
| (ϕ_0, θ_0) | Native longitude and latitude of the fiducial point | PV i_1a^\dagger , PV i_2a^\dagger |
| (α_0, δ_0) | Celestial longitude and latitude of the fiducial point | CRVAL ia |
| (ϕ_p, θ_p) | Native longitude and latitude of the celestial pole | LONPOLE a (= PV i_3a^\dagger), LATPOLE a , (= PV i_4a^\dagger) |
| (α_p, δ_p) | Celestial longitude and latitude of the native pole ($\delta_p = \theta_p$) | |
| $\arg()$ | Inverse tangent function that returns the correct quadrant | |

[†] Associated with *longitude* axis i .

Sect. 5.1.7. Therefore, while this work follows the AIPS approach it must of necessity generalize it.

Accordingly we specify only that a fiducial celestial coordinate pair (α_0, δ_0) given by the CRVAL ia will be associated with a fiducial native coordinate pair (ϕ_0, θ_0) defined explicitly for each projection. For example, zenithal projections all have $(\phi_0, \theta_0) = (0, 90^\circ)$, while cylindricals have $(\phi_0, \theta_0) = (0, 0)$. The AIPS convention has been honored here as far as practicable by constructing the projection equations so that (ϕ_0, θ_0) transforms to the reference point, $(x, y) = (0, 0)$. Thus, apart from the one exception noted, the fiducial celestial and native coordinates are the celestial and native coordinates of the reference point and we will not normally draw a distinction.

It is important to understand why (ϕ_0, θ_0) differs for different projection types. There are two main reasons; the first makes it difficult for it to be the same, while the second makes it desirable that it differs. Of the former, some projections such as Mercator's, diverge at the native pole, therefore they cannot have the reference point there because that would imply infinite values for CRPIX ja . On the other hand, the gnomonic projection diverges at the equator so it can't have the reference point there for the same reason. Possibly (ϕ_0, θ_0) chosen at some mid-latitude could satisfy all projections, but that leads us to the second reason.

Different projection types are best suited to different purposes. For example, zenithal projections are best for mapping the region in the vicinity of a point, often a pole; cylindrical projections are appropriate for the neighborhood of a great circle, usually an equator; and the conics are suitable for small circles such as parallels of latitude. Thus, it would be awkward if a cylindrical used to map, say, a few degrees on either side of the galactic plane, had its reference point, and thus CRPIX ja and CRVAL ia , at the native pole, way outside the map boundary. In formulating the projection equations themselves the native coordinate system is chosen to simplify the geometry as much as possible. For the zenithals the natural formulation has

$(x, y) = (0, 0)$ at the native pole, whereas for the cylindricals the equations are simplest if $(x, y) = (0, 0)$ at a point on the equator.

As discussed above, a third Euler angle must be specified and this will be given by the native longitude of the celestial pole, ϕ_p , specified by the new FITS keyword

LONPOLE a (floating-valued).

The default value of LONPOLE a will be 0 for $\delta_0 \geq \theta_0$ or 180° for $\delta_0 < \theta_0$. This is the condition for the celestial latitude to increase in the same direction as the native latitude at the reference point. Thus, for example, in zenithal projections the default is always 180° (unless $\delta_0 = 90^\circ$) since $\theta_0 = 90^\circ$. In cylindrical projections, where $\theta_0 = 0$, the default value for LONPOLE a is 0 for $\delta_0 \geq 0$, but it is 180° for $\delta_0 < 0$.

2.3. Spherical coordinate rotation

Since (ϕ_0, θ_0) differs for different projections it is apparent that the relationship between (α_0, δ_0) and the required Euler angles also differs.

For zenithal projections, $(\phi_0, \theta_0) = (0, 90^\circ)$ so the CRVAL ia specify the celestial coordinates of the native pole, i.e. $(\alpha_0, \delta_0) = (\alpha_p, \delta_p)$. There is a simple relationship between the Euler angles for consecutive rotations about the Z-, X-, and Z-axes and α_p , δ_p and ϕ_p ; the ZXZ Euler angles are $(\alpha_p + 90^\circ, 90^\circ - \delta_p, \phi_p - 90^\circ)$. Given this close correspondence it is convenient to write the Euler angle transformation formulæ directly in terms of α_p , δ_p and ϕ_p :

$$\begin{aligned}\alpha &= \alpha_p + \arg(\sin \theta \cos \delta_p - \cos \theta \sin \delta_p \cos(\phi - \phi_p), \\ &\quad - \cos \theta \sin(\phi - \phi_p)), \\ \delta &= \sin^{-1}(\sin \theta \sin \delta_p + \cos \theta \cos \delta_p \cos(\phi - \phi_p)),\end{aligned}\tag{2}$$

where $\arg()$ is an inverse tangent function that returns the correct quadrant, i.e. if $(x, y) = (r \cos \beta, r \sin \beta)$ with $r > 0$ then $\arg(x, y) = \beta$. Note that, if $\delta_p = 90^\circ$, Eqs. (2) become

$$\begin{aligned} \alpha &= \alpha_p + \phi - \phi_p - 180^\circ, \\ \delta &= \theta, \end{aligned} \quad (3)$$

which may be used to define a simple change in the origin of longitude. Likewise for $\delta_p = -90^\circ$

$$\begin{aligned} \alpha &= \alpha_p - \phi + \phi_p, \\ \delta &= -\theta. \end{aligned} \quad (4)$$

The inverse equations are

$$\begin{aligned} \phi &= \phi_p + \arg(\sin \delta \cos \delta_p - \cos \delta \sin \delta_p \cos(\alpha - \alpha_p), \\ &\quad - \cos \delta \sin(\alpha - \alpha_p)), \\ \theta &= \sin^{-1}(\sin \delta \sin \delta_p + \cos \delta \cos \delta_p \cos(\alpha - \alpha_p)). \end{aligned} \quad (5)$$

Useful relations derived from Eqs. (2) and (5) are

$$\begin{aligned} \cos \delta \cos(\alpha - \alpha_p) &= \sin \theta \cos \delta_p - \cos \theta \sin \delta_p \cos(\phi - \phi_p), \\ \cos \delta \sin(\alpha - \alpha_p) &= -\cos \theta \sin(\phi - \phi_p), \end{aligned} \quad (6)$$

$$\begin{aligned} \cos \theta \cos(\phi - \phi_p) &= \sin \delta \cos \delta_p - \cos \delta \sin \delta_p \cos(\alpha - \alpha_p), \\ \cos \theta \sin(\phi - \phi_p) &= -\cos \delta \sin(\alpha - \alpha_p). \end{aligned} \quad (7)$$

A matrix method of handling the spherical coordinate rotation is described in Appendix B.

2.4. Non-polar (ϕ_0, θ_0)

Projections such as the cylindricals and conics for which $(\phi_0, \theta_0) \neq (0, 90^\circ)$ are handled by providing formulae to compute (α_p, δ_p) from (α_0, δ_0) whence the above equations may be used.

Given that (α_0, δ_0) are the celestial coordinates of the point with native coordinates (ϕ_0, θ_0) , Eqs. (6) and (7) may be inverted to obtain

$$\begin{aligned} \delta_p &= \arg(\cos \theta_0 \cos(\phi_p - \phi_0), \sin \theta_0) \\ &\quad \pm \cos^{-1} \left(\frac{\sin \delta_0}{\sqrt{1 - \cos^2 \theta_0 \sin^2(\phi_p - \phi_0)}} \right), \end{aligned} \quad (8)$$

$$\sin(\alpha_0 - \alpha_p) = \sin(\phi_p - \phi_0) \cos \theta_0 / \cos \delta_0, \quad (9)$$

$$\cos(\alpha_0 - \alpha_p) = \frac{\sin \theta_0 - \sin \delta_p \sin \delta_0}{\cos \delta_p \cos \delta_0}, \quad (10)$$

whence Eqs. (2) may be used to determine the celestial coordinates. Note that Eq. (8) contains an ambiguity in the sign of the inverse cosine and that all three indicate that some combinations of $\phi_0, \theta_0, \alpha_0, \delta_0$, and ϕ_p are not allowed. For these projections, we must therefore adopt additional conventions:

1. Equations (9) and (10) indicate that α_p is undefined when $\delta_0 = \pm 90^\circ$. This simply represents the longitude singularity at the pole and forces us to define $\alpha_p = \alpha_0$ in this case.
2. If $\delta_p = \pm 90^\circ$ then the longitude at the native pole is $\alpha_p = \alpha_0 + \phi_p - \phi_0 - 180^\circ$ for $\delta_p = 90^\circ$ and $\alpha_p = \alpha_0 - \phi_p + \phi_0$ for $\delta_p = -90^\circ$.

3. Some combinations of $\phi_0, \theta_0, \delta_0$, and ϕ_p produce an invalid argument for the $\cos^{-1}()$ in Eq. (8). This is indicative of an inconsistency for which there is no solution for δ_p . Otherwise Eq. (8) produces two solutions for δ_p . Valid solutions are ones that lie in the range -90° to $+90^\circ$, and it is possible in some cases that neither solution is valid.

Note, however, that if $\phi_0 = 0$, as is usual, then when LONPOLEa ($\equiv \phi_p$) takes its default value of 0 or 180° (depending on θ_0) then *any* combination of δ_0 and θ_0 produces a valid argument to the $\cos^{-1}()$ in Eq. (8), and at least one of the solutions is valid.

4. Where Eq. (8) has two valid solutions the one closest to the value of the new FITS keyword

LATPOLEa (floating-valued)

is chosen. It is acceptable to set LATPOLEa to a number greater than $+90^\circ$ to choose the northerly solution (the default if LATPOLEa is omitted), or a number less than -90° to select the southern solution.

5. Equation (8) often only has one valid solution (because the other lies outside the range -90° to $+90^\circ$). In this case LATPOLEa is ignored.
6. For the special case where $\theta_0 = 0, \delta_0 = 0$, and $\phi_p - \phi_0 = \pm 90^\circ$ then δ_p is not determined and LATPOLEa specifies it completely. LATPOLEa has no default value in this case.

These rules governing the application of Eqs. (8–10) are certainly the most complex of this formalism. FITS writers are well advised to check the values of $\phi_0, \theta_0, \alpha_0, \delta_0$, and ϕ_p against them to ensure their validity.

2.5. User-specified (ϕ_0, θ_0)

In Sect. 2.2 we formally decoupled (α_0, δ_0) from the reference point and associated it with (ϕ_0, θ_0) . One implication of this is that it should be possible to allow (ϕ_0, θ_0) to be user-specifiable. This may be useful in some circumstances, mainly to allow CRVALia to match a point of interest rather than some predefined point which may lie well outside the image and be of no particular interest. We therefore reserve keywords PV*i*.1a and PV*i*.2a attached to *longitude* coordinate *i* to specify ϕ_0 and θ_0 respectively.

By itself, this prescription discards the AIPS convention and lacks utility because it breaks the connection between CRVALia and any point whose pixel coordinates are given in the FITS header. New keywords could be invented to define these pixel coordinates but this would introduce additional complexity and still not satisfy the AIPS convention. The solution adopted here is to provide an option to force $(x, y) = (0, 0)$ at (ϕ_0, θ_0) by introducing an implied offset (x_0, y_0) which is computed for (ϕ_0, θ_0) from the relevant projection equations given in Sect. 5. This is to be applied to the (x, y) coordinates when converting to or from pixel coordinates. The operation is controlled by the value of PV*i*.0a attached to *longitude* coordinate *i*; the offset is to be applied only when this differs from its default value of zero.

This construct should be considered advanced usage, of which Figs. 33 and 34 provide an example. Normally we

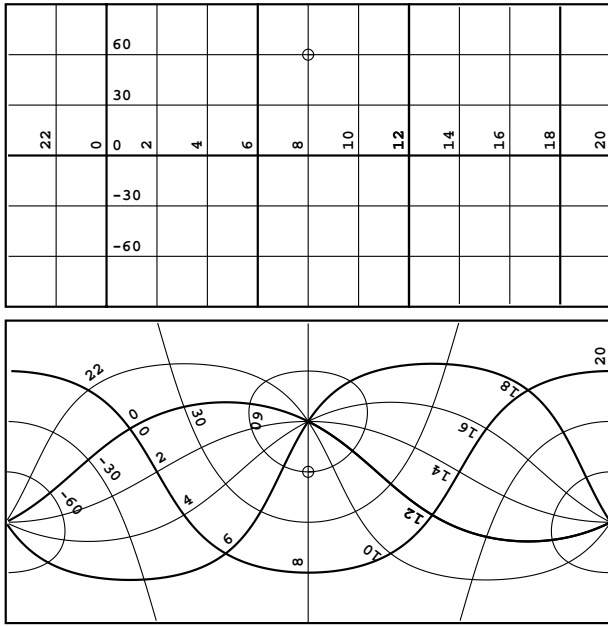


Fig. 2. A linear equatorial coordinate system (top) defined via the methods of Wells et al. (1981), and the corresponding oblique system constructed using the methods of this paper. The reference coordinate (α_0, δ_0) for each is at right ascension 8^{hr} , declination $+60^\circ$ (marked). The two sets of FITS header cards differ only in their CTYPE*ia* keyword values. The non-oblique graticule could be obtained in the current system by setting $(\alpha_0, \delta_0, \phi_p) = (120^\circ, 0, 0)$.

expect that PVi_1a and PVi_2a will either be omitted or set to the projection-specific defaults given in Sect. 5.

2.6. Encapsulation

So that all required transformation parameters can be contained completely within the recognized world coordinate system (WCS) header cards, the values of LONPOLE*a* and LATPOLE*a* may be recorded as PVi_3a and PVi_4a, attached to *longitude* coordinate *i*, and these take precedence where a conflict arises.

We recommend that FITS writers include the PVi_1a, PVi_2a, PVi_3a, and PVi_4a cards in the header, even if only to denote the correct use of the default values.

Note carefully that these are associated with the *longitude* coordinate, whereas the projection parameters defined later are all associated with the *latitude* coordinate.

2.7. Change of coordinate system

A change of coordinate system may be effected in a straightforward way if the transformation from the original system, (α, δ) , to the new system, (α', δ') , and its inverse are known. The new coordinates of the (ϕ_0, θ_0) , namely (α'_0, δ'_0) , are obtained simply by transforming (α_0, δ_0) . To obtain ϕ'_p , first transform the coordinates of the pole of the new system to the original celestial system and then transform the result to native coordinates via Eq. (5) to obtain (ϕ'_p, θ'_p) . As a check, compute δ'_p via Eq. (8) and verify that $\theta'_p = \delta'_p$.

2.8. Comparison with linear coordinate systems

It must be stressed that the coordinate transformation described here differs from the linear transformation defined by Wells et al. (1981) even for some simple projections where at first glance they may appear to be the same. Consider the plate carrée projection defined in Sect. 5.2.3 with $\phi = x$, $\theta = y$ and illustrated in Fig. 18. Figure 1 shows that while the transformation from (x, y) to (ϕ, θ) may be linear (in fact identical), there still remains the non-linear transformation from (ϕ, θ) to (α, δ) . Hence the linear coordinate description defined by the unqualified CTYPE*ia* pair of RA, DEC which uses the Wells et al. prescription will generally differ from that of RA---CAR, DEC---CAR with the same CRVAL*ia*, etc. If LONPOLE*a* assumes its default value then they will agree to first order at points near the reference point but gradually diverge at points away from it.

Figure 2 illustrates this point for a plate carrée projection with reference coordinates of 8^{hr} right ascension and $+60^\circ$ declination and with $\phi_p = 0$. It is evident that since the plate carrée has $(\phi_0, \theta_0) = (0, 0)$, a non-oblique graticule may only be obtained by setting $\delta_0 = 0$ with $\phi_p = 0$. It should also be noted that where a larger map is to be composed of tiled submaps the coordinate description of a submap should only differ in the value of its reference pixel coordinate.

3. Celestial coordinate systems

As mentioned in Sect. 2.1, Paper I defined “4–3” form for the CTYPE*ia* keyword value; i.e., the first four characters specify the coordinate type, the fifth character is a “-”, and the remaining three characters specify an algorithm code for computing the world coordinate value. Thus while the right half specifies the transformation to be applied in computing the spherical coordinate pair, (α, δ) , the left half simply identifies the celestial system with which (α, δ) are to be associated. In this sense CTYPE*ia* contains an active part which drives the transformation and a passive part which describes the results.

Consistent with past practice, an equatorial coordinate pair is denoted by RA-- and DEC-, and other celestial systems are of the form xLON and xLAT for longitude and latitude pairs, where $x = G$ for galactic⁴, E for ecliptic, H for helioecliptic⁵, and S for supergalactic coordinates. Since representation of planetary, lunar and solar coordinate systems could exceed the 26 possibilities afforded by the single character x , we also here allow yzLN and yzLT pairs. Additional values of x and yz will undoubtedly be defined. A basic requirement, however, is that the coordinate system be right-handed and that the pole be at latitude $+90^\circ$. A coordinate pair such as azimuth and zenith distance would have to be represented as a negative azimuth and elevation with implied conversion. In some situations negation of the longitude coordinate may be implemented via a sign reversal of the

⁴ “New” galactic coordinates are assumed here, Blaauw et al. (1960). Users of the older system or future systems should adopt a different value of x and document its meaning.

⁵ Ecliptic and helioecliptic systems each have their equator on the ecliptic. However, the reference point for ecliptic longitude is the vernal equinox while that for helioecliptic longitude is the sun vector.

Table 2. Allowed values of RADESYS*a*.

| RADESYS <i>a</i> | Definition |
|------------------|---|
| ICRS | International Celestial Reference System |
| FK5 | mean place, new (IAU 1984) system |
| FK4 | mean place, old (Bessell-Newcomb) system |
| FK4-NO-E | mean place, old system but without e-terms |
| GAPPT | geocentric apparent place, IAU 1984 system |

appropriate CDEL*Tia*. It remains the responsibility of the authors of new coordinate system types to define them properly and to gain general recognition for them from the FITS community. However, FITS interpreters should be able to associate coordinate pairs even if the particular coordinate system is not recognized.

Paper I clarified that, while the subscript of CRPIX*ja* and the *j* subscript of PC*i_ja* and CD*i_ja* refer to pixel coordinate elements, the *i* subscript of PC*i_ja* and CD*i_ja* and the subscripts of CDEL*Tia*, CTY*PEia* and CRVAL*ia* refer to world coordinate elements. However we now have three different sets of world coordinates, (x, y) , (ϕ, θ) , and (α, δ) . This leads us to associate x, ϕ , and α on the one hand, and y, θ , and δ on the other. This simply means, for example, that if CTY*PE3* = 'GLON-AIT', then the third element of the intermediate world coordinate calculated via Eq. (1) corresponds to what we have been calling the x -coordinate in the plane of projection, the association being between α and x . In this way pairs of CTY*PEia* with complementary left halves and matching right halves define which elements of the intermediate world coordinate vector form the plane of projection.

3.1. Equatorial and ecliptic coordinates

Several systems of equatorial coordinates (right ascension and declination) are in common use. Apart from the International Celestial Reference System (ICRS, IAU 1998), the axes of which are by definition fixed with respect to the celestial sphere, each system is parameterized by time. In particular, mean equatorial coordinates (Hohenkerk et al. 1992) are defined in terms of the epoch (i.e. instant of time) of the mean equator and equinox (i.e. pole and origin of right ascension). The same applies for ecliptic coordinate systems. Several additional keywords are therefore required to specify these systems fully. We introduce the new keyword

RADESYS*a* (character-valued)

to specify the particular system. Recognized values are given in Table 2. Apart from FK4-NO-E these keywords are applicable to ecliptic as well as equatorial coordinates.

Wells et al. (1981) introduced the keyword EPOCH to mean the epoch of the mean equator and equinox. However we here replace it with

EQUINOX*a* (floating-valued),

since the word “epoch” is often used in astrometry to refer to the time of observation. The new keyword⁶ takes preference over EPOCH if both are given. Note that EQUINOX*a* applies to ecliptic as well as to equatorial coordinates.

For RADESYS*a* values of FK4 and FK4-NO-E, any stated equinox is Besselian and, if neither EQUINOX*a* nor EPOCH are given, a default of 1950.0 is to be taken. For FK5, any stated equinox is Julian and, if neither keyword is given, it defaults to 2000.0.

If the EQUINOX*a* keyword is given it should always be accompanied by RADESYS*a*. However, if it should happen to appear by itself then RADESYS*a* defaults to FK4 if EQUINOX*a* < 1984.0, or to FK5 if EQUINOX*a* ≥ 1984.0. Note that these defaults, while probably true of older files using the EPOCH keyword, are not required of them.

RADESYS*a* defaults to ICRS if both it and EQUINOX*a* are absent.

Geocentric apparent equatorial and ecliptic coordinates (GAPPT) require the epoch of the equator and equinox of date. This will be taken as the time of observation rather than EQUINOX*a*. The time of observation may also be required for other astrometric purposes in addition to the usual astrophysical uses, for example, to specify when the mean place was correct in accounting for proper motion, including “fictitious” proper motions in the conversion between the FK4 and FK5 systems. The old DATE-OBS keyword may be used for this purpose. However, to provide a more convenient specification we here introduce the new keyword

MJD-OBS (floating-valued),

that provides DATE-OBS as a Modified Julian Date (JD – 2 400 000.5) but is identical to it in all other respects. MJD-OBS does not have a version code since there can only be one time of observation. Following the year-2000 conventions for DATE keywords (Bunclark & Rots 1996), this time refers by default to the start of the observation unless another interpretation is clearly explained in the comment field. In the present case the distinction is not important. We leave it to future agreements to clarify systems of time measurement and other matters related to time.

The combination of CTY*PEia*, RADESYS*a*, and EQUINOX*a* define the coordinate system of the CRVAL*ia* and of the celestial coordinates that result from the sequence of transformations summarized by Fig. 1. However, FK4 coordinates are not strictly spherical since they include a contribution from the elliptic terms of aberration, the so-called “e-terms” which amount to ≤343 milliarcsec. Strictly speaking, therefore, a map obtained from, say, a radio synthesis telescope, should be regarded as FK4-NO-E unless it has been appropriately resampled or a distortion correction provided (Paper IV). In common usage, however, CRVAL*ia* for such maps is usually given in FK4 coordinates. In doing so, the e-terms are effectively corrected to first order only.

⁶ EQUINOX has since been adopted by Hanisch et al. (2001) which deprecates EPOCH.

4. Alternate FITS image representations

4.1. Random groups visibility data

The random-groups extension to FITS (Greisen & Harten 1981) has been used to transmit interferometer fringe visibility sample data. It has been customary among users of this format to convey the suggested projection type as the last four characters of the random parameter types (PTYPE n) of the Fourier plane coordinates (u, v, w). Any rotation of these coordinates was carried, however, by CROTA i associated with the one-pixel array axis used to convey the field declination. Within the new convention users of random groups for visibility data should be prepared to read, carry forward, and use as needed, the new keywords PC i _ja, CD i _ja, LONPOLE a , LATPOLE a , PV i _ja, MJD-OBS, EQUINOX a , and RADESYS a . In particular, any rotation of the (u, v) coordinate system should be represented via PC i _ja or CD i _ja (but not both) attached to the two degenerate axes used to convey the celestial coordinates of the field center.

4.2. Pixel list and image array column elements

Paper I defined the coordinate keywords used to describe a multi-dimensional image array in a single element of a FITS binary table and a tabulated list of pixel coordinates in a FITS ASCII or binary table. In this section we extend this to the keywords specific to celestial coordinates.

4.2.1. Keyword naming convention

Table 3 lists the corresponding set of coordinate system keywords for use with each type of FITS image representation.

The data type of the alternate keyword matches that of the primary keyword and the allowed values are the same. The following notes apply to the naming conventions used in Table 3:

- a is a 1-character coordinate version code and may be blank (for the primary version of the coordinate description) or any single uppercase character from A through Z.
- n is an integer table column number without any leading zeros (1 – 999).

When using the BINTABLE image array format (Cotton et al. 1995), if the table only contains a single image column or if there are multiple image columns but they all have the same value for any of the keywords in Table 3 then the simpler form of the keyword name, as used for primary arrays, may be used. For example, if all the images in the table have the same epoch then one may use a single EQUINOX a keyword rather than multiple EQUI na keywords. The other keywords, however, must always be specified using the more complex keyword name with the column number suffix and the axis number prefix.

In principle, more than one pixel list image can be stored in a single FITS table by defining more than one pair of p_1 and p_2 pixel coordinate columns. Under the convention defined here, however, all the images must share the same values for the keywords in Table 3.

Example binary table and pixel list headers are given in Sect. 7.3.2.

Table 3. Alternate coordinate keywords; the data type of the alternate keyword matches that of the primary keyword.

| Keyword Description | Primary Array | BINTABLE Array | Pixel List |
|---------------------|---------------|----------------|------------|
| Coord Rotation | LONPOLE a | LONP na | LONP na |
| Coord Rotation | LATPOLE a | LATP na | LATP na |
| Coord Epoch | EQUINOX a | EQUI na | EQUI na |
| Date of Obs | MJD-OBS | MJDOB n | MJDOB n |
| Reference Frame | RADESYS a | RADE na | RADE na |

5. Spherical map projections

In this section we present the transformation equations for all spherical map projections likely to be of use in astronomy. Many of these such as the gnomonic, orthographic, zenithal equidistant, Sanson-Flamsteed, Hammer-Aitoff and COBE quadrilateralized spherical cube are in common use. Others with special properties such as the stereographic, Mercator, and the various equal area projections could not be excluded. A selection of the conic and polyconic projections, much favored by cartographers for their minimal distortion properties, has also been included. However, we have omitted numerous other projections which we considered of mathematical interest only. Evenden (1991) presents maps of the Earth for 73 different projections, although without mathematical definition, including most of those described here. These are particularly useful in judging the distortion introduced by the various projections. Snyder (1993) provides fascinating background material on the subject; historical footnotes in this paper, mainly highlighting astronomical connections, are generally taken from this source. It should be evident from the wide variety of projections described here that new projections could readily be accommodated, the main difficulty being in obtaining general recognition for them from the FITS community.

Cartographers have often given different names to special cases of a class of projection. This applies particularly to oblique projections which, as we have seen in Sect. 2, the current formalism handles in a general way. While we have tended to avoid such special cases, the gnomonic, stereographic, and orthographic projections, being specializations of the zenithal perspective projection, are included for conformance with the AIPS convention. It is also true that zenithal and cylindrical projections may be thought of as special cases of conic projections (see Sect. 5.4). However, the limiting forms of the conic equations tend to become intractable and infinite-valued projection parameters may be involved. Even when the conic equations don't have singularities in these limits it is still likely to be less efficient to use them than the simpler special-case equations. Moreover, we felt that it would be unwise to disguise the true nature of simple projections by implementing them as special cases of more general ones. In the same vein, the cylindrical equal area projection, being a specialization of the cylindrical perspective projection, stands on its own right, as does the Sanson-Flamsteed projection which is a limiting case of Bonne's projection. A list of aliases is provided in Appendix A, Table A.1.

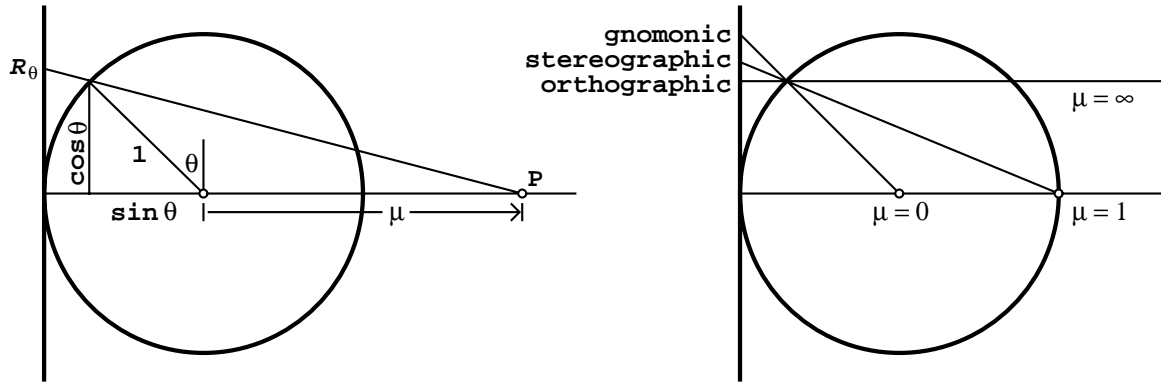


Fig. 4. (Left) geometry of the zenithal perspective projections, the point of projection at P is μ spherical radii from the center of the sphere; (right) the three important special cases. This diagram is at 3:2 scale compared to the graticules of Figs. 8, 9 and 10.

In accordance with the image display convention of Paper I we think of the p_1 -pixel coordinate increasing to the right with p_2 increasing upwards, i.e. a right-handed system. This means that the (x, y) coordinates must be *left-handed* as shown in Fig. 3. Note, however, that the approximation $(\alpha, \delta) \approx (\alpha_0, \delta_0) + (x, y)$ cannot hold unless 1) (ϕ_0, θ_0) , and hence (α_0, δ_0) , do actually map to the reference point (Sect. 2.2), 2) ϕ_p assumes its default value (Sect. 2.8), and 3) the projection is scaled true at the reference point (some are not as discussed in Sect. 7.2). Figure 3 also illustrates the orientation of the native coordinate system with respect to the (x, y) coordinate system for the two main cases.

Cartographers, for example Kellaway (1946), think of spherical projections as being a projection of the surface of a sphere onto a plane, this being the *forward* direction; the deprojection from plane back to sphere is thus the *inverse* or *reverse* direction. However, this is at variance with common usage in FITS where the transformation from pixel coordinates to world coordinates is considered the forward direction. We take the cartographic view in this section as being the natural one and trust that any potential ambiguity may readily be resolved by context.

The requirement stated in Sect. 1 that (x, y) coordinates in the plane of projection be measured in “degrees” begs clarification. Spherical projections are usually defined mathematically in terms of a scale factor, r_0 , known as the “radius of the generating sphere”. However, in this work r_0 is set explicitly to $180^\circ/\pi$ in order to maintain backwards compatibility with the AIPS convention. This effectively sets the circumference of the generating sphere to 360° so that arc length is measured naturally in degrees (rather than radians as for a unit sphere). However, this true angular measure on the generating sphere becomes distorted when the sphere is projected onto the plane of projection. So while the “degree” units of r_0 are notionally carried over by conventional dimensional analysis to the (x, y) they no longer represent a true angle except near the reference point (for most projections).

In addition to the (x, y) coordinates, the native spherical coordinates, (ϕ, θ) , celestial coordinates, (α, δ) , and all other angles in this paper are measured in degrees. In the equations given below, the arguments to all trigonometric functions are in degrees and all inverse trigonometric functions return their

result in degrees. Whenever a conversion between radians and degrees is required it is shown explicitly. All of the graticules presented in this section have been drawn to the same scale in (x, y) coordinates in order to represent accurately the exaggeration and foreshortening found in some projections. It will also be apparent that since FITS image planes are rectangular and the boundaries of many projections are curved, there may sometimes be cases when the FITS image must contain pixels that are outside the boundary of the projection. These pixels should be blanked correctly and geometry routines should return a sensible error code to indicate that their celestial coordinates are undefined.

5.1. Zenithal (azimuthal) projections

Zenithal or *azimuthal* projections all map the sphere directly onto a plane. The native coordinate system is chosen to have the polar axis orthogonal to the plane of projection at the reference point as shown on the left side of Fig. 3. Meridians of native longitude are projected as uniformly spaced rays emanating from the reference point and the parallels of native latitude are mapped as concentric circles centered on the same point. Since all zenithal projections are constructed with the pole of the native coordinate system at the reference point we set

$$(\phi_0, \theta_0)_{\text{zenithal}} = (0, 90^\circ). \quad (11)$$

Zenithal projections are completely specified by defining the radius as a function of native latitude, R_θ . Rectangular Cartesian coordinates, (x, y) , in the plane of projection as defined by Eq. (1), are then given by

$$x = R_\theta \sin \phi, \quad (12)$$

$$y = -R_\theta \cos \phi, \quad (13)$$

which may be inverted as

$$\phi = \arg(-y, x), \quad (14)$$

$$R_\theta = \sqrt{x^2 + y^2}. \quad (15)$$

5.1.1. AZP: Zenithal perspective

Zenithal (azimuthal) perspective projections are generated from a point and carried through the sphere to the plane of

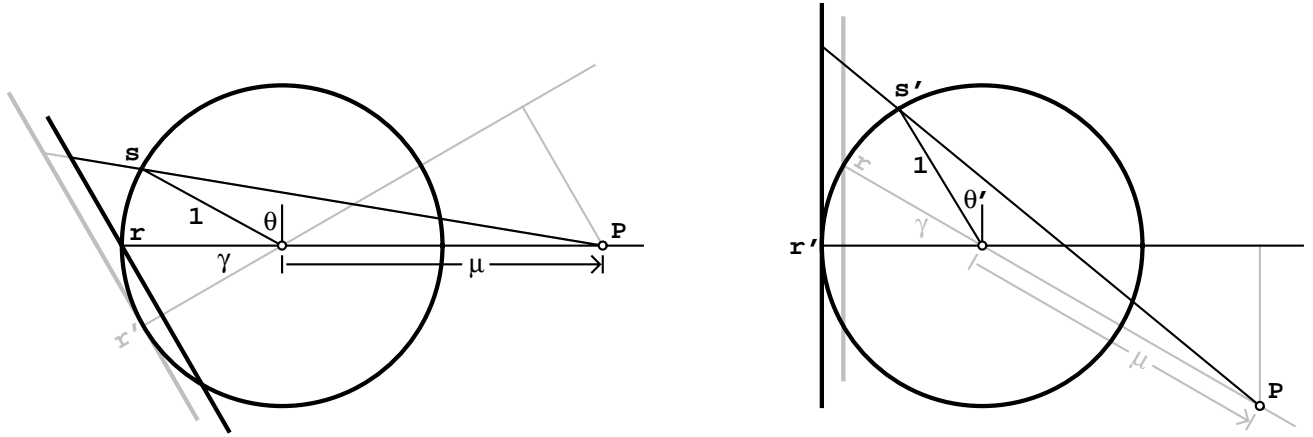


Fig. 5. Alternate geometries of slant zenithal perspective projections with $\mu = 2$ and $\gamma = 30^\circ$: (left) tilted plane of projection (AZP), (right) displaced point of projection P (SZP). Grey lines in each diagram indicate the other point of view. They differ geometrically only by a scale factor, the effect of translating the plane of projection. Each projection has its native pole at the reference point, r and r' , but these are geometrically different points. Thus the native latitudes θ and θ' of the geometrically equivalent points s and s' differ. Consequently the two sets of projection equations have a different form. This diagram is at 3:2 scale compared to the graticules of Figs. 6 and 7.

projection as illustrated in Fig. 4. We need consider only the case where the plane of projection is tangent to the sphere at its pole; the projection is simply rescaled if the plane intersects some other parallel of native latitude. If the source of the projection is at a distance μ spherical radii from the center of the sphere with μ increasing in the direction away from the plane of projection, then it is straightforward to show that

$$R_\theta = \frac{180^\circ (\mu + 1) \cos \theta}{\pi (\mu + \sin \theta)}, \quad (16)$$

with $\mu \neq -1$ being the only restriction. When R_θ is given Eq. (16) has two solutions for θ , one for each side of the sphere. The following form of the inverse equation always gives the planeward solution for any μ

$$\theta = \arg(\rho, 1) - \sin^{-1} \left(\frac{\rho \mu}{\sqrt{\rho^2 + 1}} \right), \quad (17)$$

where

$$\rho = \frac{\pi R_\theta}{180^\circ \mu + 1}. \quad (18)$$

For $|\mu| \neq 1$ the sphere is divided by a native parallel at latitude θ_x into two unequal segments that are projected in superposition:

$$\theta_x = \begin{cases} \sin^{-1}(-1/\mu) \dots |\mu| > 1 \\ \sin^{-1}(-\mu) \dots |\mu| < 1 \end{cases}. \quad (19)$$

For $|\mu| > 1$, the projection is bounded and both segments are projected in the correct orientation, whereas for $|\mu| \leq 1$ the projection is unbounded and the anti-planewards segment is inverted.

A *near-sided* perspective projection may be obtained with $\mu < -1$. This correctly represents the image of a sphere, such as a planet, when viewed from a distance $|\mu|$ times the planetary radius. The coordinates of the reference point may be expressed in planetary longitude and latitude, (λ, β) . Also, the signs of the relevant CDELT *ia* may be chosen so that longitude increases as

appropriate for a sphere seen from the outside rather than from within.

It is particularly with regard to planetary mapping that we must generalize AZP to the case where the plane of projection is tilted with respect to the axis of the generating sphere, as shown on the left side of Fig. 5. It can be shown (Sect. 7.4.1) that this geometry is appropriate for spacecraft imaging with non-zero look-angle, γ , the angle between the camera's optical axis and the line to the center of the planet.

Such *slant* zenithal perspective projections are not radially symmetric and their projection equations must be expressed directly in terms of x and y :

$$x = R \sin \phi, \quad (20)$$

$$y = -R \sec \gamma \cos \phi, \quad (21)$$

where

$$R = \frac{180^\circ (\mu + 1) \cos \theta}{\pi (\mu + \sin \theta) + \cos \theta \cos \phi \tan \gamma} \quad (22)$$

is a function of ϕ as well as θ . Equations (20) and (21) reduce to the non-slant case for $\gamma = 0$. The inverse equations are

$$\phi = \arg(-y \cos \gamma, x), \quad (23)$$

$$\theta = \begin{cases} \psi - \omega \\ \psi + \omega + 180^\circ \end{cases}, \quad (24)$$

where

$$\psi = \arg(\rho, 1), \quad (25)$$

$$\omega = \sin^{-1} \left(\frac{\rho \mu}{\sqrt{\rho^2 + 1}} \right), \quad (26)$$

$$\rho = \frac{R}{\frac{180^\circ}{\pi} (\mu + 1) + y \sin \gamma}, \quad (27)$$

$$R = \sqrt{x^2 + y^2 \cos^2 \gamma}. \quad (28)$$

For $|\mu| < 1$ only one of the solutions for θ will be valid, i.e. lie in the range $[-90^\circ, 90^\circ]$ after normalization. Otherwise there will be two valid solutions; the one closest to 90° should be chosen.

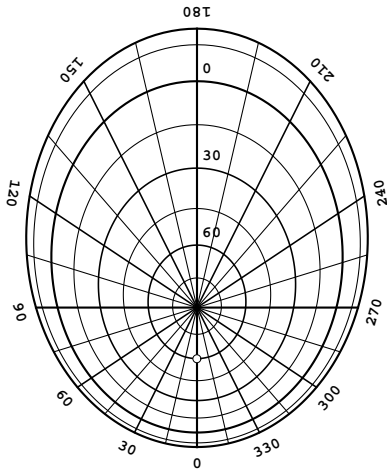


Fig. 6. Slant zenithal perspective (AZP) projection with $\mu = 2$ and $\gamma = 30^\circ$ which corresponds to the left-hand side of Fig. 5. The reference point of the corresponding SZP projection is marked at $(\phi, \theta) = (0, 60^\circ)$.

With $\gamma \neq 0$ the projection is not scaled true at the reference point. In fact the x scale is correct but the y scale is magnified by $\sec \gamma$, thus stretching parallels of latitude near the pole into ellipses (see Fig. 6). This also shows the native meridians projected as rays emanating from the pole. For constant θ , each parallel of native latitude defines a cone with apex at the point of projection. This cone intersects the tilted plane of projection in a conic section. Equations (20) and (21) reduce to the parametric equations of an ellipse, parabola, or hyperbola; the quantity

$$C = (\mu + \sin \theta)^2 - \tan^2 \gamma \cos^2 \theta \quad (29)$$

determines which:

$$\begin{aligned} C > 0 &\dots \text{ellipse,} \\ C = 0 &\dots \text{parabola,} \\ C < 0 &\dots \text{hyperbola.} \end{aligned} \quad (30)$$

If $|\mu \cos \gamma| \leq 1$ then the open conic sections are possible and $C = 0$ when

$$\theta = \pm \gamma - \sin^{-1}(\mu \cos \gamma). \quad (31)$$

For $C > 0$ the eccentricity of the ellipse is a function of θ , as is the offset of its center in y .

Definition of the perimeter of the projection is more complicated for the slant projection than the orthogonal case. As before, for $|\mu| > 1$ the sphere is divided into two unequal segments that are projected in superposition. The boundary between these two segments is what would be seen as the limb of the planet in spacecraft photography. It corresponds to native latitude

$$\theta_x = \sin^{-1}(-1/\mu), \quad (32)$$

which is projected as an ellipse, parabola, or hyperbola for $|\mu \cos \gamma|$ greater than, equal to, or less than 1 respectively.

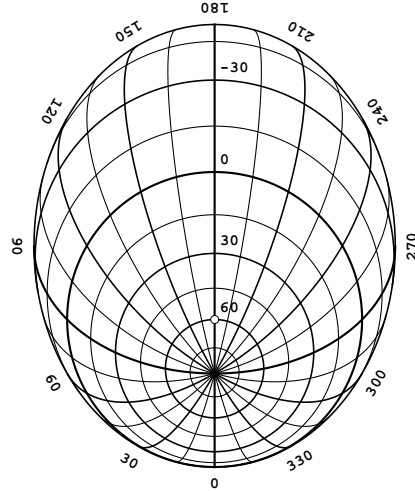


Fig. 7. Slant zenithal perspective (SZP) projection with $\mu = 2$ and $(\phi_c, \theta_c) = (180^\circ, 60^\circ)$, which corresponds to the right-hand side of Fig. 5. The reference point of the corresponding AZP projection is marked at $(\phi, \theta) = (180^\circ, 60^\circ)$.

In general, for $|\mu \cos \gamma| > 1$, the projection is bounded, otherwise it is unbounded. However, the latitude of divergence is now a function of ϕ :

$$\theta_\infty = \begin{cases} \psi - \omega \\ \psi + \omega + 180^\circ \end{cases}, \quad (33)$$

where

$$\psi = -\tan^{-1}(\tan \gamma \cos \phi), \quad (34)$$

$$\omega = \sin^{-1}\left(\frac{\mu}{\sqrt{1 + \tan^2 \gamma \cos^2 \phi}}\right). \quad (35)$$

Zero, one, or both of the values of θ_∞ given by Eq. (33) may be valid, i.e. lie in the range $[-90^\circ, 90^\circ]$ after normalization.

The FITS keywords `PVi_1a` and `PVi_2a`, attached to *latitude* coordinate i , will be used to specify, respectively, μ in spherical radii and γ in degrees, both with default value 0.

5.1.2. SZP: Slant zenithal perspective

While the generalization of the AZP projection to tilted planes of projection is useful for certain applications it does have a number of drawbacks, in particular, unequal scaling at the reference point.

Figure 5 shows that moving the point of projection, P, off the axis of the generating sphere is equivalent, to within a scale factor, to tilting the plane of projection. However this approach has the advantage that the plane of projection remains tangent to the sphere. Thus the projection is conformal at the native pole as can be seen by the circle around the native pole in Fig. 7. It is also quite straightforward to formulate the projection equations with P offset in x as well as y .

It is interesting to note that this slant zenithal perspective (SZP) projection also handles the case that corresponds to $\gamma = 90^\circ$ in AZP. AZP fails in this extreme since P falls in the plane of projection – effectively a scale factor of zero is applied to AZP over the corresponding SZP case. One of the more

important aspects of SZP is the application of its limiting case with $\mu = \infty$ in aperture synthesis radio astronomy as discussed in Sect. 5.1.5. One minor disadvantage is that the native meridians are projected as curved conic sections rather than straight lines.

If the Cartesian coordinates of P measured in units of the spherical radius are (x_p, y_p, z_p) , then

$$x = \frac{180^\circ z_p \cos \theta \sin \phi - x_p(1 - \sin \theta)}{\pi \frac{z_p - (1 - \sin \theta)}{z_p - (1 - \sin \theta)}}, \quad (36)$$

$$y = -\frac{180^\circ z_p \cos \theta \cos \phi + y_p(1 - \sin \theta)}{\pi \frac{z_p - (1 - \sin \theta)}{z_p - (1 - \sin \theta)}}. \quad (37)$$

To invert these equations, compute θ first via

$$\theta = \sin^{-1} \left(\frac{-b \pm \sqrt{b^2 - ac}}{a} \right), \quad (38)$$

where

$$a = X'^2 + Y'^2 + 1, \quad (39)$$

$$b = X'(X - X') + Y'(Y - Y'), \quad (40)$$

$$c = (X - X')^2 + (Y - Y')^2 - 1, \quad (41)$$

$$(X, Y) = \frac{\pi}{180^\circ}(x, y), \quad (42)$$

$$(X', Y') = (X - x_p, Y - y_p)/z_p. \quad (43)$$

Choose θ closer to 90° if Eq. (38) has two valid solutions; then ϕ is given by

$$\phi = \arg(-Y - Y'(1 - \sin \theta), X - X'(1 - \sin \theta)). \quad (44)$$

The Cartesian coordinates of P are simply related to the parameters used in AZP. If μ is the distance of P from the center of the sphere O, and the line through P and O intersects the sphere at (ϕ_c, θ_c) on the planewards side (point r in Fig. 5, right), then $\gamma = 90^\circ - \theta_c$ and

$$x_p = -\mu \cos \theta_c \sin \phi_c, \quad (45)$$

$$y_p = \mu \cos \theta_c \cos \phi_c, \quad (46)$$

$$z_p = \mu \sin \theta_c + 1, \quad (47)$$

where μ is positive if P lies on the opposite side of O from r and negative otherwise. For a non-degenerate projection we require $z_p \neq 0$ and this is the only constraint on the projection parameters.

For $|\mu| > 1$ the sphere is divided into two unequal segments that are projected in superposition. The limb is defined by computing the native latitude θ_x as a function of ϕ

$$\theta_x = \begin{cases} \psi - \omega \\ \psi + \omega + 180^\circ \end{cases}, \quad (48)$$

where

$$\psi = \arg(\rho, \sigma), \quad (49)$$

$$\omega = \sin^{-1} \left(\frac{1}{\sqrt{\rho^2 + \sigma^2}} \right), \quad (50)$$

$$(\rho, \sigma) = (z_p - 1, x_p \sin \phi - y_p \cos \phi), \quad (51)$$

$$= (\mu \sin \theta_c, -\mu \cos \theta_c \cos(\phi - \phi_c)). \quad (52)$$

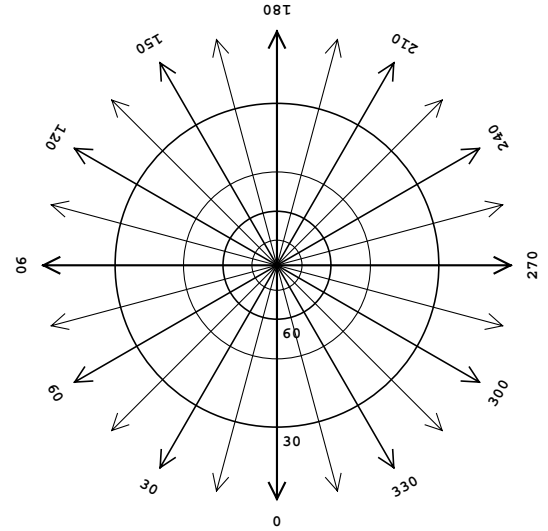


Fig. 8. Gnomonic (TAN) projection; diverges at $\theta = 0$.

Zero, one, or both of the values of θ_x given by Eq. (48) may be valid, i.e. lie in the range $[-90^\circ, 90^\circ]$ after normalization. A second boundary constraint applies if $|1 - z_p| \leq 1$ in which case the projection diverges at native latitude:

$$\theta_\infty = \sin^{-1}(1 - z_p). \quad (53)$$

The FITS keywords `PVi_1a`, `PVi_2a`, and `PVi_3a`, attached to *latitude* coordinate *i*, will be used to specify, respectively, μ in spherical radii with default value 0, ϕ_c in degrees with default value 0, and θ_c in degrees with default value 90° .

5.1.3. TAN: Gnomonic

The zenithal perspective projection with $\mu = 0$, the gnomonic projection⁸, is widely used in optical astronomy and was given its own code within the AIPS convention, namely `TAN`⁹. For $\mu = 0$, Eq. (16) reduces to

$$R_\theta = \frac{180^\circ}{\pi} \cot \theta, \quad (54)$$

with inverse

$$\theta = \tan^{-1} \left(\frac{180^\circ}{\pi R_\theta} \right). \quad (55)$$

The gnomonic projection is illustrated in Fig. 8. Since the projection is from the center of the sphere, all great circles are projected as straight lines. Thus, the shortest distance between two points on the sphere is represented as a straight line interval, which, however, is not uniformly divided. The gnomonic projection diverges at $\theta = 0$, but one may use a gnomonic projection onto the six faces of a cube to display the whole sky. See Sect. 5.6.1 for details.

⁸ The gnomonic projection is the oldest known, dating to Thales of Miletus (ca. 624–547 B.C.). The stereographic and orthographic date to Hipparchus (ca. 190–after 126 B.C.).

⁹ Referring to the dependence of R_θ on the angular separation between the tangent point and field point, i.e. the native *co*-latitude.

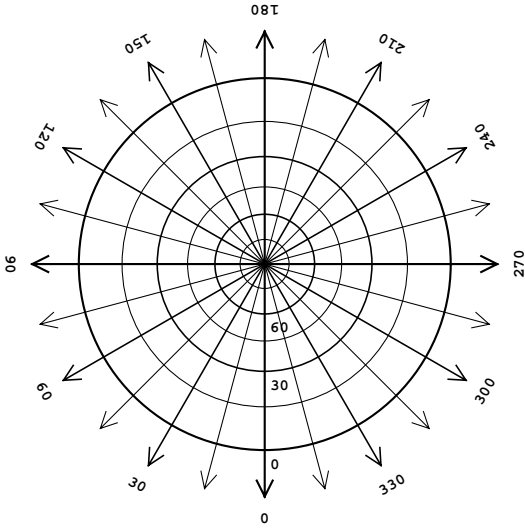


Fig. 9. Stereographic (STG) projection; diverges at $\theta = -90^\circ$.

5.1.4. STG: Stereographic

The stereographic projection, the second important special case of the zenithal perspective projection defined by the AIPS convention, has $\mu = 1$, for which Eq. (16) becomes

$$R_\theta = \frac{180^\circ}{\pi} \frac{2 \cos \theta}{1 + \sin \theta}, \quad (56)$$

$$= \frac{360^\circ}{\pi} \tan\left(\frac{90^\circ - \theta}{2}\right),$$

with inverse

$$\theta = 90^\circ - 2 \tan^{-1}\left(\frac{\pi R_\theta}{360^\circ}\right). \quad (57)$$

The stereographic projection illustrated in Fig. 9 is the conformal (orthomorphic) zenithal projection¹⁰, everywhere satisfying the isoscaling requirement

$$\frac{\partial R_\theta}{\partial \theta} = \frac{-\pi R_\theta}{180^\circ \cos \theta}. \quad (58)$$

This allows its use as a replacement for retroazimuthal projections, as discussed in Sect. 5.

The stereographic projection also has the amazing property that it maps all circles on the sphere to circles in the plane of projection, although concentric circles on the sphere are not necessarily concentric in the plane of projection. This property made it the projection of choice for Arab astronomers in constructing astrolabes. In more recent times it has been used by the Astrogeology Center for maps of the Moon, Mars, and Mercury containing craters, basins, and other circular features.

5.1.5. SIN: Slant orthographic

The zenithal perspective projection with $\mu = \infty$, the orthographic projection, is illustrated in the upper portion of Fig. 10 (at consistent scale). It represents the visual appearance of a sphere, e.g. a planet, when seen from a great distance.

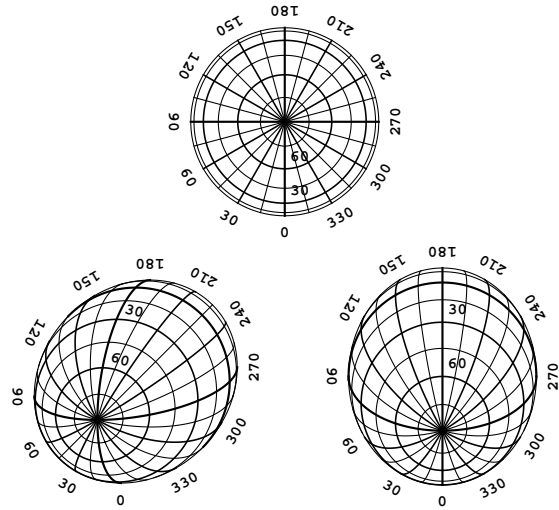


Fig. 10. Slant orthographic (SIN) projection: (top) the orthographic projection, $(\xi, \eta) = (0, 0)$, north and south sides begin to overlap at $\theta = 0$; (bottom left) $(\phi_c, \theta_c) = (225^\circ, 60^\circ)$, i.e. $(\xi, \eta) = (-1/\sqrt{6}, 1/\sqrt{6})$; (bottom right) projection appropriate for an east-west array observing at $\delta_0 = 60^\circ$, $(\phi_c, \theta_c) = (180^\circ, 60^\circ)$, $(\xi, \eta) = (0, 1/\sqrt{3})$.

The orthographic projection is widely used in aperture synthesis radio astronomy and was given its own code within the AIPS convention, namely SIN¹¹. Use of this projection code obviates the need to specify an infinite value as a parameter of AZP. In this case, Eq. (16) becomes

$$R_\theta = \frac{180^\circ}{\pi} \cos \theta, \quad (59)$$

with inverse

$$\theta = \cos^{-1}\left(\frac{\pi}{180^\circ} R_\theta\right). \quad (60)$$

In fact, use of the orthographic projection in radio interferometry is an approximation, applicable only for small field sizes. However, an exact solution exists where the interferometer baselines are co-planar. It reduces to what Greisen (1983) called the NCP projection for the particular case of an East-West interferometer (Brouw 1971). The projection equations (derived in Appendix C) are

$$x = \frac{180^\circ}{\pi} [\cos \theta \sin \phi + \xi (1 - \sin \theta)], \quad (61)$$

$$y = -\frac{180^\circ}{\pi} [\cos \theta \cos \phi - \eta (1 - \sin \theta)]. \quad (62)$$

These are the equations of the ‘‘slant orthographic’’ projection, equivalent to Eqs. (36) and (37) of the SZP projection in the limit $\mu = \infty$, with

$$\xi = \cot \theta_c \sin \phi_c, \quad (63)$$

$$\eta = -\cot \theta_c \cos \phi_c. \quad (64)$$

It can be shown that the slant orthographic projection is equivalent to an orthographic projection centered at $(x, y) = \frac{180^\circ}{\pi} (\xi, \eta)$ which has been stretched in the ϕ_c direction by a

¹⁰ First noted by astronomer Edmond Halley (1656–1742).

¹¹ Similar etymology to TAN.

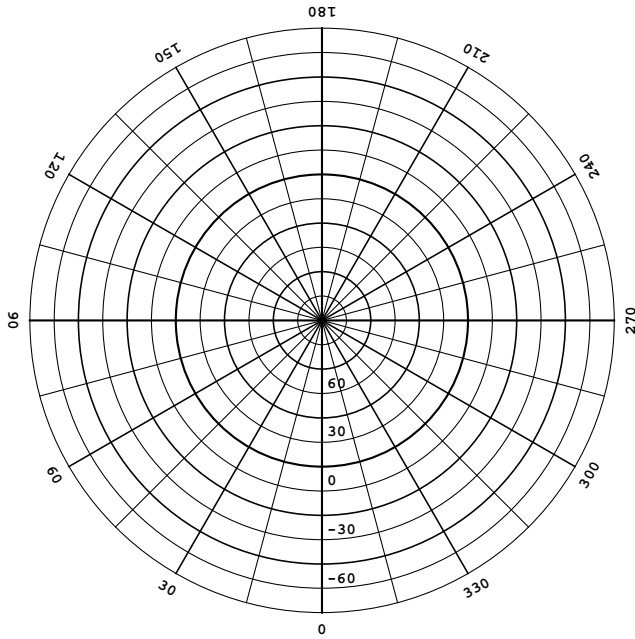


Fig. 11. Zenithal equidistant (ARC) projection; no limits.

factor of $\text{cosec } \theta_c$. The projection equations may be inverted using Eqs. (38) and (44) except that Eq. (43) is replaced with

$$(X', Y') = (\xi, \eta). \quad (65)$$

The outer boundary of the SIN projection is given by Eq. (48) in the limit $\mu = \infty$:

$$\theta_x = -\tan^{-1}(\xi \sin \phi - \eta \cos \phi). \quad (66)$$

Two example graticules are illustrated in the lower portion of Fig. 10. We here extend the original SIN projection of the AIPS convention to encompass the slant orthographic projection, with the dimensionless ξ and η given by keywords *PVi_1a* and *PVi_2a*, respectively, attached to *latitude* coordinate *i*, both with default value 0.

5.1.6. ARC: Zenithal equidistant

Some non-perspective zenithal projections are also of interest in astronomy. The zenithal equidistant projection first appeared in Greisen (1983) as ARC. It is widely used as the approximate projection of Schmidt telescopes. As illustrated in Fig. 11, the native meridians are uniformly divided to give equispaced parallels. Thus

$$R_\theta = 90^\circ - \theta, \quad (67)$$

which is trivially invertible. This projection was also known in antiquity.

5.1.7. ZPN: Zenithal polynomial

The zenithal polynomial projection, ZPN, generalizes the ARC projection by adding polynomial terms up to a large degree in the zenith distance. We define it as

$$R_\theta = \frac{180^\circ}{\pi} \sum_{m=0}^{20} P_m \left(\frac{\pi}{180^\circ} (90^\circ - \theta) \right)^m. \quad (68)$$

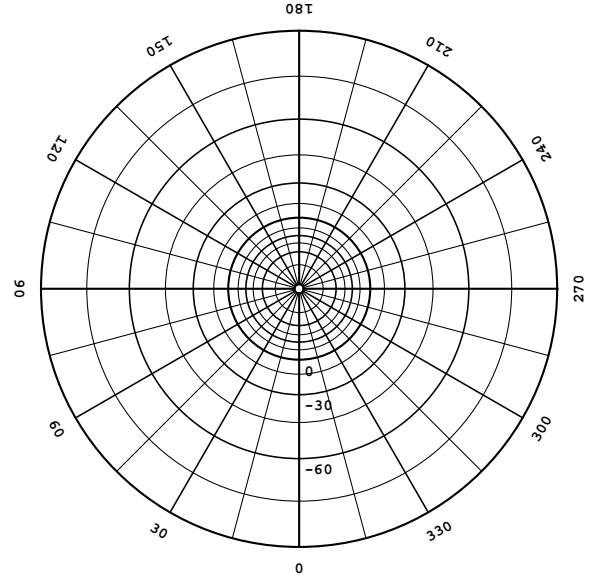


Fig. 12. Zenithal polynomial projection (ZPN) with parameters, 0.050, 0.975, -0.807, 0.337, -0.065, 0.010, 0.003, -0.001; limits depend upon the parameters.

Note the dimensionless units of P_m imparted by $\pi/180^\circ$. Allowance is made for a polynomial of degree up to 20 as a conservative upper limit that should encompass all practical applications. For speed and numerical precision the polynomial should be evaluated in Horner form, i.e.

$$(\dots(P_{20}\gamma + P_{19})\gamma + \dots P_2)\gamma + P_1)\gamma + P_0$$

where $\gamma = (180^\circ/\pi)(90^\circ - \theta)$.

Since its inverse cannot be expressed analytically, ZPN should only be used when the geometry of the observations require it. In particular, it should never be used as an *n*th-degree expansion of one of the standard zenithal projections.

If P_0 is non-zero the native pole is mapped to an open circle centered on the reference point as illustrated in Fig. 12. In other words, $(\phi_0, \theta_0) = (0, 90^\circ)$ is not at $(x, y) = (0, 0)$, which in fact lies outside the boundary of the projection. However, we do not dismiss $P_0 \neq 0$ as a possibility since it is not inconsistent with the formalism presented in Sect. 2.2 and could conceivably be useful for images which do not contain the reference point. Needless to say, care should be exercised in constructing and interpreting such systems particularly in that (α_0, δ_0) (i.e. the *CRVAL ia*) do not specify the celestial coordinates of the reference point (the *CRPIX ja*).

P_m (dimensionless) is given by the keywords *PVi_0a*, *PVi_1a*, ..., *PVi_20a*, attached to *latitude* coordinate *i*, all of which have default values of zero.

5.1.8. ZEA: Zenithal equal-area

Lambert's zenithal equal-area projection illustrated in Fig. 13 is constructed by defining R_θ so that the area enclosed by the native parallel at latitude θ in the plane of projection is equal to the area of the corresponding spherical cap. It may be generated

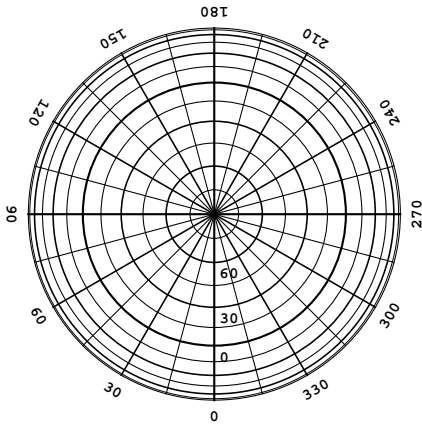


Fig. 13. Zenithal equal area projection (ZEA); no limits.

using

$$R_\theta = \frac{180^\circ}{\pi} \sqrt{2(1 - \sin \theta)}$$

$$= \frac{360^\circ}{\pi} \sin\left(\frac{90^\circ - \theta}{2}\right),$$

with inverse

$$\theta = 90^\circ - 2 \sin^{-1}\left(\frac{\pi R_\theta}{360^\circ}\right).$$

5.1.9. AIR: Airy projection

The Airy projection¹² minimizes the error for the region within latitude θ_b (Evenden 1991). It is defined by

$$R_\theta = -2 \frac{180^\circ}{\pi} \left(\frac{\ln(\cos \xi)}{\tan \xi} + \frac{\ln(\cos \xi_b)}{\tan^2 \xi_b} \tan \xi \right),$$

where

$$\xi = \frac{90^\circ - \theta}{2},$$

$$\xi_b = \frac{90^\circ - \theta_b}{2}.$$

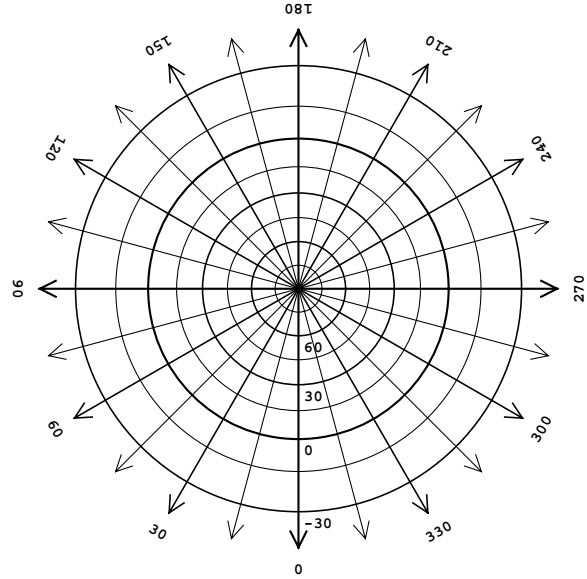
When θ_b approaches 90° , the second term of Eq. (71) approaches its asymptotic value of $-\frac{1}{2}$. For all θ_b , the projection is unbounded at the native south pole. Inversion of Eq. (71), a transcendental equation in θ , must be done via iterative methods.

The FITS keyword `PVi_1a`, attached to *latitude* coordinate *i*, will be used to specify θ_b in degrees with a default of 90° . This projection is illustrated in Fig. 14.

5.2. Cylindrical projections

Cylindrical projections are so named because the surface of projection is a cylinder. The native coordinate system is chosen to have its polar axis coincident with the axis of the cylinder. Meridians and parallels are mapped onto a rectangular graticule so that cylindrical projections are described by formulæ

¹² Devised in 1861 by astronomer royal George Biddell Airy, 1801–1892.



(69) Fig. 14. Airy projection (AIR) with $\theta_b = 45^\circ$; diverges at $\theta = -90^\circ$.

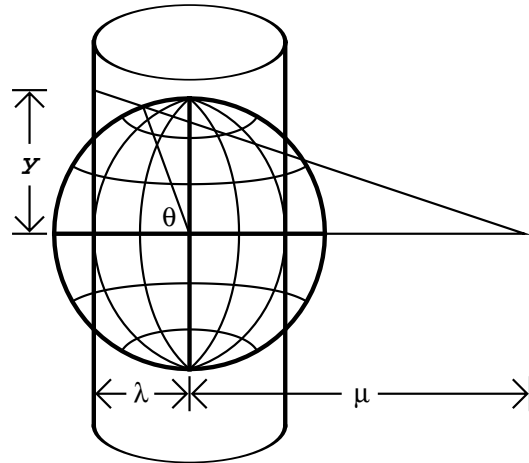


Fig. 15. Geometry of cylindrical projections.

which return x and y directly. Since all cylindrical projections are constructed with the native coordinate system origin at the reference point, we set

$$(\phi_0, \theta_0)_{\text{cylindrical}} = (0, 0).$$

Furthermore, all cylindrical projections have

$$x \propto \phi.$$

Cylindrical projections are often chosen to map the regions adjacent to a great circle, usually the equator, with minimal distortion.

5.2.1. CYP: Cylindrical perspective

Figure 15 illustrates the geometry for the construction of cylindrical perspective projections. The sphere is projected onto a cylinder of radius λ spherical radii from points in the equatorial plane of the native system at a distance μ spherical radii measured from the center of the sphere in the direction opposite the projected surface. The cylinder intersects the sphere at

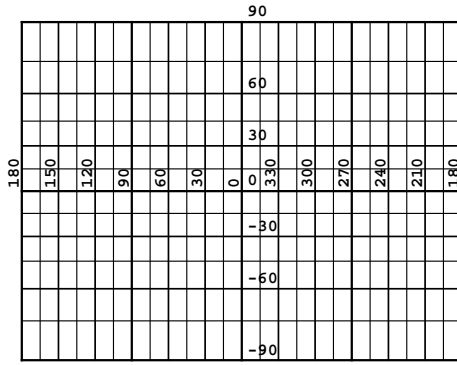


Fig. 16. Gall's stereographic projection, CYP with $\mu = 1$, $\theta_x = 45^\circ$; no limits.

latitudes $\theta_x = \cos^{-1} \lambda$. It is straightforward to show that

$$x = \lambda \phi, \quad (74)$$

$$y = \frac{180^\circ}{\pi} \left(\frac{\mu + \lambda}{\mu + \cos \theta} \right) \sin \theta. \quad (75)$$

This may be inverted as

$$\phi = \frac{x}{\lambda}, \quad (76)$$

$$\theta = \arg(1, \eta) + \sin^{-1} \left(\frac{\eta \mu}{\sqrt{\eta^2 + 1}} \right), \quad (77)$$

where

$$\eta = \frac{\pi}{180^\circ} \frac{y}{\mu + \lambda}. \quad (78)$$

Note that all values of μ are allowable except $\mu = -\lambda$. For FITS purposes, we define the keywords `PVi_1a` to convey μ and `PVi_2a` for λ , both measured in spherical radii, both with default value 1, and both attached to *latitude* coordinate i .

The case with $\mu = \infty$ is covered by the class of cylindrical equal area projections. No other special-cases need be defined since cylindrical perspective projections have not previously been used in FITS. Aliases for a number of special cases are listed in Appendix A, Table A.1. Probably the most important of these is Gall's stereographic projection, which minimizes distortions in the equatorial regions. It has $\mu = 1$, $\lambda = \sqrt{2}/2$, giving

$$x = \phi / \sqrt{2},$$

$$y = \frac{180^\circ}{\pi} \left(1 + \frac{\sqrt{2}}{2} \right) \tan \left(\frac{\theta}{2} \right).$$

It is illustrated in Fig. 16.

5.2.2. CEA: Cylindrical equal area

The cylindrical equal area projection is the special case of the cylindrical perspective projection with $\mu = \infty$. It is conformal at latitudes $\pm \theta_c$ where $\lambda = \cos^2 \theta_c$. The formulæ are

$$x = \phi, \quad (79)$$

$$y = \frac{180^\circ}{\pi} \frac{\sin \theta}{\lambda}, \quad (80)$$

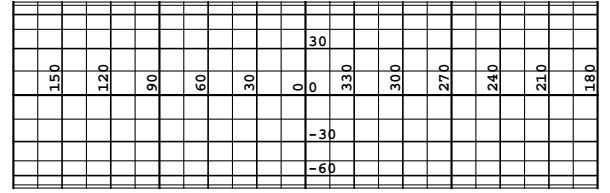


Fig. 17. Lambert's equal area projection, CEA with $\lambda = 1$; no limits.

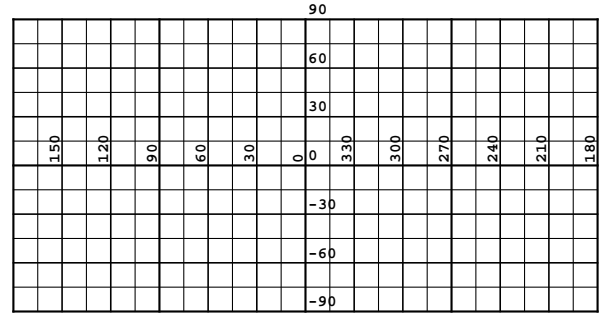


Fig. 18. The plate carrée projection (CAR); no limits.

which reverse to

$$\phi = x, \quad (81)$$

$$\theta = \sin^{-1} \left(\frac{\pi}{180^\circ} \lambda y \right). \quad (82)$$

Note that the scaling parameter λ is applied to the y -coordinate rather than the x -coordinate as in CYP. The keyword `PVi_1a` attached to *latitude* coordinate i is used to specify the dimensionless λ with default value 1.

Lambert's¹³ equal area projection, the case with $\lambda = 1$, is illustrated in Fig. 17. It shows the extreme compression of the parallels of latitude at the poles typical of all cylindrical equal area projections.

5.2.3. CAR: Plate carrée

The equator and all meridians are correctly scaled in the plate carrée projection¹⁴, whose main virtue is that of simplicity. Its formulæ are

$$x = \phi, \quad (83)$$

$$y = \theta. \quad (84)$$

The projection is illustrated in Fig. 18.

5.2.4. MER: Mercator

Since the meridians and parallels of all cylindrical projections intersect at right angles the requirement for conformality

¹³ The mathematician, astronomer and physicist Johann Heinrich Lambert (1728–1777) was the first to make significant use of calculus in constructing map projections. He formulated and gave his name to a number of important projections as listed in Table A.1.

¹⁴ Although colloquially referred to as “Cartesian”, Claudius Ptolemy (ca. 90-ca. 170 A.D.), influential cartographer and author of the Ptolemaic model of the solar system, credits Marinus of Tyre with its invention in about A.D. 100, thus predating Descartes by some 1500 years.

reduces to that of equiscaling at each point. This is expressed by the differential equation

$$\frac{\partial y}{\partial \theta} = \frac{-1}{\cos \theta} \frac{\partial x}{\partial \phi}, \quad (85)$$

the solution¹⁵ of which gives us Mercator's projection:

$$x = \phi, \quad (86)$$

$$y = \frac{180^\circ}{\pi} \ln \tan \left(\frac{90^\circ + \theta}{2} \right), \quad (87)$$

with inverse

$$\theta = 2 \tan^{-1} \left(e^{y\pi/180^\circ} \right) - 90^\circ. \quad (88)$$

This projection, illustrated in Fig. 19, has been widely used in navigation since it has the property that lines of constant bearing (known as *rhumbs lines* or *loxodromes*) are projected as straight lines. This is a direct result of its conformality and the fact that its meridians do not converge.

Refer to Sect. 6.1.4 for a discussion of the usage of MER in AIPS.

5.3. Pseudocylindrical and related projections

Pseudocylindricals are like cylindrical projections except that the parallels of latitude are projected at diminishing lengths towards the polar regions in order to reduce lateral distortion there. Consequently the meridians are curved. Pseudocylindrical projections lend themselves to the construction of *interrupted* projections in terrestrial cartography. However, this technique is unlikely to be of use in celestial mapping and is not considered here. Like ordinary cylindrical projections, the pseudocylindricals are constructed with the native coordinate system origin at the reference point. Accordingly we set

$$(\phi_0, \theta_0)_{\text{pseudocylindrical}} = (0, 0). \quad (89)$$

The Hammer-Aitoff projection is a modified zenithal projection, not a pseudocylindrical, but is presented with this group on account of its superficial resemblance to them.

5.3.1. SFL: Sanson-Flamsteed

Bonne's projection (Sect. 5.5.1) reduces to the pseudocylindrical Sanson-Flamsteed¹⁶ projection when $\theta_1 = 0$. Parallels are equispaced and projected at their true length which makes it an equal area projection. The formulæ are

$$x = \phi \cos \theta, \quad (90)$$

$$y = \theta, \quad (91)$$

¹⁵ Gerardus Mercator (1512–1594), a prominent Flemish map-maker, effectively solved this equation by numerical integration. Presented in 1569 it thus predates Newton's *theory of fluxions* by nearly a century.

¹⁶ Nicolas Sanson d'Abbeville (1600–1667) of France and John Flamsteed (1646–1719), the first astronomer royal of England, popularized this projection, which was in existence at least as early as 1570.

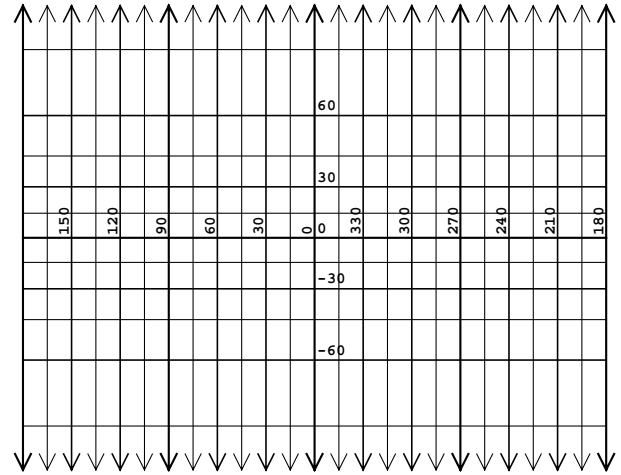


Fig. 19. Mercator's projection (MER); diverges at $\theta = \pm 90^\circ$.

which reverse into

$$\phi = \frac{x}{\cos y}, \quad (92)$$

$$\theta = y. \quad (93)$$

This projection is illustrated in Fig. 20. Refer to Sect. 6.1.4 for a discussion relating SFL to the GLS projection in AIPS.

5.3.2. PAR: Parabolic

The parabolic or Craster pseudocylindrical projection is illustrated in Fig. 21. The meridians are projected as parabolic arcs which intersect the poles and correctly divide the equator, and the parallels of latitude are spaced so as to make it an equal area projection. The formulæ are

$$x = \phi \left(2 \cos \frac{2\theta}{3} - 1 \right), \quad (94)$$

$$y = 180^\circ \sin \frac{\theta}{3}, \quad (95)$$

with inverse

$$\theta = 3 \sin^{-1} \left(\frac{y}{180^\circ} \right), \quad (96)$$

$$\phi = \frac{180^\circ}{\pi} \frac{x}{1 - 4(y/180^\circ)^2}. \quad (97)$$

5.3.3. MOL: Mollweide's

In Mollweide's pseudocylindrical projection¹⁷, the meridians are projected as ellipses that correctly divide the equator and the parallels are spaced so as to make the projection equal area. The formulæ are

$$x = \frac{2\sqrt{2}}{\pi} \phi \cos \gamma, \quad (98)$$

$$y = \sqrt{2} \frac{180^\circ}{\pi} \sin \gamma, \quad (99)$$

¹⁷ Presented in 1805 by astronomer and mathematician Karl Brandan Mollweide (1774–1825).

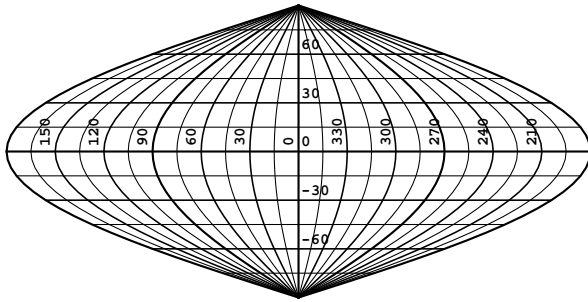


Fig. 20. Sanson-Flamsteed projection (SFL); no limits.

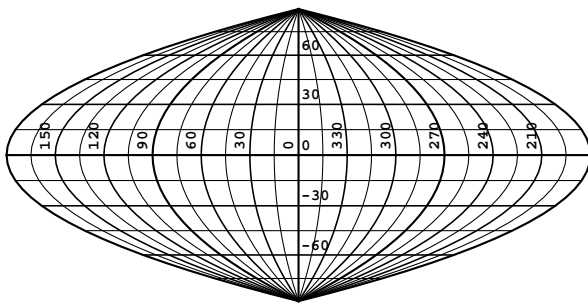


Fig. 21. Parabolic projection (PAR); no limits.

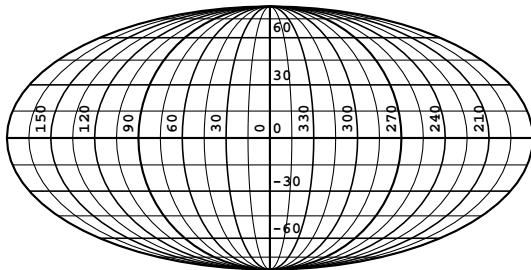


Fig. 22. Mollweide's projection (MOL); no limits.

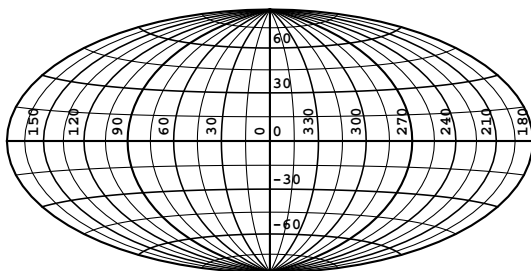


Fig. 23. Hammer-Aitoff projection (AIT); no limits.

where γ is defined as the solution of the transcendental equation

$$\sin \theta = \frac{\gamma}{90^\circ} + \frac{\sin 2\gamma}{\pi} \quad (100)$$

The inverse equations may be written directly without reference to γ ,

$$\phi = \pi x / \left(2 \sqrt{2 - \left(\frac{\pi}{180^\circ} y \right)^2} \right), \quad (101)$$

$$\theta = \sin^{-1} \left(\frac{1}{90^\circ} \sin^{-1} \left(\frac{\pi}{180^\circ} \frac{y}{\sqrt{2}} \right) + \frac{y}{180^\circ} \sqrt{2 - \left(\frac{\pi}{180^\circ} y \right)^2} \right). \quad (102)$$

Mollweide's projection is illustrated in Fig. 22.

5.3.4. AIT: Hammer-Aitoff

The Hammer-Aitoff¹⁸ projection illustrated in Fig. 23 is developed from the equatorial case of the zenithal equal area projection by doubling the equatorial scale and longitude coverage. The whole sphere is mapped thereby while preserving the equal area property. Note, however, that the equator is not evenly divided.

This projection reduces distortion in the polar regions compared to pseudocylindricals by making the meridians and parallels more nearly orthogonal. Together with its equal area property this makes it one of most commonly used all-sky projections.

The formulæ for the projection and its inverse are derived in Greisen (1986) and Calabretta (1992) among others. They are

$$x = 2\gamma \cos \theta \sin \frac{\phi}{2}, \quad (103)$$

$$y = \gamma \sin \theta, \quad (104)$$

where

$$\gamma = \frac{180^\circ}{\pi} \sqrt{\frac{2}{1 + \cos \theta \cos(\phi/2)}}. \quad (105)$$

The reverse equations are

$$\phi = 2 \arg \left(2Z^2 - 1, \frac{\pi}{180^\circ} \frac{Z}{2} x \right), \quad (106)$$

$$\theta = \sin^{-1} \left(\frac{\pi}{180^\circ} y Z \right), \quad (107)$$

where

$$Z = \sqrt{1 - \left(\frac{\pi}{180^\circ} \frac{x}{4} \right)^2 - \left(\frac{\pi}{180^\circ} \frac{y}{2} \right)^2}, \quad (108)$$

$$= \sqrt{\frac{1}{2} \left(1 + \cos \theta \cos \frac{\phi}{2} \right)}. \quad (109)$$

Note that $\frac{1}{2} \leq Z^2 \leq 1$. Refer to Sect. 6.1.4 for a discussion of the usage of AIT in AIPS.

¹⁸ David Aitoff (1854–1933) developed his projection from the zenithal equidistant projection in 1889 and in 1892 Ernst Hammer (1858–1925) applied his idea more usefully to the zenithal equal area projection. See Jones (1993).

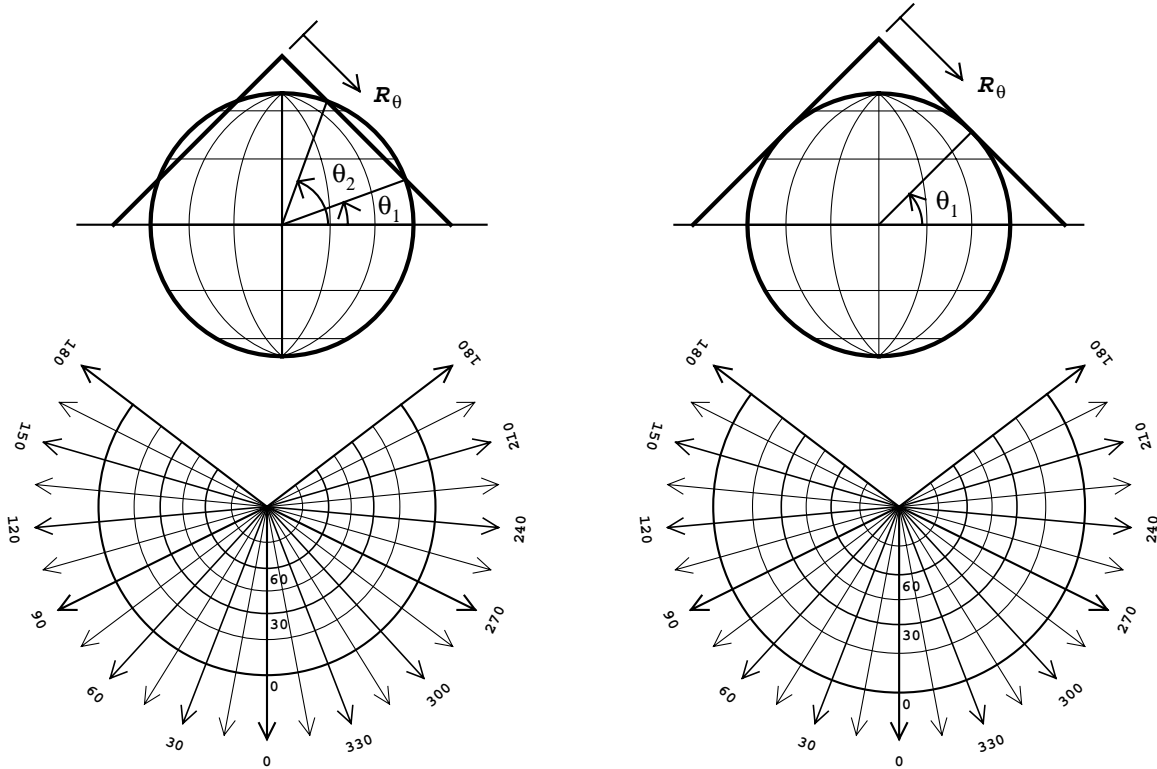


Fig. 24. Construction of conic perspective projections (COP) and the resulting graticules; (left) two-standard projection with $\theta_1 = 20^\circ$, $\theta_2 = 70^\circ$; (right) one-standard projection with $\theta_1 = \theta_2 = 45^\circ$. Both projections have $\theta_a = 45^\circ$ and this accounts for their similarity. Both diverge at $\theta = \theta_a \pm 90^\circ$.

5.4. Conic projections

In conic projections the sphere is thought to be projected onto the surface of a cone which is then opened out. The native coordinate system is chosen so that the poles are coincident with the axis of the cone. Native meridians are then projected as uniformly spaced rays that intersect at a point (either directly or by extrapolation), and parallels are projected as equiangular arcs of concentric circles.

Two-standard conic projections are characterized by two latitudes, θ_1 and θ_2 , whose parallels are projected at their true length. In the conic perspective projection these are the latitudes at which the cone intersects the sphere. *One-standard* conic projections have $\theta_1 = \theta_2$ and the cone is tangent to the sphere as shown in Fig. 24. Since conics are designed to minimize distortion in the regions between the two standard parallels they are constructed so that the point on the prime meridian mid-way between the two standard parallels maps to the reference point so we set

$$(\phi_0, \theta_0)_{\text{conic}} = (0, \theta_a), \quad (110)$$

where

$$\theta_a = (\theta_1 + \theta_2)/2. \quad (111)$$

Being concentric, the parallels may be described by R_θ , the radius for latitude θ , and A_ϕ , the angle for longitude ϕ . An offset in y is also required to force $(x, y) = (0, 0)$ at $(\phi, \theta) = (0, \theta_a)$. All one- and two-standard conics have

$$A_\phi = C\phi, \quad (112)$$

where C , a constant known as the constant of the cone, is such that the apical angle of the projected cone is $360^\circ C$. Since the standard parallels are projected as concentric arcs at their true length we have

$$C = \frac{180^\circ \cos \theta_1}{\pi R_{\theta_1}} = \frac{180^\circ \cos \theta_2}{\pi R_{\theta_2}}. \quad (113)$$

Cartesian coordinates in the plane of projection are

$$x = R_\theta \sin(C\phi), \quad (114)$$

$$y = -R_\theta \cos(C\phi) + Y_0, \quad (115)$$

and these may be inverted as

$$R_\theta = \text{sign } \theta_a \sqrt{x^2 + (Y_0 - y)^2}, \quad (116)$$

$$\phi = \arg\left(\frac{Y_0 - y}{R_\theta}, \frac{x}{R_\theta}\right)/C. \quad (117)$$

To complete the inversion the equation for θ as a function of R_θ is given for each projection. The equations given here correctly invert southern conics, i.e. those with $\theta_a < 0$. An example is shown in Fig. 25.

The conics will be parameterized in FITS by θ_a (given by Eq. (111)) and η where

$$\eta = |\theta_1 - \theta_2|/2. \quad (118)$$

The keywords `PVi_1a` and `PVi_2a` attached to *latitude* coordinate i will be used to specify θ_a and η respectively, both measured in degrees. `PVi_1a` has no default while `PVi_2a` defaults

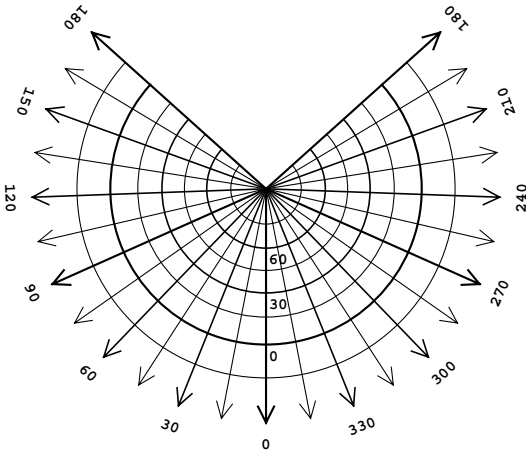


Fig. 27. Conic orthomorphic projection (COO) with $\theta_1 = 20^\circ$ and $\theta_2 = 70^\circ$; diverges at $\theta = -90^\circ$.

5.4.4. COO: Conic orthomorphic

The requirement for conformality of conic projections is

$$\frac{\partial R_\theta}{\partial \theta} = \frac{-\pi R_\theta}{180^\circ \cos \theta} C. \quad (138)$$

Solution of this differential equation gives rise to the formulæ for Lambert's conic orthomorphic projection:

$$C = \frac{\ln \left(\frac{\cos \theta_2}{\cos \theta_1} \right)}{\ln \left[\frac{\tan \left(\frac{90^\circ - \theta_2}{2} \right)}{\tan \left(\frac{90^\circ - \theta_1}{2} \right)} \right]}, \quad (139)$$

$$R_\theta = \psi \left[\tan \left(\frac{90^\circ - \theta}{2} \right) \right]^C, \quad (140)$$

$$Y_0 = \psi \left[\tan \left(\frac{90^\circ - \theta_a}{2} \right) \right]^C, \quad (141)$$

where

$$\psi = \frac{180^\circ}{\pi} \frac{\cos \theta_1}{C \left[\tan \left(\frac{90^\circ - \theta_1}{2} \right) \right]^C}, \quad (142)$$

$$= \frac{180^\circ}{\pi} \frac{\cos \theta_2}{C \left[\tan \left(\frac{90^\circ - \theta_2}{2} \right) \right]^C}. \quad (143)$$

The inverse may be computed with

$$\theta = 90^\circ - 2 \tan^{-1} \left(\left[\frac{R_\theta}{\psi} \right]^{\frac{1}{C}} \right). \quad (144)$$

When $\theta_1 = \theta_2$ the expression for C may be replaced with $C = \sin \theta_1$. This projection is illustrated in Fig. 27.

5.5. Polyconic and pseudoconic projections

Polyconics are generalizations of the standard conic projections; the parallels of latitude are projected as circular arcs which may or may not be concentric, and meridians are curved rather than straight as in the standard conics. *Pseudoconics* are

a sub-class with concentric parallels. The two polyconics presented here have parallels projected at their true length and use the fact that for a cone tangent to the sphere at latitude θ_1 , as shown in Fig. 24, we have $R_{\theta_1} = \frac{180^\circ}{\pi} \cot \theta_1$. Since both are constructed with the native coordinate system origin at the reference point we set

$$(\phi_0, \theta_0)_{\text{polyconic}} = (0, 0). \quad (145)$$

5.5.1. BON: Bonne's equal area

In Bonne's pseudoconic projection¹⁹ all parallels are projected as concentric equidistant arcs of circles of true length and true spacing. This is sufficient to guarantee that it is an equal area projection. It is parameterized by the latitude θ_1 for which $R_{\theta_1} = \frac{180^\circ}{\pi} \cot \theta_1$. The projection is conformal at this latitude and along the central meridian. The equations for Bonne's projection become divergent for $\theta_1 = 0$ and this special case is handled as the Sanson-Flamsteed projection. The projection formulæ are

$$x = R_\theta \sin A_\phi, \quad (146)$$

$$y = -R_\theta \cos A_\phi + Y_0, \quad (147)$$

where

$$A_\phi = \frac{180^\circ}{\pi R_\theta} \phi \cos \theta, \quad (148)$$

$$R_\theta = Y_0 - \theta, \quad (149)$$

$$Y_0 = \frac{180^\circ}{\pi} \cot \theta_1 + \theta_1. \quad (150)$$

The inverse formulæ are then

$$\theta = Y_0 - R_\theta, \quad (151)$$

$$\phi = \frac{\pi}{180^\circ} A_\phi R_\theta / \cos \theta, \quad (152)$$

where

$$R_\theta = \text{sign } \theta_1 \sqrt{x^2 + (Y_0 - y)^2}, \quad (153)$$

$$A_\phi = \arg \left(\frac{Y_0 - y}{R_\theta}, \frac{x}{R_\theta} \right). \quad (154)$$

This projection is illustrated in Fig. 28. The keyword `PVi_1a` attached to *latitude* coordinate *i* will be used to give θ_1 in degrees with no default value.

5.5.2. PC0: Polyconic

Each parallel in Hassler's polyconic projection is projected as an arc of a circle of radius $\frac{180^\circ}{\pi} \cot \theta$ at its true length, $360^\circ \cos \theta$, and correctly divided. The scale along the central

¹⁹ The ancestry of this important projection may be traced back to Ptolemy. Attribution for its invention is uncertain but it was certainly used before the birth of Rigobert Bonne (1727–1795) who did much to popularize it.

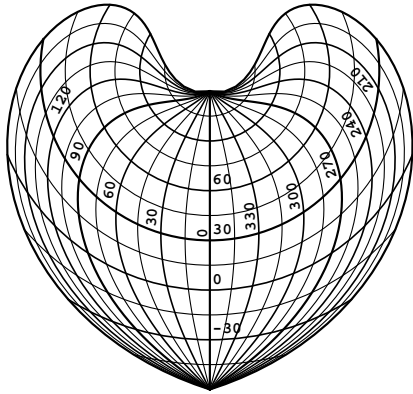


Fig. 28. Bonne's projection (BON) with $\theta_1 = 45^\circ$; no limits.

meridian is true and consequently the parallels are not concentric. The projection formulæ are

$$x = \frac{180^\circ}{\pi} \cot \theta \sin(\phi \sin \theta), \quad (155)$$

$$y = \theta + \frac{180^\circ}{\pi} \cot \theta [1 - \cos(\phi \sin \theta)]. \quad (156)$$

Inversion requires iterative solution for θ of the equation

$$x^2 - \frac{360^\circ}{\pi} (y - \theta) \cot \theta + (y - \theta)^2 = 0. \quad (157)$$

Once θ is known ϕ is given by

$$\phi = \frac{1}{\sin \theta} \arg \left(\frac{180^\circ}{\pi} - (y - \theta) \tan \theta, x \tan \theta \right). \quad (158)$$

The polyconic projection is illustrated in Fig. 29.

5.6. Quad-cube projections

Quadrilateralized spherical cube (quad-cube) projections belong to the class of polyhedral projections²⁰ in which the sphere is projected onto the surface of an enclosing polyhedron, typically one of the five Platonic polyhedra: the tetrahedron, hexahedron (cube), octahedron, dodecahedron, and icosahedron.

The starting point for polyhedral projections is the gnomonic projection of the sphere onto the faces of an enclosing polyhedron. This may then be modified to make the projection equal area or impart other special properties. However, minimal distortion claims often made for polyhedral projections should be balanced against the many interruptions of the flattened polyhedron; the breaks should be counted as extreme distortions. Their importance in astronomy is not so much in visual representation but in solving the problem of distributing N points as uniformly as possible over the sphere. This may be of particular importance in optimizing computationally intensive applications. The general problem may be tackled by

²⁰ Polyhedral projections date from renaissance times when the artist and mathematician Albrecht Dürer (1471–1528) described, although did not implement, the tetrahedral, dodecahedral, and icosahedral cases. Snyder (1993) traces subsequent development into the twentieth century, including one by R. Buckminster Fuller onto the non-Platonic “cuboctahedron” with constant scale along each edge.

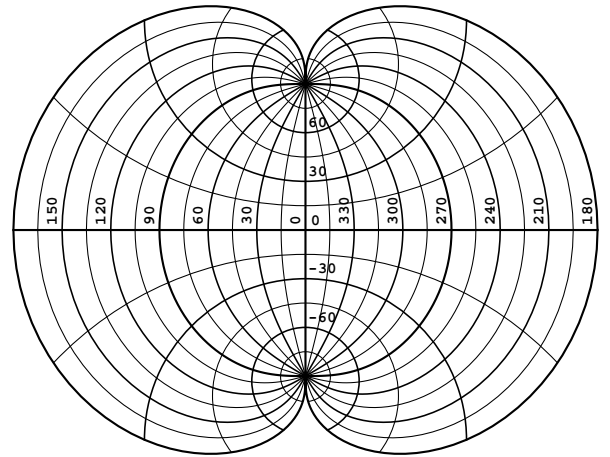


Fig. 29. Polyconic projection (PCO); no limits.

pixelizations such as HEALPix (Hierarchical Equal Area iso-Latitude PIXelization, Górski & Hivon 1999), which define a distribution of points on the sphere but do not relate these to points in a plane of projection and are therefore outside the scope of this paper.

The quad-cubes have been used extensively in the COBE project and are described by Chan & O'Neill (1975) and O'Neill & Laubscher (1976). The icosahedral case has also been studied by Tegmark (1996). It is close to optimal, providing a 10% improvement over the cubic case. However, we have not included it here since it relies on image pixels being organized in an hexagonal close-packed arrangement rather than the simple rectangular arrangement supported by FITS.

The six faces of quad-cube projections are numbered and laid out as

$$\begin{array}{c} 0 \\ 4 \ 3 \ 2 \ 1 \ 4 \ 3 \ 2 \\ 5 \end{array}$$

where faces 2, 3 and 4 may appear on one side or the other (or both). The layout used depends only on the FITS writer's choice of ϕ_c in Table 4. It is also permissible to split faces between sides, for example to put half of face 3 to the left and half to the right to create a symmetric layout. FITS readers should have no difficulty determining the layout since the origin of (x, y) coordinates is at the center of face 1 and each face is 90° on a side. The range of x therefore determines the layout. Other arrangements are possible and Snyder (1993) illustrates the “saw-tooth” layout of Reichard's 1803 map of the Earth. While these could conceivably have benefit in celestial mapping we judged the additional complication of representing them in FITS to be unwarranted. The layout used in the COBE project itself has faces 2, 3, and 4 to the left.

The native coordinate system has its pole at the center of face 0 and origin at the center of face 1 (see Fig. 30) which is the reference point whence

$$(\phi_0, \theta_0)_{\text{quad-cube}} = (0, 0). \quad (159)$$

Table 4. Assignment of parametric variables and central longitude and latitude by face number for quadrilateralized spherical cube projections.

| Face | ξ | η | ζ | ϕ_c | θ_c |
|------|-------|--------|---------|-----------------------------|-------------|
| 0 | m | $-l$ | n | 0° | 90° |
| 1 | m | n | l | 0° | 0° |
| 2 | $-l$ | n | m | -270° or 90° | 0° |
| 3 | $-m$ | n | $-l$ | -180° or 180° | 0° |
| 4 | l | n | $-m$ | -90° or 270° | 0° |
| 5 | m | l | $-n$ | 0° | -90° |

The face number may be determined from the native longitude and latitude by computing the direction cosines:

$$\begin{aligned}
l &= \cos \theta \cos \phi, \\
m &= \cos \theta \sin \phi, \\
n &= \sin \theta.
\end{aligned} \tag{160}$$

The face number is that which maximizes the value of ζ in Table 4. That is, if ζ is the largest of n , l , m , $-l$, $-m$, and $-n$, then the face number is 0 through 5, respectively. Each face may then be given a Cartesian coordinate system, (ξ, η) , with origin in the center of each face as per Table 4. The formulæ for quad-cubes are often couched in terms of the variables

$$\chi = \xi/\zeta, \tag{161}$$

$$\psi = \eta/\zeta. \tag{162}$$

Being composed of six square faces the quad-cubes admit the possibility of efficient data storage in FITS. By stacking them on the third axis of a three-dimensional data structure the storage required for an all-sky map may be halved. This axis will be denoted by a CTYPE*ia* value of CUBEFACE. In this case the value of (x, y) computed via Eq. (1) for the center of each face must be $(0, 0)$ and the FITS interpreter must increment this by (ϕ_c, θ_c) using its choice of layout. Since the CUBEFACE axis type is purely a storage mechanism the linear transformation of Eq. (1) must preserve the CUBEFACE axis pixel coordinates.

5.6.1. TSC: Tangential spherical cube

While perspective quad-cube projections could be developed by projecting a sphere onto an enclosing cube from any point of projection, inside or outside the sphere, it is clear that only by projecting from the center of the sphere will every face be treated equally. Thus the tangential spherical cube projection (TSC) consists of six faces each of which is a gnomonic projection of a portion of the sphere. As discussed in Sect. 5.1.1, gnomonic projections map great circles as straight lines but unfortunately diverge very rapidly away from the poles and can only represent a portion of the sphere without extreme distortion. The TSC projection partly alleviates this by projecting great circles as piecewise straight lines. To compute the forward projection first determine χ and ψ as described above, then

$$x = \phi_c + 45^\circ \chi, \tag{163}$$

$$y = \theta_c + 45^\circ \psi. \tag{164}$$

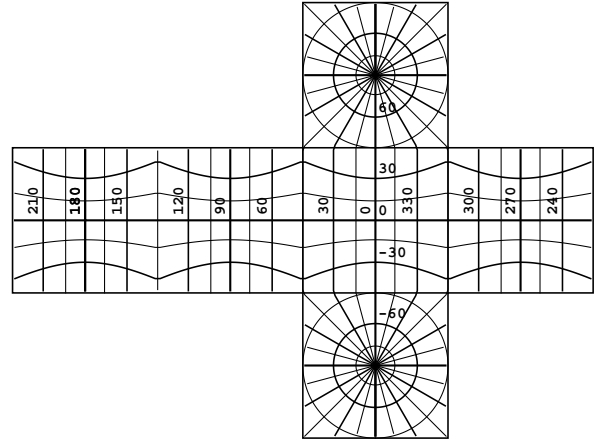


Fig. 30. Tangential spherical cube projection (TSC); no limits.

To invert these first determine to which face the (x, y) coordinates refer, then compute

$$\chi = (x - \phi_c)/45^\circ, \tag{165}$$

$$\psi = (y - \theta_c)/45^\circ, \tag{166}$$

then

$$\zeta = 1 / \sqrt{1 + \chi^2 + \psi^2}. \tag{167}$$

Once ζ is known ξ and η are obtained via

$$\xi = \chi \zeta, \tag{168}$$

$$\eta = \psi \zeta. \tag{169}$$

The direction cosines (l, m, n) may be identified with (ξ, η, ζ) with the aid of Table 4, whence (ϕ, θ) may readily be computed. The projection is illustrated in Fig. 30 for the full sphere.

5.6.2. CSC: COBE quadrilateralized spherical cube

The COBE quadrilateralized spherical cube projection illustrated in Fig. 31 modifies the tangential spherical cube projection in such a way as to make it approximately equal area. The forward equations are

$$x = \phi_c + 45^\circ F(\chi, \psi), \tag{170}$$

$$y = \theta_c + 45^\circ F(\psi, \chi), \tag{171}$$

where the function F is given by

$$\begin{aligned}
F(\chi, \psi) &= \chi \gamma^* + \chi^3 (1 - \gamma^*) \\
&\quad + \chi \psi^2 (1 - \chi^2) \left[\Gamma + (M - \Gamma) \chi^2 \right. \\
&\quad \left. + (1 - \psi^2) \sum_{i=0}^{\infty} \sum_{j=0}^{\infty} C_{ij} \chi^{2i} \psi^{2j} \right] \\
&\quad + \chi^3 (1 - \chi^2) \left[\Omega_1 - (1 - \chi^2) \sum_{i=0}^{\infty} D_i \chi^{2i} \right].
\end{aligned} \tag{172}$$

C_{ij} and D_i are derived from c_{ij}^* and d_i^* as given by Chan & O'Neill (1975). The other parameters are given by exact formulæ developed by O'Neill & Laubscher (1976), who provide

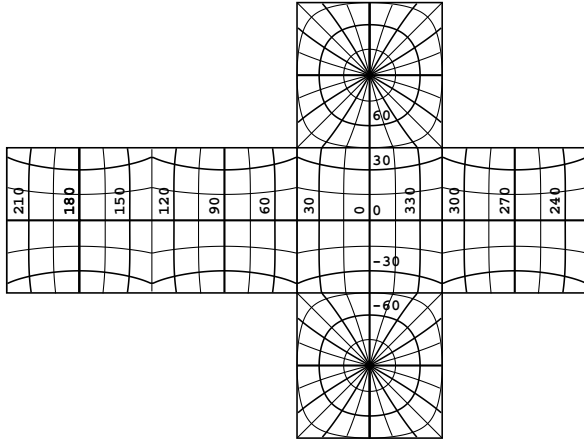


Fig. 31. COBE quadrilateralized spherical cube projection (CSC); no limits.

the numeric values of their parameters in tables and software listings. Both disagree with their formulæ, but the software listings do contain the actual numeric parameters still in use for the COBE Project (Immanuel Freedman, private communication, 1993). They are

$$\begin{aligned}
 \gamma^* &= 1.37484847732 \\
 M &= 0.004869491981 \\
 \Gamma &= -0.13161671474 \\
 \Omega_1 &= -0.159596235474 \\
 C_{00} &= 0.141189631152 \\
 C_{10} &= 0.0809701286525 \\
 C_{01} &= -0.281528535557 \\
 C_{20} &= -0.178251207466 \\
 C_{11} &= 0.15384112876 \\
 C_{02} &= 0.106959469314 \\
 D_0 &= 0.0759196200467 \\
 D_1 &= -0.0217762490699
 \end{aligned}$$

Chan & O'Neill (1975) actually defined the projection via the inverse equations. Their formulation may be rewritten in a more convenient form which is now the current usage in the COBE Project (Immanuel Freedman, private communication, 1993):

$$\chi = f(x - \phi_c, y - \theta_c), \quad (173)$$

$$\psi = f(y - \theta_c, x - \phi_c), \quad (174)$$

where

$$f(x - \phi_c, y - \theta_c) = X + X \left(1 - X^2\right) \sum_{j=0}^N \sum_{i=0}^{N-j} P_{ij} X^{2i} Y^{2j}, \quad (175)$$

and

$$X = (x - \phi_c)/45^\circ,$$

$$Y = (y - \theta_c)/45^\circ.$$

For COBE, $N = 6$ and the best-fit parameters have been taken to be

$$\begin{aligned}
 P_{00} &= -0.27292696 & P_{04} &= 0.93412077 \\
 P_{10} &= -0.07629969 & P_{50} &= 0.25795794 \\
 P_{01} &= -0.02819452 & P_{41} &= 1.71547508 \\
 P_{20} &= -0.22797056 & P_{32} &= 0.98938102 \\
 P_{11} &= -0.01471565 & P_{23} &= -0.93678576 \\
 P_{02} &= 0.27058160 & P_{14} &= -1.41601920 \\
 P_{30} &= 0.54852384 & P_{05} &= -0.63915306 \\
 P_{21} &= 0.48051509 & P_{60} &= 0.02584375 \\
 P_{12} &= -0.56800938 & P_{51} &= -0.53022337 \\
 P_{03} &= -0.60441560 & P_{42} &= -0.83180469 \\
 P_{40} &= -0.62930065 & P_{33} &= 0.08693841 \\
 P_{31} &= -1.74114454 & P_{24} &= 0.33887446 \\
 P_{22} &= 0.30803317 & P_{15} &= 0.52032238 \\
 P_{13} &= 1.50880086 & P_{06} &= 0.14381585.
 \end{aligned}$$

Given the face number, χ , and ψ , the native coordinates (ϕ, θ) may be computed as for the tangential spherical cube projection.

Equations (172) and (175), the forward and reverse projection equations used by COBE, are not exact inverses. Each set could of course be inverted to any required degree of precision via iterative methods (in that case Eq. (175) should be taken to define the projection). However, the aim here is to describe the projection in use within the COBE project. One may evaluate the closure error in transforming $(x - \phi_c, y - \theta_c)$ to (χ, ψ) with Eq. (175) and then transforming back to $(x - \phi_c, y - \theta_c)$ with Eq. (172), i.e.

$$\begin{aligned}
 E_{ij}^2 &= \left(F(f(x_i, y_j), f(y_j, x_i)) - x_i \right)^2 \\
 &\quad + \left(F(f(y_j, x_i), f(x_i, y_j)) - y_j \right)^2.
 \end{aligned}$$

The COBE parameterization produces an average error of 4.7 arcsec over the full field. The root mean square and peak errors are 6.6 and 24 arcsec, respectively. In the central parts of the image $(|X|, |Y| \leq 0.8)$, the average and root mean square errors are 5.9 and 8.0 arcsec, larger than for the full field.

Measures of equal-area conformance obtained for Eq. (175) show that the rms deviation is 1.06% over the full face and 0.6% over the inner 64% of the area of each face. The maximum deviation is +13.7% and -4.1% at the edges of the face and only $\pm 1.3\%$ within the inner 64% of the face.

5.6.3. QSC: Quadrilateralized spherical cube

O'Neill & Laubscher (1976) derived an exact expression for an equal-area transformation from a sphere to the six faces of a cube. At that time, their formulation was thought to be computationally intractable, but today, with modern computers and telescopes of higher angular resolution than COBE, their formulation has come into use. Fred Patt (1993, private communication) has provided us with the inverse of the O'Neill & Laubscher formula and their expression in Cartesian coordinates.

O'Neill & Laubscher's derivation applies only in the quadrant $-45^\circ \leq \phi \leq 45^\circ$ and must be reflected into the other

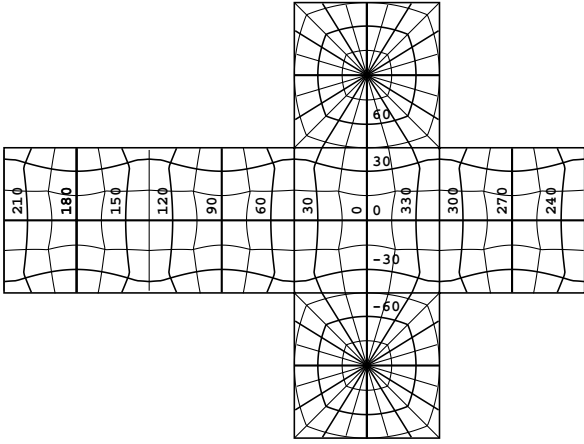


Fig. 32. Quadrilateralized spherical cube projection (QSC); no limits.

quadrants. This has the effect of making the projection non-differentiable along the diagonals as is evident in Fig. 32. To compute the forward projection first identify the face and find (ξ, η, ζ) and (ϕ_c, θ_c) from Table 4. Then

$$(x, y) = (\phi_c, \theta_c) + \begin{cases} (u, v) & \text{if } |\xi| > |\eta| \\ (v, u) & \text{otherwise} \end{cases}, \quad (176)$$

where

$$u = 45^\circ S \sqrt{\frac{1 - \zeta}{1 - 1/\sqrt{2 + \omega^2}}}, \quad (177)$$

$$v = \frac{u}{15^\circ} \left[\tan^{-1}(\omega) - \sin^{-1}\left(\frac{\omega}{\sqrt{2(1 + \omega^2)}}\right) \right], \quad (178)$$

$$\omega = \begin{cases} \eta/\xi & \text{if } |\xi| > |\eta| \\ \xi/\eta & \text{otherwise} \end{cases},$$

$$S = \begin{cases} +1 & \text{if } \xi > |\eta| \text{ or } \eta > |\xi| \\ -1 & \text{otherwise} \end{cases}.$$

To compute the inverse first identify the face from the (x, y) coordinates, then determine (u, v) via

$$(u, v) = \begin{cases} (x - \phi_c, y - \theta_c) & \text{if } |x - \phi_c| > |y - \theta_c| \\ (y - \theta_c, x - \phi_c) & \text{otherwise} \end{cases}. \quad (179)$$

Then

$$\zeta = 1 - \left(\frac{u}{45^\circ}\right)^2 \left(1 - \frac{1}{\sqrt{2 + \omega^2}}\right), \quad (180)$$

where

$$\omega = \frac{\sin(15^\circ v/u)}{\cos(15^\circ v/u) - 1/\sqrt{2}}. \quad (181)$$

If $|x - \phi_c| > |y - \theta_c|$ then

$$\xi = \sqrt{\frac{1 - \zeta^2}{1 + \omega^2}}, \quad (182)$$

$$\eta = \xi\omega, \quad (183)$$

otherwise

$$\eta = \sqrt{\frac{1 - \zeta^2}{1 + \omega^2}}, \quad (184)$$

$$\xi = \eta\omega. \quad (185)$$

Given the face number and (ξ, η, ζ) , the native coordinates (ϕ, θ) may be computed with reference to Table 4 as for the tangential spherical cube projection.

6. Support for the AIPS convention

A large number of FITS images have been written using the AIPS coordinate convention and a substantial body of software exists to interpret it. Consequently, the AIPS convention has acquired the status of a de facto standard and FITS interpreters will need to support it indefinitely in order to obey the maxim “once FITS always FITS”. Translations between the old and new system are therefore required.

6.1. Interpreting old headers

In the AIPS convention, CROTA i assigned to the latitude axis was used to define a bulk rotation of the image plane. Since this rotation was applied *after* CDELTA i the translation to the current formalism follows from

$$\begin{pmatrix} \text{CDELTA1} & 0 \\ 0 & \text{CDELTA2} \end{pmatrix} \begin{pmatrix} \text{PC1}_1 \text{PC1}_2 \\ \text{PC2}_1 \text{PC2}_2 \end{pmatrix} = \begin{pmatrix} \cos \rho - \sin \rho & 0 \\ \sin \rho & \cos \rho \end{pmatrix} \begin{pmatrix} \text{CDELTA1} & 0 \\ 0 & \text{CDELTA2} \end{pmatrix}, \quad (186)$$

where we have used subscript 1 for the longitude axis, 2 for latitude, and written ρ for the value of CROTA2. Equation (186), which includes the added constraint of preserving CDELTA i in the translation, is readily solved for the elements of the PC i - ja matrix

$$\begin{pmatrix} \text{PC1}_1 \text{PC1}_2 \\ \text{PC2}_1 \text{PC2}_2 \end{pmatrix} = \begin{pmatrix} \cos \rho - \lambda \sin \rho \\ \frac{1}{\lambda} \sin \rho & \cos \rho \end{pmatrix}, \quad (187)$$

where

$$\lambda = \text{CDELTA2}/\text{CDELTA1}. \quad (188)$$

Note that Eq. (187) defines a rotation if and only if $\lambda = \pm 1$, which is often the case. In fact, the operations of scaling and rotation are commutative if and only if the scaling is isotropic, i.e. $\lambda = +1$; for $\lambda = -1$ the direction of the rotation is reversed. However, whatever the value of λ , the interpretation of Eq. (186) as that of a scale followed by a rotation is preserved.

The translation for CD i - ja is simpler, effectively because the CDELTA i have an implied value of unity and the constraint on preserving them in the translation is dropped:

$$\begin{pmatrix} \text{CD1}_1 \text{CD1}_2 \\ \text{CD2}_1 \text{CD2}_2 \end{pmatrix} = \begin{pmatrix} \text{CDELTA1} \cos \rho - \text{CDELTA2} \sin \rho \\ \text{CDELTA1} \sin \rho & \text{CDELTA2} \cos \rho \end{pmatrix}. \quad (189)$$

The expressions in Hanisch & Wells (1988) and Geldzahler & Schlesinger (1997) yield the same results as Eq. (189) for the usual left-handed sky coordinates and right-handed pixel coordinates, but can lead to an incorrect interpretation (namely, possible sign errors for the off-diagonal elements) for other configurations of the coordinate systems. The Hanisch & Wells draft and the coordinate portions of Geldzahler & Schlesinger are superseded by this paper.

6.1.1. SIN

The SIN projection defined by Greisen (1983) is here generalized by the addition of projection parameters. However, these parameters assume default values which reduce to the simple orthographic projection of the AIPS convention. Therefore no translation is required.

6.1.2. NCP

The “north-celestial-pole” projection defined by Greisen (1983) is a special case of the new generalized SIN projection. The old header cards

```
CTYPE1 = 'RA---NCP',
CTYPE2 = 'DEC--NCP',
```

should be translated to the current formalism as

```
CTYPE1 = 'RA---SIN',
CTYPE2 = 'DEC--SIN',
PV2_1 = 0,
PV2_2 = cot δ0.
```

6.1.3. TAN, ARC and STG

The TAN, ARC and STG projections defined by Greisen (1983, 1986) are directly equivalent to those defined here and no translation is required.

6.1.4. AIT, GLS and MER

Special care is required in interpreting the AIT (Hammer-Aitoff), GLS (Sansón-Flamsteed), and MER (Mercator) projections in the AIPS convention as defined by Greisen (1986). As explained in Sect. 7.1, the AIPS convention cannot represent oblique celestial coordinate graticules such as the one shown in Fig. 2. CRVAL*i* for these projections in AIPS does not correspond to the celestial coordinates (α_0, δ_0) of the reference point, as understood in this formalism, unless they are both zero in which case no translation is required.

A translation into the new formalism exists for non-zero CRVAL*i* but only if CROTA*i* is zero. It consists of setting CRVAL*i* to zero and adjusting CRPIX*j* and CDELTA*i* accordingly in the AIPS header whereupon the above situation is obtained. The corrections to CRPIX*j* are obtained by computing the pixel coordinates of (α, δ) = (0, 0) within the AIPS convention. For AIT and MER (but not GLS), CDELTA*i* must also be corrected for the scaling factors f_α and f_δ incorporated into the AIPS projection equations.

Of the three projections only GLS is known to have been used with non-zero CRVAL*i*. Consequently we have renamed it as SFL as a warning that translation is required.

6.2. Supporting old interpreters

As mentioned in Sect. 6, FITS interpreters will need to recognize the AIPS convention virtually forever. It stands to reason,

therefore, that if modern FITS-writers wish to assist older FITS interpreters they may continue to write older style headers, assuming of course that it is possible to express the coordinate system in the AIPS convention.

Modern FITS-writers must not attempt to help older interpreters by including CROTA*i* together with the new keyword values (assuming the combination of CDELTA*i* and PC*i-ja* matrix, or CD*i-ja* matrix, is amenable to such translation). We make this requirement primarily to minimize confusion.

Assuming that a header has been developed using the present formalism the following test may be applied to determine whether the combination of CDELTA*i* and PC*i-ja* matrix represents a scale followed by a rotation as in Eq. (186). Firstly write

$$\begin{pmatrix} CD1_1 & CD1_2 \\ CD2_1 & CD2_2 \end{pmatrix} = \begin{pmatrix} CDELTA1 & 0 \\ 0 & CDELTA2 \end{pmatrix} \begin{pmatrix} PC1_1 & PC1_2 \\ PC2_1 & PC2_2 \end{pmatrix}, \quad (190)$$

where 1 is the longitude coordinate and 2 the latitude coordinate, then evaluate ρ_a and ρ_b as

$$\rho_a = \begin{cases} \arg(CD1_1, CD2_1) & \text{if } CD2_1 > 0 \\ 0 & \text{if } CD2_1 = 0 \\ \arg(-CD1_1, -CD2_1) & \text{if } CD2_1 < 0 \end{cases},$$

$$\rho_b = \begin{cases} \arg(-CD2_2, CD1_2) & \text{if } CD1_2 > 0 \\ 0 & \text{if } CD1_2 = 0 \\ \arg(CD2_2, -CD1_2) & \text{if } CD1_2 < 0 \end{cases}. \quad (191)$$

If $\rho_a = \rho_b$ to within reasonable precision (Geldzahler & Schlesinger 1997), then compute

$$\rho = (\rho_a + \rho_b)/2 \quad (192)$$

as the best estimate of the rotation angle, the older keywords are

$$\begin{aligned} CDELTA1 &= CD1_1 / \cos \rho, \\ CDELTA2 &= CD2_2 / \cos \rho, \\ CROTA2 &= \rho. \end{aligned} \quad (193)$$

Note that the translated values of CDELTA*i* in Eqs. (193) may differ from the starting values in Eq. (190).

Solutions for CROTA2 come in pairs separated by 180°. The above formulæ give the solution which falls in the half-open interval [0, 180°). The other solution is obtained by subtracting 180° from CROTA2 and negating CDELTA1 and CDELTA2. While each solution is equally valid, if one makes CDELTA1 < 0 and CDELTA2 > 0 then it would normally be the one chosen.

Of course, the projection must be one of those supported by the AIPS convention, which only recognizes SIN, NCP, TAN, ARC, STG, AIT, GLS and MER. Of these, we strongly recommend that the AIPS version of AIT, GLS, and MER not be written because of the problems described in Sect. 6.1.4. It is interesting to note that a translation does exist for the slant orthographic (SIN) projection defined in Sect. 5.1.5 to the simple orthographic projection of AIPS. However, we advise against such translation because of the likelihood of creating confusion and so we do not define it here. The exception is where the SIN projection may be translated as NCP as defined in Sect. 6.1.2.

7. Discussion

7.1. Oblique projections

The term *oblique projection* is often used when a projection's native coordinate system does not coincide with the coordinate system of interest. Texts on terrestrial cartography often separately name and derive projection equations for particular oblique projections. Thus the Cassini, Transverse Mercator, and Bartholomew nordic projections are nothing more than the plate carrée, Mercator, and Mollweide projections in disguise.

The view of obliqueness as being a property of a projection arose mainly because of the computational difficulty of producing oblique graticules in the days before electronic computers. The particular aspects chosen were those for which geometrical construction was possible or for which the mathematical formulation had a simple form, and this tended to entrench particular oblique projections as separate entities. In addition, terrestrial longitude and latitude are so closely tied to the visual representation of the Earth's surface that it is shown predominantly in the usual north-south orientation. The only other natural terrestrial coordinate system is that defined by the magnetic pole but the difference between it and the geographic graticule is sufficiently small that it is usually treated as a local correction to the magnetic bearing. The special view of obliqueness was probably also reinforced by traditional methods of map making using sextant and chronometer, which were based on geographic longitude and latitude.

The situation in astronomical cartography is quite different. The celestial sphere has a variety of natural coordinate systems – equatorial, ecliptic, galactic, etc. – and oblique and non-oblique graticules are often plotted together on the same map. It wouldn't make sense to describe such a projection as being simultaneously oblique and non-oblique; clearly it is the particular coordinate *graticule* which may be oblique, not the projection. Visually, an area of the sky may be seen in different orientations depending on whether it's rising, transiting, or setting, or whether seen from the northern or southern hemisphere. Moreover, oblique graticules arise as a normal feature of observations in optical, infrared, radio, and other branches of astronomy, just as they do now in terrestrial mapping based on aerial and satellite photography. The center of the field of view, wherever it may happen to be, typically corresponds to the native pole of a zenithal projection. Thus the aim of this paper has been to provide a formalism whereby obliquity may be handled in a general way.

Figures 33 and 34 illustrate the same four oblique celestial graticules for the zenithal equal area, conic equidistant, Hammer-Aitoff, and COBE quadrilateralized spherical cube projections (at variable (x, y) scale). For the sake of intercomparison, these graticules are defined in terms of the celestial coordinates of the native pole, (α_p, δ_p) , together with ϕ_p by setting $(\phi_0, \theta_0) = (0, 90^\circ)$ as described in Sect. 2.5.

The first graticule, A, when compared to the non-oblique native coordinate graticules presented earlier for each projection, illustrates the effect of changing δ_p (and hence δ_0). Comparison of graticules A and B shows that changing α_p (and hence α_0) results in a simple change in origin of

longitude. Graticules A, C, and D show the more interesting effect of varying ϕ_p (conveyed by LONPOLE*a*). For the zenithal projections the result is indistinguishable from a bulk rotation of the image plane, but this is not the case for any other class of projection. This explains why the role of LONPOLE*a* was covered by CROTA*i* in the AIPS convention for the zenithal projections introduced by Greisen (1983), but why this does not work for any other class of projection.

7.2. Choice of projection

The projected meridians and parallels in Figs. 33 and 34 also serve to illustrate the distortions introduced by the various projections. In particular, the quad-cube projection, while doing a good job within each face, is very distorted over the sphere as a whole, especially where the faces join, so much so that it is difficult even to trace the path of some of the meridians and parallels. However, as indicated previously, this projection is designed for efficient numerical computation rather than visual representation of the sphere.

This leads us to the question of the choice of projection for a particular application. In some cases the projection is the natural result of the geometry of the observation and there is no choice. For example, maps produced by rotational synthesis radio telescopes are orthographic (SIN) projections with native pole at the phase center of the observation. Photographic plates produced by Schmidt telescopes are best described by the zenithal equidistant (ARC) projection, while the field of view of other optical telescopes is closer to a gnomonic (TAN) projection. On the other hand, the great circle scanning technique of the Sloan Digital Sky Survey produces a cylindrical projection. Similarly a map of the surface of the Moon as it appears from Earth requires a zenithal perspective (AZP) projection with $\mu \approx -220$. The same is true for spacecraft generated images of distant moons and planets. All-sky cameras should be well served by a ZPN projection with empirically determined parameters.

Sometimes observational data will be regridded onto a projection chosen for a particular purpose. Equal area projections are often used since they preserve surface density and allow integration, whether numerical or visual, to be performed with reasonable accuracy by summing pixel values. The Hammer-Aitoff (AIT) projection is probably the most widely used for all-sky maps. However, the Sanson-Flamsteed (SFL) may be preferred as being easier to take measurements from. The humble plate carrée (CAR) excels in this regard and may be considered adequate, say, for mapping a few degrees on either side of the galactic plane. In general terms, zenithal projections are good for mapping the region in the vicinity of a point, often a pole; cylindrical projections are good for the neighborhood of a great circle, usually an equator; and the conics are suitable for small circles such as parallels of latitude. A conic projection might be a good choice for mapping a hemisphere; distortion at most points is reduced compared to a zenithal projection although at the expense of the break between native longitudes $\pm 180^\circ$. However, in some cases this break might be considered an extreme distortion which outweighs other reductions in

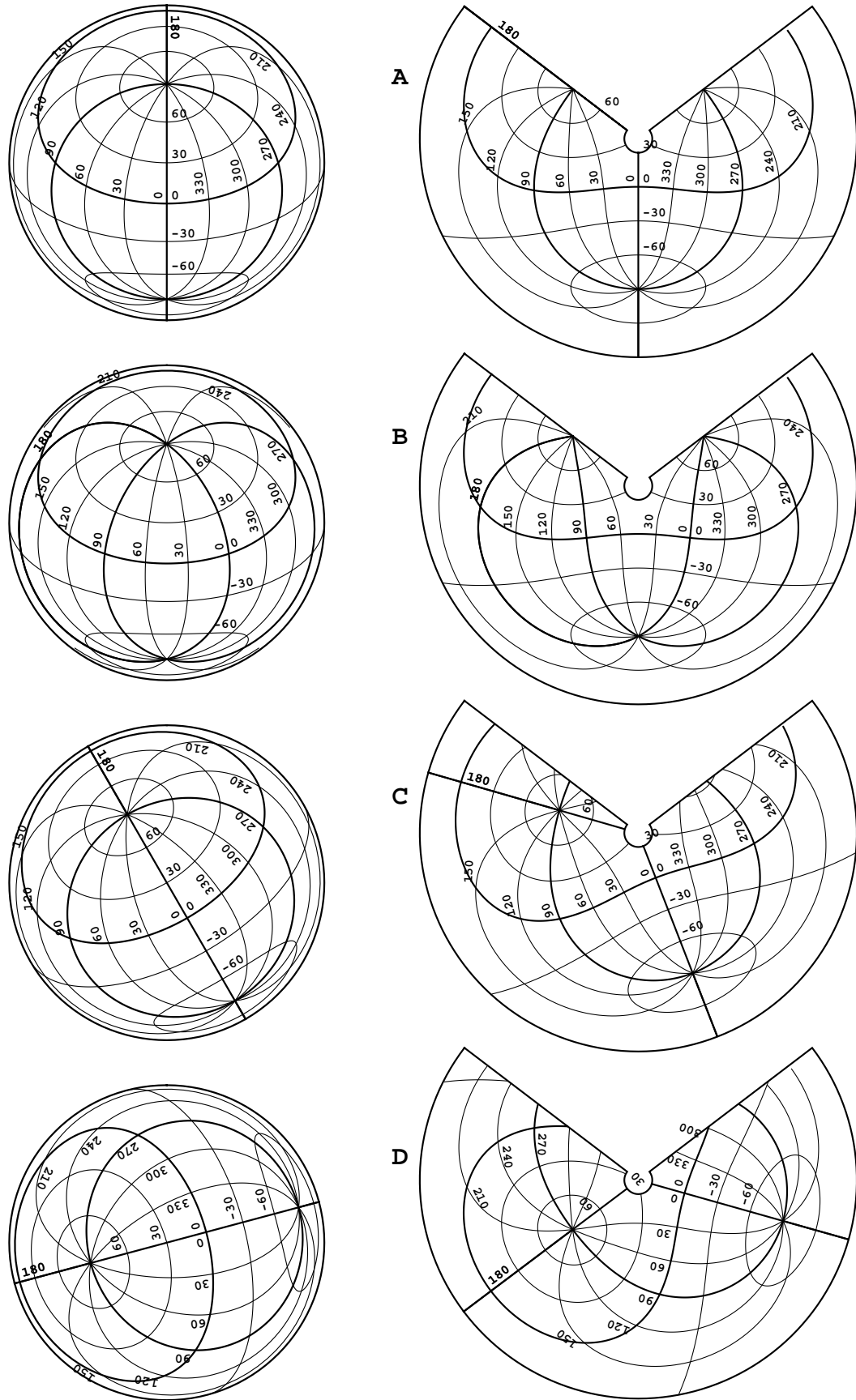


Fig. 33. Oblique (α, δ) graticules plotted for the zenithal equal area (ZEA) and conic equidistant (COD) projections with parameters (A) $\alpha_p = 0$, $\delta_p = 30^\circ$, $\phi_p = 180^\circ$; (B) $\alpha_p = 45^\circ$, $\delta_p = 30^\circ$, $\phi_p = 180^\circ$; (C) $\alpha_p = 0$, $\delta_p = 30^\circ$, $\phi_p = 150^\circ$; (D) $\alpha_p = 0$, $\delta_p = 30^\circ$, $\phi_p = 75^\circ$.

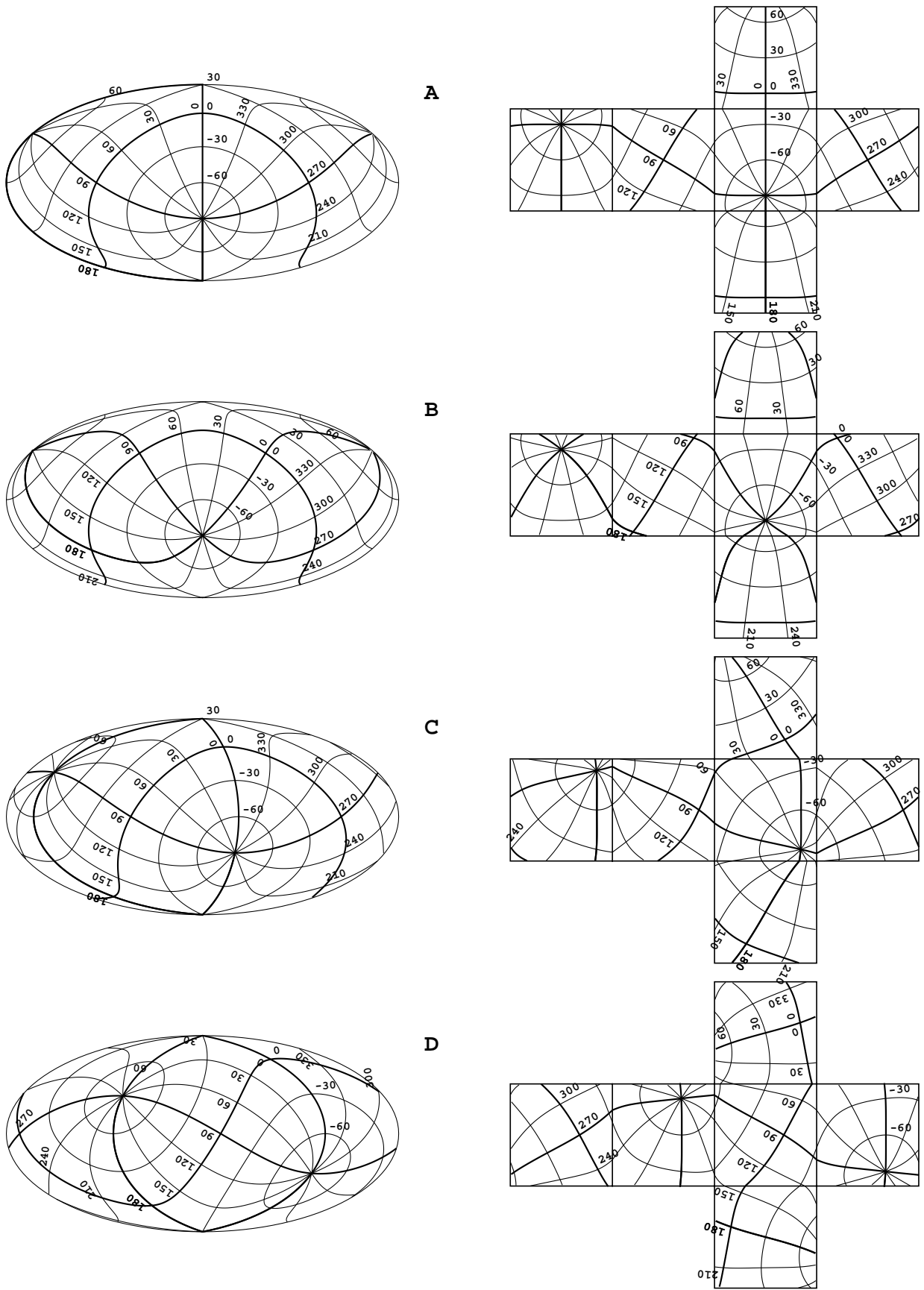


Fig. 34. Oblique (α, δ) graticules plotted for the Hammer-Aitoff (AIT) and COBE quadrilateralized spherical cube (CSC) projections using the same parameters as Fig. 33.

distortion and, depending on the application, may mandate the use of a zenithal projection. Cartographers typically favor conics and polyconics for “Australia-sized” regions of the sphere and at this they excel. Oblique forms of the zenithal equal-area projection are also commonly used. Celestial applications might include large scale maps of the Magellanic clouds. Tables 3.1 and 4.1 of Snyder (1993) summarize actual usage in a variety of 19th and 20th century atlases.

As mentioned in Sect. 5, some projections are not scaled true at the reference point. In most cases this is deliberate, usually because the projection is designed to minimize distortion over a wide area; the scale will be true at some other place on the projection, typically along a parallel of latitude. If the projection is required to have $(\alpha, \delta) \approx (\alpha_0, \delta_0) + (x, y)$ then a number of projections will serve provided also that ϕ_p takes its default value. The following are always scaled true at the reference point: SZP, TAN, SIN, STG, ARC, ZEA, CAR, MER, BON, PCO, SFL, and AIT. The following are scaled true at the reference point for the particular conditions indicated: AZP ($\gamma = 0$), ZPN ($P_0 = 0, P_1 = 1$), AIR ($\theta_b = 90^\circ$), CYP ($\lambda = 1$), CEA ($\lambda = 1$), COP ($\eta = 0$), COD ($\eta = 0$), COE ($\eta = 0$), and COO ($\eta = 0$). The following are never scaled true at the reference point: PAR (but is scaled true in x), MOL, TSC, CSC, and QSC; the latter three are equiscaled at the reference point.

Of course CDEL Tia may be used to control scaling of (x, y) with respect to (p_1, p_2) . Thus, for example, the plate carrée projection (CAR) also serves as the more general equirectangular projection.

7.3. Header interpretation examples

We now consider three examples chosen to illustrate how a FITS reader would interpret a celestial coordinate header.

Example 1 is a simple header whose interpretation is quite straightforward.

Example 2 is more complicated; it also serves to illustrate the WCS header cards for 1) image arrays in binary tables, and 2) pixel lists.

Example 3 highlights a subtle problem introduced into a header by the FITS writer and considers how this should be corrected. As such, it introduces the generally more difficult task of composing WCS headers, considered in greater detail in Sect. 7.4.

7.3.1. Header interpretation example 1

Consider as the first example the relatively simple optical image whose header is given in Table 5. The NAXIS and NAXIS j keywords indicate that we have a four-dimensional image consisting of 512 columns, 512 rows, 196 planes, and one polarization. The degenerate STOKES axis is used simply to convey a coordinate value which applies to every pixel in the image. The CRPIX j keywords tell us that the reference point is at pixel coordinate (256, 257, 1, 1). The PC i_ja keywords default to the unit matrix which indicates that no bulk rotation or shear is applied to the pixel coordinates. Intermediate world coordinates

may thus be computed from Eq. (1) as

$$\begin{pmatrix} x \\ y \\ z \\ s \end{pmatrix} = \begin{pmatrix} -0.003 & 0 & 0 & 0 \\ 0 & 0.003 & 0 & 0 \\ 0 & 0 & 7128.30 & 0 \\ 0 & 0 & 0 & 1 \end{pmatrix} \begin{pmatrix} p_1 - 256 \\ p_2 - 257 \\ p_3 - 1 \\ p_4 - 1 \end{pmatrix}.$$

Since VELOCITY and STOKES are linear axis types, the velocity and Stokes value of each point are found simply by adding the coordinate value at the reference point to the relative coordinate. Thus,

$$\text{Velocity} = 500000.0 + 7128.3 (p_3 - 1) \text{ m s}^{-1},$$

$$\text{Stokes} = 1 \text{ (I polarization)}.$$

The CTYPE1 and CTYPE2 keywords denote a TAN (gnomonic) projection for which (x, y) are projection plane coordinates for the zenithal perspective projection with the source of the projection at the center of the sphere. Thus the native longitude and latitude are given by

$$\begin{aligned} \phi &= \arg(-y, x), \\ \theta &= \tan^{-1} \left(\frac{180^\circ}{\pi} \frac{1}{\sqrt{x^2 + y^2}} \right), \end{aligned}$$

which, on substitution, become

$$\begin{aligned} \phi &= \arg(p_2 - 257, p_1 - 256) + 180^\circ, \\ \theta &= \tan^{-1} \left(\frac{19098.5932}{\sqrt{(p_1 - 256)^2 + (p_2 - 257)^2}} \right), \end{aligned}$$

where we have used Eqs. (15), (14), and (55).

The celestial coordinate system is equatorial since the CTYPE ia begin with RA and DEC and the RADESYS a and EQUINOX a cards denote that these are in the IAU 1984 system. Zenithal projections have $(\phi_0, \theta_0) = (0, 90^\circ)$ for which the CRVAL i give equatorial coordinates $\alpha_p = 45^\circ.83$ in right ascension and $\delta_p = 63^\circ.57$ in declination. The equatorial north pole has a longitude of 180° in the native coordinate system from the LONPOLE a keyword. LATPOLE a is never required for zenithal projections and was not given. Thus, Eqs. (6) for the right ascension and declination become

$$\begin{aligned} \sin \delta &= \sin \theta \sin(63^\circ.57) - \cos \theta \cos \phi \cos(63^\circ.57), \\ \cos \delta \sin(\alpha - 45^\circ.83) &= \cos \theta \sin \phi, \\ \cos \delta \cos(\alpha - 45^\circ.83) &= \sin \theta \cos(63^\circ.57) \\ &\quad + \cos \theta \cos \phi \sin(63^\circ.57). \end{aligned}$$

Sample calculations for points on the diagonal near the three corners of the image are shown in Table 6.

If we define the projection non-linearity as the departure of θ from $r = \sqrt{x^2 + y^2}$, then in this 1.5×1.5 image it amounts to ~ 0.5 at the corners. However, in a $6^\circ \times 6^\circ$ image it quickly escalates to ~ 0.5 , sixty times larger. Comparison of α for the southeast and northeast corners indicates the significant effect of grid convergence even in this moderate sized image. The two differ by $22^\circ.16$, most of which is attributable to the $\cos \delta$ term in converting longitude offsets to true angular distances. The effect of grid convergence is small for (α_0, δ_0) near the equator and large near the poles.

Table 5. FITS header for example 1.

| 123456789 | 123456789 | 123456789 | 123456789 | 123456789 | 123456789 | 123456789 | 123456789 |
|-----------|-----------|------------|-----------|-----------------------|--------------------------------------|-----------|-----------|
| NAXIS | = | | 4 | / | 4-dimensional cube | | |
| NAXIS1 | = | | 512 | / | x axis (fastest) | | |
| NAXIS2 | = | | 512 | / | y axis (2nd fastest) | | |
| NAXIS3 | = | | 196 | / | z axis (planes) | | |
| NAXIS4 | = | | 1 | / | Dummy to give a coordinate | | |
| CRPIX1 | = | | 256 | / | Pixel coordinate of reference point | | |
| CDELTA1 | = | -0.003 | / | 10.8 arcsec per pixel | | | |
| CTYPE1 | = | 'RA---TAN' | | / | Gnomonic projection | | |
| CRVAL1 | = | | 45.83 | / | RA at reference point | | |
| CUNIT1 | = | 'deg' | | / | Angles are degrees always | | |
| CRPIX2 | = | | 257 | / | Pixel coordinate of reference point | | |
| CDELTA2 | = | | 0.003 | / | 10.8 arcsec per pixel | | |
| CTYPE2 | = | 'DEC--TAN' | | / | Gnomonic projection | | |
| CRVAL2 | = | | 63.57 | / | Dec at reference point | | |
| CUNIT2 | = | 'deg' | | / | Angles are degrees always | | |
| CRPIX3 | = | | 1 | / | Pixel coordinate of reference point | | |
| CDELTA3 | = | 7128.3 | / | Velocity increment | | | |
| CTYPE3 | = | 'VELOCITY' | | / | Each plane at a velocity | | |
| CRVAL3 | = | 500000.0 | / | Velocity in m/s | | | |
| CUNIT3 | = | 'm/s' | | / | metres per second | | |
| CRPIX4 | = | | 1 | / | Pixel coordinate of reference point | | |
| CDELTA4 | = | | 1 | / | Required here. | | |
| CTYPE4 | = | 'STOKES' | | / | Polarization | | |
| CRVAL4 | = | | 1 | / | Unpolarized | | |
| CUNIT4 | = | | | / | Conventional unitless = I pol | | |
| LONPOLE | = | | 180 | / | Native longitude of celestial pole | | |
| RADESYS | = | 'FK5' | | / | Mean IAU 1984 equatorial coordinates | | |
| EQUINOX | = | | 2000.0 | / | Equator and equinox of J2000.0 | | |

Figure 35 investigates the effect of projective nonlinearities for moderate field sizes for the commonly used zenithal projections. It shows the difference in R_θ between the various projections and the SIN projection as a function of native latitude θ . The SIN projection is used as reference since it always has R_θ less than the other zenithal projections. The difference for all projections exceeds 1 arcsec for values of θ less than 88° and the difference for the TAN projection exceeds one milliarcsec only 440 arcsec from the native pole. Such nonlinearities would be significant in optical, VLBI, and other high resolution observations.

7.3.2. Header interpretation example 2

While the previous header was a realistic example it overlooked many of the concepts introduced in this paper. Consider now the header given in Table 7. Although contrived to illustrate as much as possible in one example, this header could conceivably arise as a “tile” from a conic equal area projection of a region of the southern galactic hemisphere centered at galactic coordinates $(\ell, b) = (90^\circ, -25^\circ)$. The tile size of 2048×2048 pixels is approximately $10^\circ \times 10^\circ$, and this particular tile is situated immediately to the north of the central tile.

The header defines ecliptic coordinates as an alternate coordinate system, perhaps to help define the distribution of zodiacal light. This has the same reference point and transformation

Table 6. Sample calculations for example 1.

| parameter | units | SE corner | NE corner | NW corner |
|--------------|------------------|----------------|----------------|----------------|
| (p_1, p_2) | pixel | (1, 2) | (1, 512) | (511, 512) |
| (p_3, p_4) | pixel | (1, 1) | (1, 1) | (196, 1) |
| x | deg | 0:765000 | 0:765000 | -0:765000 |
| y | deg | -0:765000 | 0:765000 | 0:765000 |
| ϕ | deg | 45:000000 | 135:000000 | 225:000000 |
| θ | deg | 88:918255 | 88:918255 | 88:918255 |
| α | deg | 47:503264 | 47:595581 | 44:064419 |
| δ | deg | 62:795111 | 64:324332 | 64:324332 |
| Velocity | ms ⁻¹ | 500000.00 | 500000.00 | 1890018.50 |
| Stokes | | 1.0 \equiv I | 1.0 \equiv I | 1.0 \equiv I |

matrix as the primary description and the reference values are translated according to the prescription given in Sect. 2. The RADESYS card indicates that the ecliptic coordinates are mean coordinates in the IAU 1984 system, though the author of the header has been sloppy in omitting the EQUINOXA card which therefore defaults to J2000.0. Note that, in accord with Paper I, all keywords for the alternate description are reproduced, even those which do not differ from the primary description.

The problem will be to determine the galactic and ecliptic coordinates corresponding to a field point with pixel

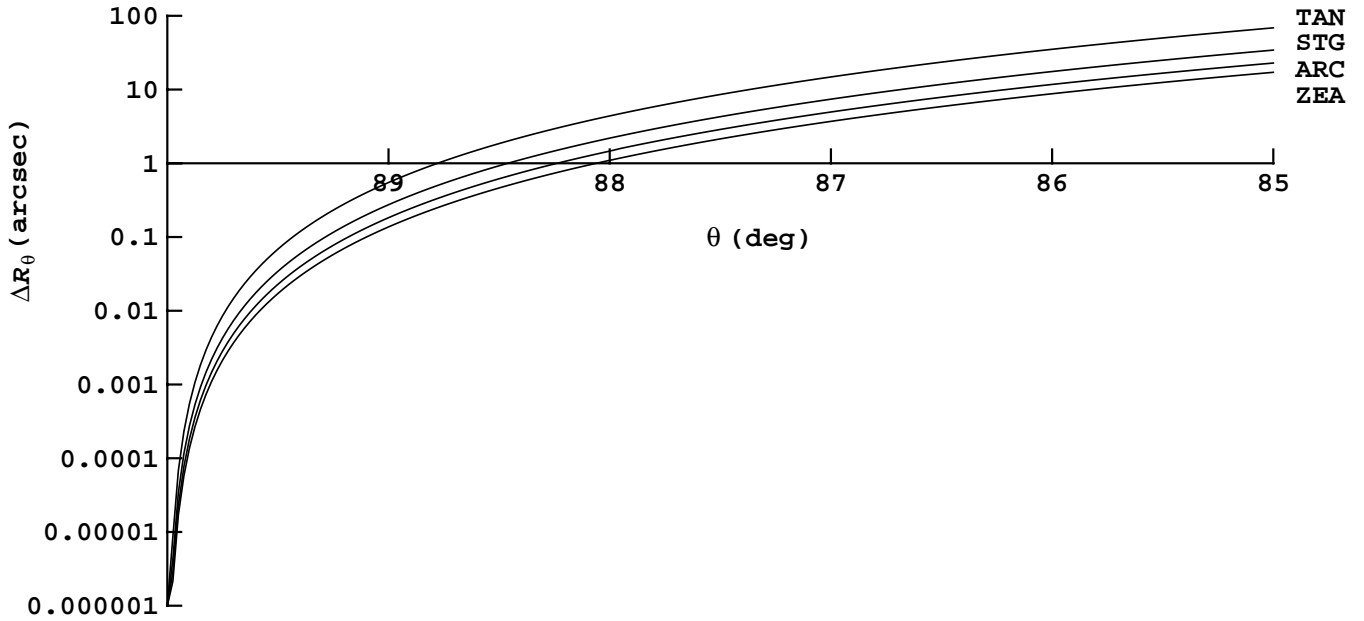


Fig. 35. $R_\theta(\text{projection}) - R_\theta(\text{SIN})$ in arcsec plotted versus θ for various projections.

coordinates (1957.2, 775.4). We begin as before by substituting in Eq. (1)

$$\begin{pmatrix} x \\ y \end{pmatrix} = \begin{pmatrix} -0.005 & 0.00002 \\ -0.00001 & 0.005 \end{pmatrix} \begin{pmatrix} p_1 - 1024.5 \\ p_2 + 1023.5 \end{pmatrix}.$$

Note that this transformation matrix describes a slight skewness and rotation; the x -, and y -axes correspond to the following two non-orthogonal lines in the pixel plane;

$$p_2 = 0.002(p_1 - 1024.5) - 1023.5,$$

$$p_2 = 250(p_1 - 1024.5) - 1023.5.$$

The values of the (x, y) projection plane coordinates for the chosen point are shown in Table 8 together with the remaining calculations for this example.

The next step is to compute the native longitude and latitude. Like all standard conics, the conic equal area projection has two parameters, θ_a and η , given by the keywords `PVi.1a` and `PVi.2a` attached to latitude coordinate i . In this example `PV2.1` is given but the author has again been sloppy in omitting `PV2.2`, which thus defaults to 0. Explicit inclusion of this keyword in the header would obviate any suspicion that it had been accidentally omitted. The native coordinates, (ϕ, θ) are obtained from (x, y) using Eqs. (117) and (129) via the intermediaries C , Y_0 , and R_θ given by Eqs. (125), (127), and (116). These in turn are expressed in terms of γ , θ_1 , and θ_2 given by Eqs. (128), (119), and (120). The calculations are shown in Table 8.

At this stage we have deprojected the field point. In this example the alternate coordinate description defines the same projection as the primary description. Indeed, it may seem odd that the formalism even admits the possibility that they may differ. However, this is a realistic possibility, for example in defining multiple optical plate solutions based on the TAN projection. It now remains to transform the native spherical coordinates into galactic coordinates, (ℓ, b) , and ecliptic coordinates, (λ, β) . To do this we need to apply Eqs. (2) and in order to do that we need (ℓ_p, b_p) and (λ_p, β_p) .

Looking first at galactic coordinates, we have $(\ell_0, b_0) = (90^\circ, -25^\circ)$ and $\phi_p = 0$. This conic projection has $(\phi_0, \theta_0) = (0^\circ, -25^\circ)$, and because $b_0 = \theta_0$ and $\phi_p = 0^\circ$, the native and galactic coordinate systems must coincide to within an offset in longitude. However, it is not obvious what ℓ_p should be to produce this offset. Equation (8) has one valid solution, namely $b_p = 90^\circ$. The special case in point 2 in the usage notes for Eqs. (9) and (10) must therefore be used to obtain $(\ell_p, b_p) = (-90^\circ, 90^\circ)$. The galactic coordinates of the field point listed in Table 8 are then readily obtained by application of Eqs. (2).

The header says that the ecliptic coordinates of the reference point are $(\lambda_0, \beta_0) = (-7^\circ.0300934, 34^\circ.8474143)$ and the native longitude of the ecliptic pole is $\phi_p = 6^\circ.3839706$. It also specifies `LATPOLEA` as `29.8114400`. In this case Eq. (8) has two valid solutions, $\beta_p = -25^\circ.1367794 \pm 54^\circ.9482194$, and the one closest in value to `LATPOLEA` (in fact equal to it) is chosen. If `LATPOLEA` had been omitted from the header its default value of `+90` would have selected the northerly solution anyway, but of course it is good practice to make the choice clear. The value of λ_p may be obtained by a straightforward application of Eqs. (9) and (10), and the ecliptic coordinates of the field point computed via Eqs. (2) are listed in Table 8 as the final step of the calculation. The reader may verify the calculation by transforming the computed galactic coordinates of the field point to mean ecliptic coordinates.

7.3.3. Binary table representations of example 2

Table 9 shows the FITS header for a set of images stored in binary table image array column format. The images are similar to that described in header interpretation example 2, Sect. 7.3.2, with primary image header illustrated in Table 7.

In this example the images are stored as 2-D arrays in Col. 5 of the table and each row of the table contains a 2048×2048 pixel image of a different region on the sky. This might

Table 7. Second example FITS header (blank lines have been inserted for clarity).

| | | | | | | | |
|-----------|-----------|---------------|------------|-----------|---------------------------------------|-----------|-----------|
| 123456789 | 123456789 | 123456789 | 123456789 | 123456789 | 123456789 | 123456789 | 123456789 |
| NAXIS | = | | 2 | / | 2-dimensional image | | |
| NAXIS1 | = | | 2048 | / | x axis (fastest) | | |
| NAXIS2 | = | | 2048 | / | y axis (2nd fastest) | | |
| MJD-OBS | = | 44258.7845612 | | / | MJD at start of observation | | |
| CRPIX1 | = | | 1024.5 | / | Pixel coordinate of reference point | | |
| CRPIX2 | = | | -1023.5 | / | Pixel coordinate of reference point | | |
| PC1_1 | = | | 1 | / | Transformation matrix element | | |
| PC1_2 | = | | -0.004 | / | Transformation matrix element | | |
| PC2_1 | = | | -0.002 | / | Transformation matrix element | | |
| PC2_2 | = | | 1 | / | Transformation matrix element | | |
| CDEL1 | = | | -0.005 | / | x-scale | | |
| CDEL2 | = | | 0.005 | / | y-scale | | |
| CTYPE1 | = | 'GLON-COE' | | / | Conic equal area projection | | |
| CTYPE2 | = | 'GLAT-COE' | | / | Conic equal area projection | | |
| PV2_1 | = | | -25.0 | / | Conic mid-latitude | | |
| CRVAL1 | = | | 90.0 | / | Galactic longitude at reference point | | |
| CRVAL2 | = | | -25.0 | / | Galactic latitude at reference point | | |
| CRPIX1A | = | | 1024.5 | / | Pixel coordinate of reference point | | |
| CRPIX2A | = | | -1023.5 | / | Pixel coordinate of reference point | | |
| PC1_1A | = | | 1 | / | Transformation matrix element | | |
| PC1_2A | = | | -0.004 | / | Transformation matrix element | | |
| PC2_1A | = | | -0.002 | / | Transformation matrix element | | |
| PC2_2A | = | | 1 | / | Transformation matrix element | | |
| CDEL1A | = | | -0.005 | / | x-scale | | |
| CDEL2A | = | | 0.005 | / | y-scale | | |
| CTYPE1A | = | 'ELON-COE' | | / | Conic equal area projection | | |
| CTYPE2A | = | 'ELAT-COE' | | / | Conic equal area projection | | |
| PV2_1A | = | | -25.0 | / | Conic mid-latitude | | |
| CRVAL1A | = | | -7.0300934 | / | Ecliptic longitude at reference point | | |
| CRVAL2A | = | | 34.8474143 | / | Ecliptic latitude at reference point | | |
| LONPOLEA | = | | 6.3839706 | / | Native longitude of ecliptic pole | | |
| LATPOLEA | = | | 29.8114400 | / | Ecliptic latitude of native pole | | |
| RADESYSA | = | 'FK5' | | / | Mean IAU 1984 ecliptic coordinates | | |

represent a set of smaller images extracted from a single larger image. In this case all coordinate system parameters except for the reference pixel coordinate are the same for each image and are given as header keywords. The reference pixel coordinate for the primary and secondary description are given in Cols. 1 to 4 of the binary table.

Table 10 shows the header for the same image given in pixel list format. There are 10 000 rows in this table, each one listing the pixel coordinates (XPOS, YPOS) of every detected “event” or photon in the image. For illustration purposes, this table also contains an optional DATA_QUALITY column that could be used to flag the reliability or statistical significance of each event. A real image may be constructed from this virtual image as the 2-dimensional histogram of the number of events that occur within each pixel. The additional TLMIN n and TLMAX n keywords shown here are used to specify the minimum and maximum legal values in XPOS and YPOS columns and are useful for determining the range of each axis when constructing the image histogram.

Table 8. Calculations for example 2.

| | | |
|------------------------|--------------|--------------|
| (p_1, p_2) | 1957.2 | 775.4 |
| (x, y) | -4:6275220 | 8:9851730 |
| θ_a, η | -25:0000000 | 0:0000000 |
| θ_1, θ_2 | -25:0000000 | -25:0000000 |
| γ | -0.8452365 | |
| C, Y_0 | -0.4226183 | -122:8711957 |
| (ϕ, θ) | -4:7560186 | -15:8973800 |
| (ℓ_p, b_p) | -90:0000000 | 90:0000000 |
| (ℓ, b) | 85:2439814 | -15:8973800 |
| (λ_p, β_p) | -179:9767827 | 29:8114400 |
| (λ, β) | -14:7066741 | 43:0457292 |

7.3.4. Header interpretation example 3

This example has been adapted from a real-life FITS data file. The simplicity of the header shown in Table 11 is deceptive; it is actually presented as an example of how *not* to write a FITS

Table 9. Example binary table image array header (blank lines have been inserted for clarity).

```

123456789 123456789 123456789 123456789 123456789 123456789 123456789 123456789
XTENSION= 'BINTABLE' / Binary table extension
BITPIX = 8 / 8-bit bytes
NAXIS = 2 / 2-dimensional binary table
NAXIS1 = 16777232 / Width of table in bytes
NAXIS2 = 4 / Number of rows in table
PCOUNT = 0 / Size of special data area
GCOUNT = 1 / One data group (required keyword)

TFIELDS = 5 / number of fields in each row
TTYPE1 = '1CRP5 ' / Axis 1: reference pixel coordinate
TFORM1 = '1J ' / Data format of column 1: I*4 integer
TTYPE2 = '2CRP5 ' / Axis 2: reference pixel coordinate
TFORM2 = '1J ' / Data format of column 2: I*4 integer
TTYPE3 = '1CRP5A ' / Axis 1A: reference pixel coordinate
TFORM3 = '1J ' / Data format of column 3: I*4 integer
TTYPE4 = '2CRP5A ' / Axis 2A: reference pixel coordinate
TFORM4 = '1J ' / Data format of column 4: I*4 integer
TTYPE5 = 'Image ' / 2-D image array
TFORM5 = '4194304J' / Data format of column 5: I*4 vector
TDIM5 = '(2048,2048)' / Dimension of column 5 array
MJD0B5 = 44258.7845612 / MJD at start of observation

COMMENT The following keywords define the primary coordinate description
COMMENT of the images contained in Column 5 of the table.

11PC5 = 1 / Transformation matrix element
12PC5 = -0.004 / Transformation matrix element
21PC5 = -0.002 / Transformation matrix element
22PC5 = 1 / Transformation matrix element
1CDE5 = -0.005 / Axis 1: scale
2CDE5 = 0.005 / Axis 2: scale
1CTY5 = 'GLON-COE' / Axis 1: conic equal area projection
2CTY5 = 'GLAT-COE' / Axis 2: conic equal area projection
2PV5_1 = -25.0 / Conic mid-latitude
1CRV5 = 90.0 / Axis 1: galactic longitude at reference point
2CRV5 = -25.0 / Axis 2: galactic latitude at reference point

COMMENT The following keywords define the secondary coordinate description
COMMENT of the images contained in Column 5 of the table.

11PC5A = 1 / Transformation matrix element
12PC5A = -0.004 / Transformation matrix element
21PC5A = -0.002 / Transformation matrix element
22PC5A = 1 / Transformation matrix element
1CDE5A = -0.005 / Axis 1A: scale
2CDE5A = 0.005 / Axis 2A: scale
1CTY5A = 'ELON-COE' / Axis 1A: conic equal area projection
2CTY5A = 'ELAT-COE' / Axis 2A: conic equal area projection
2PV5_1A = -25.0 / Conic mid-latitude
1CRV5A = -7.0300934 / Axis 1A: ecliptic longitude at reference point
2CRV5A = 34.8474143 / Axis 2A: ecliptic latitude at reference point
LONP5A = 6.3839706 / Native longitude of ecliptic pole
LATP5A = 29.8114400 / Ecliptic latitude of native pole
RADE5A = 'FK5 ' / Mean IAU 1984 ecliptic coordinates
EQUI5A = 2000.0 / Coordinate epoch
END

```

Table 10. Example pixel list header (blank lines have been inserted for clarity).

| 123456789 | 123456789 | 123456789 | 123456789 | 123456789 | 123456789 | 123456789 | 123456789 |
|-----------|---|----------------|-----------|-----------|--|-----------|-----------|
| XTENSION= | 'BINTABLE' | | | / | Binary table extension | | |
| BITPIX | = | 8 | | / | 8-bit bytes | | |
| NAXIS | = | 2 | | / | 2-dimensional binary table | | |
| NAXIS1 | = | 5 | | / | Width of table in bytes | | |
| NAXIS2 | = | 10000 | | / | Number of rows in table | | |
| PCOUNT | = | 0 | | / | Size of special data area | | |
| GCOUNT | = | 1 | | / | One data group (required keyword) | | |
| | | | | | | | |
| TFIELDS | = | 3 | | / | Number of fields in each row | | |
| TTYPE1 | = | 'DATA_QUALITY' | | / | Quality flag value of the photon | | |
| TFORM1 | = | '1B' | | / | Data format of the field: 1-byte integer | | |
| TTYPE2 | = | 'XPOS' | | / | Axis 1: pixel coordinate of the photon | | |
| TFORM2 | = | '1I' | | / | Data format of column 2: I*2 integer | | |
| TLMIN2 | = | 1 | | / | Lower limit of axis in column 2 | | |
| TLMAX2 | = | 2048 | | / | Upper limit of axis in column 2 | | |
| TTYPE3 | = | 'YPOS' | | / | Axis 2: pixel coordinate of the photon | | |
| TFORM3 | = | '1I' | | / | Data format of column 3: I*2 integer | | |
| TLMIN3 | = | 1 | | / | Lower limit of axis in column 3 | | |
| TLMAX3 | = | 2048 | | / | Upper limit of axis in column 3 | | |
| MJDOB3 | = | 44258.7845612 | | / | MJD at start of observation | | |
| | | | | | | | |
| COMMENT | The following keywords define the primary coordinate description. | | | | | | |
| | | | | | | | |
| TCRP2 | = | 1024.5 | | / | Axis 1: reference pixel coordinate | | |
| TCRP3 | = | -1023.5 | | / | Axis 2: reference point pixel coordinate | | |
| TPC2_2 | = | 1 | | / | Transformation matrix element | | |
| TPC2_3 | = | -0.004 | | / | Transformation matrix element | | |
| TPC3_2 | = | -0.002 | | / | Transformation matrix element | | |
| TPC3_3 | = | 1 | | / | Transformation matrix element | | |
| TCDE2 | = | -0.005 | | / | Axis 1: scale | | |
| TCDE3 | = | 0.005 | | / | Axis 2: scale | | |
| TCTY2 | = | 'GLON-COE' | | / | Axis 1: conic equal area projection | | |
| TCTY3 | = | 'GLAT-COE' | | / | Axis 2: conic equal area projection | | |
| TPV3_1 | = | -25.0 | | / | Conic mid-latitude | | |
| TCRV2 | = | 90.0 | | / | Axis 1: galactic longitude at reference point | | |
| TCRV3 | = | -25.0 | | / | Axis 2: galactic latitude at reference point | | |
| | | | | | | | |
| COMMENT | The following keywords define the secondary coordinate description. | | | | | | |
| | | | | | | | |
| TCRP2A | = | 1024.5 | | / | Axis 1A: reference pixel coordinate | | |
| TCRP3A | = | -1023.5 | | / | Axis 2A: reference point pixel coordinate | | |
| TP2_2A | = | 1 | | / | Transformation matrix element | | |
| TP2_3A | = | -0.004 | | / | Transformation matrix element | | |
| TP3_2A | = | -0.002 | | / | Transformation matrix element | | |
| TP3_3A | = | 1 | | / | Transformation matrix element | | |
| TCDE2A | = | -0.005 | | / | Axis 1A: scale | | |
| TCDE3A | = | 0.005 | | / | Axis 2A: scale | | |
| TCTY2A | = | 'ELON-COE' | | / | Axis 1A: conic equal area projection | | |
| TCTY3A | = | 'ELAT-COE' | | / | Axis 2A: conic equal area projection | | |
| TV3_1A | = | -25.0 | | / | Conic mid-latitude | | |
| TCRV2A | = | -7.0300934 | | / | Axis 1A: ecliptic longitude at reference point | | |
| TCRV3A | = | 34.8474143 | | / | Axis 2A: ecliptic latitude at reference point | | |
| LONP3A | = | 6.3839706 | | / | Native longitude of ecliptic pole | | |
| LATP3A | = | 29.8114400 | | / | Ecliptic latitude of native pole | | |
| RADE3A | = | 'FK5' | | / | Mean IAU 1984 ecliptic coordinates | | |
| EQUI3A | = | 2000.0 | | / | Coordinate epoch | | |
| END | | | | | | | |

Table 11. Third example FITS header.

| 123456789 | 123456789 | 123456789 | 123456789 | 123456789 | 123456789 | 123456789 | 123456789 |
|-----------|-----------|------------|-----------|---------------------------------------|----------------------|-----------|-----------|
| NAXIS | = | | 2 | / | 2-dimensional image | | |
| NAXIS1 | = | | 181 | / | x axis (fastest) | | |
| NAXIS2 | = | | 91 | / | y axis (2nd fastest) | | |
| CRPIX1 | = | 226.0 | / | Pixel coordinate of reference point | | | |
| CRPIX2 | = | 46.0 | / | Pixel coordinate of reference point | | | |
| CDEL1 | = | -1.0 | / | x-scale | | | |
| CDEL2 | = | 1.0 | / | y-scale | | | |
| CTYPE1 | = | 'GLON-CAR' | / | Plate carree projection | | | |
| CTYPE2 | = | 'GLAT-CAR' | / | Plate carree projection | | | |
| CRVAL1 | = | 30.0 | / | Galactic longitude at reference point | | | |
| CRVAL2 | = | 35.0 | / | Galactic latitude at reference point | | | |

header, although the latent problem with its interpretation is quite subtle.

Observe that the image spans 180° in native longitude and 90° in native latitude and that the reference pixel lies outside the image. In fact, the reference pixel is located so that the native longitude runs from 45° to 225° and hence the image lies partly inside and partly outside the normal range of native longitude, $[-180^\circ, 180^\circ]$.

In fact, as might be expected, this makes no difference to the computation of celestial coordinates. For example, in computing the celestial coordinates of pixel (1, 1) we readily find from Eqs. (83) and (84) that the native coordinates are $(\phi, \theta) = (225^\circ, -45^\circ)$. The fact that ϕ exceeds 180° becomes irrelevant once Eqs. (2) are applied since the trigonometric functions do not distinguish between $\phi = 225^\circ$ and $\phi = -135^\circ$. The latter value is the appropriate one to use if the cylinder of projection is considered to be “rolled out” over multiple cycles. Consequently the correct galactic coordinates are obtained.

The problem only surfaces when we come to draw a coordinate grid on the image. A meridian of longitude, for example, is traced by computing the pixel coordinates for each of a succession of latitudes along the segment of the meridian that crosses the image. As usual, in computing pixel coordinates, the celestial coordinates are first converted to native coordinates by applying Eqs. (5), and the native longitude will be returned in the normal range $[-180^\circ, 180^\circ]$. Consequently, in those parts of the image where $\phi > 180^\circ$ the pixel coordinates computed will correspond to the point at $\phi - 360^\circ$, i.e. in the part of the principle cycle of the cylindrical projection outside the image.

In principle it is possible to account for this, at least in specific cases, particularly for the cylindrical projections which are somewhat unusual in this regard. In practice, however, it is difficult to devise a general solution, especially when similar problems may arise for projection types where it is not desirable to track ϕ outside its normal range. For example, consider the case where a Hammer-Aitoff projection is used to represent the whole sky; since its boundary is curved there will be out-of-bounds areas in the corner of the image. Normally a grid drawing routine can detect these by checking whether the inverse projection equations return a value for ϕ outside its normal range. It may thus determine the proper boundary of the

projection and deal with the discontinuity that arises when a grid line passes through it.

How then should the header have been written? Note that the problem exists at the lowest level of the coordinate description, in the conversion between (x, y) and (ϕ, θ) , and the solution must be found at this level. The problem arose from a particular property of cylindrical projections in that they have $x \propto \phi$. We must use this same property, which we might call “ ϕ -translation similarity”, to recast the coordinate description into a more manageable form. ϕ -translation similarity simply means that changing the origin of ϕ corresponds to shifting the image in the x -direction. In other words, we can transfer the reference point of the projection from its current location to another location along the native equator without having to re-grid the image. The fact that the PC_{i-ja} matrix is unity in this example makes this task a little simpler than otherwise.

Note first that because the image straddles $\phi = 180^\circ$ we can't simply reset CRPIX1 so as to shift the reference point to $\phi = -360^\circ$; the image would then straddle $\phi = -180^\circ$, which is no improvement. In this example it is convenient and sufficient to shift the reference point to $(\phi, \theta) = (180^\circ, 0^\circ)$, which corresponds to pixel coordinate $(p_1, p_2) = (46.0, 46.0)$. Hence we need to reset CRPIX1 to 46.0 and adjust the keywords which define the celestial coordinate system. The reader may readily verify that the galactic coordinates of the new reference point are $(\ell, b) = (210^\circ, -35^\circ)$ and whereas the old, implied value of LONPOLE was 0° when $\delta_0 > 0$, now that $\delta_0 < 0$ its new implied value is 180° , and this is correct. However, we will set it explicitly anyway. The keywords to be changed are therefore

```
CRPIX1 = 46.0,
CRVAL1 = 210°,
CRVAL2 = -35°,
LONPOLE = 180°.
```

What if the PC_{i-ja} matrix was not unity? The problem of determining the pixel coordinates where $(\phi, \theta) = (-180^\circ, 0^\circ)$ would have presented little extra difficulty, although in general CRPIX2 would also need to be changed. On reflection it may come as a surprise that changing CRPIX j like this does not fundamentally alter the linear transformation. However it may

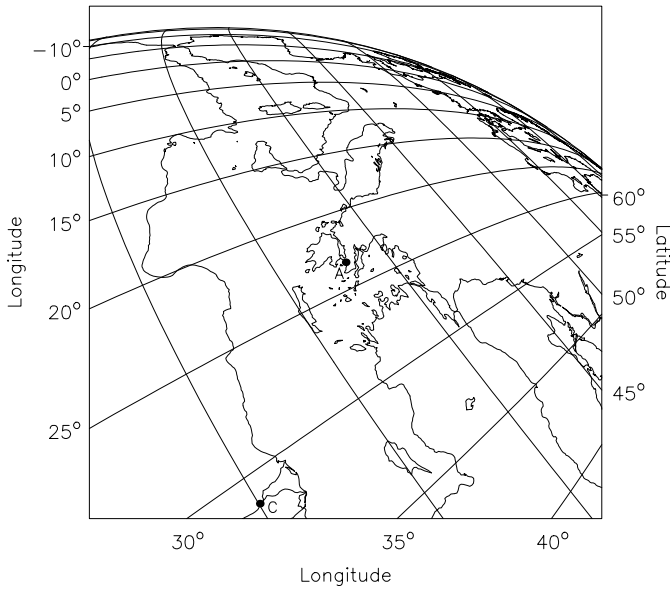


Fig. 36. The Earth from 2230 km above Cairo looking directly towards Athens.

readily be verified that the only effect of changing CRPIX j is to change the origin of the (x, y) coordinates.

7.4. Header construction examples

This section considers the more difficult problem faced by FITS writers; that of constructing world coordinate system headers.

Example 1 is contrived to illustrate the general methods used in constructing a spherical coordinate representation. Paying homage to Claudius Ptolemy, it actually constructs a terrestrial coordinate grid for the Mediterranean region as seen from space.

Example 2 constructs headers for the infra-red dust maps produced by Schlegel et al. (1998) who regridded data from the COBE/DIRBE and IRAS/ISSA surveys onto two zenithal equal area projections.

Example 3 considers the case of long-slit optical spectroscopy. It is concerned in particular with solving the problem of producing three world coordinate elements for a data array of only two dimensions.

Example 4 constructs a dual coordinate description for an image of the moon and considers the problem of producing consistent scales for each. It also suggests an extension to deal with the rings of the planet Saturn.

7.4.1. Header construction example 1

Our first example of FITS header construction concerns satellite photography of the Earth. Figure 36 shows a part of the world which probably would have been recognizable to Claudius Ptolemy.

A satellite 2230 km immediately above Cairo aims its digital camera directly towards Athens and adjusts the orientation and focal length to include Cairo in the field near the bottom edge of the frame. The 2048×2048 pixel CCD detector

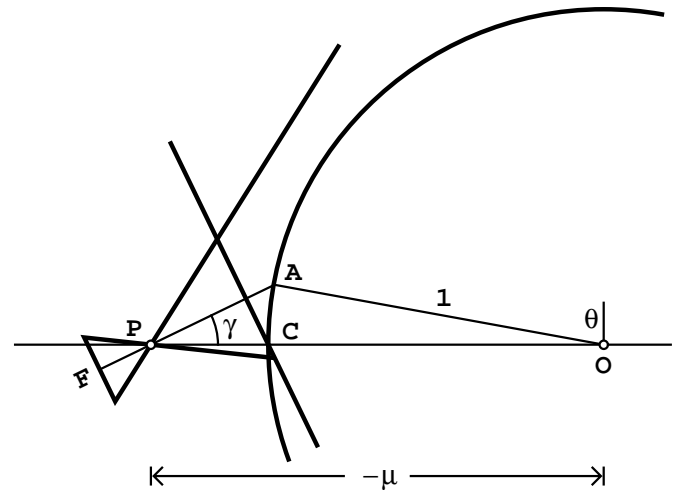


Fig. 37. The geometry of Fig. 36. Cairo at C is at the reference point of the projection with Athens at A. The camera with aperture at P and focal plane F is not drawn to scale, though the rest of the diagram is. Note that $\mu < 0$ so $-\mu$, as marked, is a positive value.

array employed by the camera is centered on its optical axis so Athens is at pixel coordinate (1024.5, 1024.5). Cairo – at the satellite’s nadir – is later found to be at (681.67, 60.12). The task is to overlay a terrestrial coordinate grid on this image.

For the sake of simplicity we will assume pin-hole camera optics. Figure 37 identifies the geometry as that of a tilted, near-sided zenithal perspective projection with the nadir at the reference point. The point of projection P corresponds to the pin-hole of the camera and the tilted plane of projection is parallel to the camera’s focal plane F. The image in the focal plane is simply scaled (and inverted) with respect to that on the plane of projection. Clearly a tilted AZP projection is a better match to the geometry than SZP in this instance.

The satellite altitude of 2230 km is 0.350 Earth radii and since the projection is near-sided we may immediately write $\mu = -1.350$.

Determination of γ requires knowledge of the coordinates of Cairo (31°15 E, 30°03 N) and Athens (23°44 E, 38°00 N). From spherical trigonometry we may deduce that the angular separation between the two cities is 10°20'72" and also that Athens is on a bearing 36°6'252" west of north from Cairo.

Now since Cairo is at the native pole of the projection the angular separation between the two cities is just their difference in native latitude, $90^\circ - \theta_A$. Using the sine rule in triangle PAO in Fig. 37 we obtain

$$90^\circ - \theta = -\gamma - \sin^{-1}(\mu \sin \gamma). \tag{194}$$

This equation, which takes account of the fact that μ is negative, may be solved iteratively to obtain $\gamma = 25^\circ 8' 458''$.

The obliqueness of this view of the Earth, occasioned by the fact that the image is not oriented along a meridian, is handled partly via LONPOLE a and partly as a bulk image rotation via PC i_ja . Note that these are not complementary; they produce distinct effects since the tilted AZP projection does not have point symmetry. Figure 37 shows the situation – the generating sphere with Cairo at the native pole must be oriented so

is easy because we know $b_p = 90^\circ$ and the simple special case Eqs. (3) apply, so

$$\ell = \phi + (\ell_p - \phi_p - 180^\circ).$$

We have a degree of freedom here since only $\ell_p - \phi_p$ is determined. It's best to let ϕ_p take its default value of 0° for zenithal projections with the celestial pole at the native pole (it's 180° otherwise), so we must have

$$\begin{aligned} \text{CRVAL1} &= 270^\circ, \\ \text{CRVAL2} &= 90^\circ, \\ \text{LONPOLE} &= 0^\circ. \end{aligned}$$

Although LONPOLE assumes its default value here it would of course be wise to write it explicitly into the header. The procedure for the south Galactic pole case is similar. The SFD equations may be rewritten

$$\begin{aligned} p_1 - 2048.5 &= 2048 \sqrt{1 - \sin(-b)} \sin(90^\circ - \ell), \\ p_2 - 2048.5 &= 2048 \sqrt{1 - \sin(-b)} \cos(90^\circ - \ell), \end{aligned}$$

whence

$$\begin{aligned} \text{CRPIX1} &= 2048.5, \\ \text{CRPIX2} &= 2048.5, \\ \text{CDELTA1} &= 180^\circ \sqrt{2}/(2048\pi), \\ \text{CDELTA2} &= -180^\circ \sqrt{2}/(2048\pi), \\ \ell &= 90^\circ - \phi, \\ b &= -\theta. \end{aligned}$$

Equations (4) apply for $b_p = -90^\circ$ so

$$\ell = (\ell_p + \phi_p) - \phi.$$

Again we let ϕ_p take its default value of 180° , so

$$\begin{aligned} \text{CRVAL1} &= 270^\circ, \\ \text{CRVAL2} &= -90^\circ, \\ \text{LONPOLE} &= 180^\circ. \end{aligned}$$

It's generally easier to interpret coordinate headers than to construct them so it's essential after formulating the header to test it at a few points and make sure that it works as expected. Note that this sort of translation exercise wouldn't be necessary if the formalism of this paper was used right from the start, i.e. in the regridding operation used to produce the maps.

7.4.3. Header construction example 3

Consider now the coordinate description for the two-dimensional image formed by a long slit spectrograph. We assume that the wavelength axis of length 1024 and dispersion $\Delta\lambda$ nm/pixel corresponds to the p_1 pixel coordinate, and the 2048 pixel spatial axis corresponds to p_2 . The slit is centered on equatorial coordinates (α_0, δ_0) and oriented at position angle ρ measured such that when $\rho = 0$ the first spectrum is northwards. We will assume that the telescope and spectrograph optics are such that the distance along the slit is in proportion to

true angular distance on the sky with a separation between pixels of σ arcsec. We do not consider curvature of the slit here, that is a distortion of the sort to be handled by the methods of Paper IV.

Equiscaling along the length of the slit together with the one-dimensional nature of the spatial geometry indicate that any projection could be used that is equiscaled along a great circle projected as a straight line. Many projections satisfy this criterion. However, in practice the zenithal equidistant (ARC) projection is the most convenient choice.

The one-dimensional spatial geometry may at first seem problematical, with each point along the slit having a different (α, δ) . However, this is easily handled by introducing a third, degenerate axis and introducing a rotation. The rotation in position angle may be handled via the linear transformation matrix. Moreover, since we've opted for a zenithal projection, bearing in mind the discussion of Sect. 7.1, the rotation can also be handled via ϕ_p (i.e. LONPOLE). We will demonstrate both methods.

Use of ϕ_p is perhaps more straightforward, and the header may be written without further ado:

$$\begin{aligned} \text{NAXIS} &= 3, \\ \text{NAXIS1} &= 1024, \\ \text{NAXIS2} &= 2048, \\ \text{NAXIS3} &= 1, \\ \text{CRPIX1} &= 1, \\ \text{CRPIX2} &= 1024.5, \\ \text{CRPIX3} &= 1, \\ \text{CDELTA1} &= \Delta\lambda, \\ \text{CDELTA2} &= -\sigma/3600, \\ \text{CDELTA3} &= 1, \\ \text{CTYPE1} &= \text{'WAVELEN'}, \\ \text{CTYPE2} &= \text{'RA---ARC'}, \\ \text{CTYPE3} &= \text{'DEC--ARC'}, \\ \text{CUNIT1} &= \text{'nm'}, \\ \text{CRVAL1} &= \lambda_0, \\ \text{CRVAL2} &= \alpha_0, \\ \text{CRVAL3} &= \delta_0, \\ \text{LONPOLE} &= 90^\circ + \rho. \end{aligned}$$

LONPOLE is the only card which requires explanation. Since no rotation is introduced by the linear transformation, the slit, which coincides with the p_2 -axis, maps directly to the x -axis. However, because CDELTA2 is negative, the two axes run in opposite directions and, given that when $\rho = 0$ the p_2 -axis runs from north to south, x must run from south to north. Referring to the left side of Fig. 3 for zenithal projections, we see that when $\rho = 0$, the north celestial pole must be at $\phi = 90^\circ$. Since position angle increases in an anticlockwise direction (i.e. north through east) in the plane of the sky, the celestial pole must rotate clockwise as ρ increases. Thus, as ρ increases so must ϕ_p , hence $\phi_p = 90^\circ + \rho$.

To verify this representation we will test it with $(\alpha_0, \delta_0) = (150^\circ, -35^\circ)$, $\rho = 30^\circ$, and $\sigma = 2''$ for pixel coordinate (1, 1, 1).

The corresponding (s, x, y) coordinates are $(0, 0^\circ.5686111, 0^\circ)$. The wavelength is therefore λ_0 . From Eqs. (15), (14), and (67) the native longitude and latitude are $(\phi, \theta) = (90^\circ, 89^\circ.4313889)$, ϕ is always $\pm 90^\circ$, and the value of θ corresponds to an offset of $2047''$ from the center of the slit as it should. From Eqs. (2) the right ascension and declination are $(\alpha, \delta) = (150^\circ.3450039, -34^\circ.5070794)$, which are in the correct quadrant.

Most optical telescopes are better described by the TAN projection. In this case the only difference in the header would be

CTYPE2 = 'RA---TAN',
CTYPE3 = 'DEC--TAN'.

Verifying it with the same values as before yields the same (s, x, y) and thus the same wavelength. From Eqs. (15), (14), and (54) we get $(\phi, \theta) = (90^\circ, 89^\circ.4314076)$, the offset of $2046''.933$ differing by only 67 mas. The right ascension and declination are $(\alpha, \delta) = (150^\circ.3449926, -34^\circ.5070956)$.

As an alternative, the original header could also have been written with the CTYPE i interchanged, so that the slit, still coincident with the p_2 -axis, maps directly to the y -axis. The header would be as above but with the following changes:

CTYPE2 = 'DEC--ARC',
CTYPE3 = 'RA---ARC',
CRVAL2 = δ_0 ,
CRVAL3 = α_0 ,
LONPOLE = $180^\circ + \rho$.

LONPOLE differs because the slit now runs along the y -axis rather than the x -axis; the negative sign on CDELTA2 is still needed to make y run counter to p_2 .

There are several practical ways to rewrite the header using the PC i - j or CD i - j matrices. Looking first at the CD i - j form we have

$$\begin{pmatrix} s \\ x \\ y \end{pmatrix} = \begin{pmatrix} \text{CD1}_1 & \text{CD1}_2 & \text{CD1}_3 \\ \text{CD2}_1 & \text{CD2}_2 & \text{CD2}_3 \\ \text{CD3}_1 & \text{CD3}_2 & \text{CD3}_3 \end{pmatrix} \begin{pmatrix} p_1 - \text{CRPIX1} \\ p_2 - \text{CRPIX2} \\ p_3 - \text{CRPIX3} \end{pmatrix}.$$

Since the third axis is degenerate, with $\text{CRPIX3} = 1$, we have $p_3 - \text{CRPIX3} = 0$, so the values of CD1_3 , CD2_3 , and CD3_3 are irrelevant. Moreover, CD1_2 , CD2_1 , and CD3_1 are all zero, hence

$$\begin{aligned} s &= \text{CD1}_1 (p_1 - \text{CRPIX1}), \\ x &= \text{CD2}_2 (p_2 - \text{CRPIX2}), \\ y &= \text{CD3}_2 (p_2 - \text{CRPIX2}). \end{aligned} \quad (195)$$

Effectively this provides (x, y) coordinates along the slit via the parametric equations of a line, where $p_2 - \text{CRPIX2}$ is the distance parameter.

As before, the main problem is to determine the correct angle of rotation. For zenithal projections $\phi_p = 180^\circ$ by default, and referring to the left side of Fig. 3 we see that this corresponds to the y -axis. Thus when $\rho = 0$ we require a rotation of 90° to transform the p_2 -axis onto the y -axis. For $\rho > 0$ we need to rotate further so the angle of rotation is $90^\circ + \rho$.

Therefore, CDELTA i and LONPOLE in the original header must be replaced with

$$\begin{aligned} \text{CD1}_1 &= \Delta\lambda, \\ \text{CD2}_2 &= \cos(90^\circ + \rho)(\sigma/3600), \\ \text{CD3}_2 &= -\sin(90^\circ + \rho)(\sigma/3600), \\ \text{CD2}_3 &= 1, \\ \text{CD3}_3 &= 1. \end{aligned}$$

The negative sign on CD3_2 is associated with the rotation, not the scale. Note that, although the value of CD3_3 is irrelevant, it must be set non-zero otherwise the zero defaults for CD i - j would make the third column zero, thereby producing a singular matrix. Likewise, in this example and similarly below, we set CD2_3 non-zero to prevent the second row of the matrix becoming zero for values of ρ such that $\cos(90^\circ + \rho) = 0$.

The PC i - j matrix formulation is similar but allows more flexibility in the way the scale is handled:

1. Since CDELTA i defaults to unity, omitting it allows PC i - j to duplicate the functionality of CD i - j . However, since PC i - j defaults to the unit matrix rather than zero, there is no need to set PC3_3 specifically, hence

$$\begin{aligned} \text{PC1}_1 &= \Delta\lambda, \\ \text{PC2}_2 &= \cos(90^\circ + \rho)(\sigma/3600), \\ \text{PC3}_2 &= -\sin(90^\circ + \rho)(\sigma/3600), \\ \text{PC2}_3 &= 1. \end{aligned}$$

2. Equation (195), as a simple scaling relation, suggests the use of CDELTA i . However, PC3_2 must be non-zero since x and y both depend on p_2 . Setting it to unity and allowing the remaining PC i - j to default to the unit matrix we have

$$\begin{aligned} \text{PC3}_2 &= 1, \\ \text{CDELTA1} &= \Delta\lambda, \\ \text{CDELTA2} &= \cos(90^\circ + \rho)(\sigma/3600), \\ \text{CDELTA3} &= -\sin(90^\circ + \rho)(\sigma/3600). \end{aligned}$$

3. The ‘‘orthodox’’ method is to encode the rotation and scale separately in PC i - j and CDELTA i :

$$\begin{aligned} \text{PC2}_2 &= \cos(90^\circ + \rho), \\ \text{PC3}_2 &= -\sin(90^\circ + \rho), \\ \text{PC2}_3 &= 1, \\ \text{CDELTA1} &= \Delta\lambda, \\ \text{CDELTA2} &= \sigma/3600, \\ \text{CDELTA3} &= \sigma/3600. \end{aligned}$$

Arguably this is more amenable to human interpretation, especially if thoughtful comments are added.

The above six methods should all be regarded as equally legitimate. In fact, there are infinitely many ways to encode this header, though most would disguise the essential simplicity of the geometry.

7.4.4. Header construction example 4

Thompson (1999) has applied the methods of this paper to the definition of solar coordinates for a variety of coordinate systems. As the final header construction example we will consider a specific coordinate description for another solar system body, the Moon.

A short exposure plate taken at Sydney Observatory at 1:00 am on 15 February 1957 AEST (GMT +1000) of the full Moon near lunar perigee has been digitized and converted to a 4096×4096 pixel image in FITS format. The scale is $1''$ per pixel with the moon centered in the image, and it is desired to construct a dual coordinate description. The first system is geocentric apparent equatorial coordinates in a gnomonic projection. The second is selenographic coordinates in a zenithal perspective projection attached to the surface of the Moon.

The ephemeris gives the geocentric apparent right ascension of the Moon at the time as $09^{\text{h}}41^{\text{m}}13^{\text{s}}.1$ and declination as $+08^{\circ}34'26''$. Diurnal parallax would have caused the Moon to appear slightly offset from this position as seen from Sydney Observatory, but to a good approximation the coordinate systems may be defined with the center of the Moon at the stated geocentric coordinates. The image was digitized in the normal orientation with north up and east to the left so the header for the primary description is straightforward:

```
NAXIS = 2,
NAXIS1 = 4096,
NAXIS2 = 4096,
MJD-OBS = 35883.625,
CRPIX1 = 2048.5,
CRPIX2 = 2048.5,
CDEL1 = -0.0002778,
CDEL2 = 0.0002778,
CTYPE1 = 'RA---TAN',
CTYPE2 = 'DEC--TAN',
CRVAL1 = 145.30458,
CRVAL2 = 8.57386,
LONPOLE = 180.0,
RADESYS = 'GAPPT'.
```

If any rotation had been introduced it could have been corrected for in the linear transformation matrix.

The first step in constructing the secondary description is to determine the distance of the observer from the Moon. The ephemeris gives the equatorial horizontal parallax as $61'29''.3$, corresponding to a distance between the centers of the Earth and Moon of 55.91 Earth radii. However, the observer may be closer or further away by up to one Earth radius depending on location and time of day and this 2% effect is deemed worthy of correction. At Sydney Observatory (longitude $10^{\text{h}}04^{\text{m}}49^{\text{s}}.2$, latitude $-33^{\circ}51'41''$) the Greenwich apparent sidereal time was $00^{\text{h}}51^{\text{m}}43^{\text{s}}.6$. Thus the apparent right ascension and declination of the zenith was $10^{\text{h}}56^{\text{m}}32^{\text{s}}.8$, $-33^{\circ}51'41''$. The vector dot product then gives the distance correction as 0.69 Earth radii. Using the ratio of the Earth and Moon radii of 3.670 the

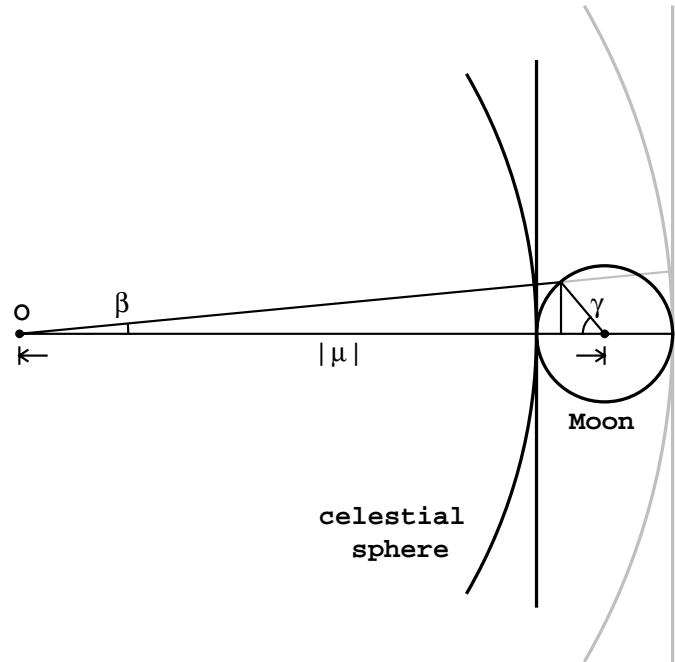


Fig. 38. Geometry of header construction example 4 (not to scale). The observer is at O, a distance of $|\mu|$ Moon radii from the center of the Moon. The Moon is projected as a near-sided zenithal perspective projection ($\mu < -1$), and the celestial sphere as a gnomonic projection. An alternative plane of projection is shown.

corrected distance of 55.22 Earth radii indicates that the distance parameter for the zenithal perspective projection is $\mu = 202.64$ Moon radii.

We now need to determine the correct relative scale. Figure 38 shows the geometry of the two projections where we note, by analogy with Fig. 4, that $\mu < -1$. From the diagram we have

$$\beta = \tan^{-1} \left(\frac{\sin \gamma}{|\mu| - \cos \gamma} \right). \quad (196)$$

The figure shows that this equation is not influenced by the choice of the plane of projection. Evaluating the derivative $d\beta/d\gamma$ at $\gamma = 0$ we find the relative scale is $1/(|\mu| - 1)$.

The ephemeris records that the selenographic coordinates of the Earth at the time were $(\ell, b) = (+0^{\circ}.26, +6^{\circ}.45)$ and the position angle of the Moon's axis was $C = 19^{\circ}.03$. However, since the Earth subtends an angle of over 2° in the lunar sky, topocentric optical libration – the correction for the observatory's location – is significant. Application of the correction formulae derived by Atkinson (1951) gives the selenographic coordinates of Sydney Observatory as $(\ell', b') = (-0^{\circ}.23, 5^{\circ}.89)$ and $C' = 18^{\circ}.94$. Since the image was taken in the normal orientation and we have a zenithal projection it is convenient to account for the position angle by setting $\phi_p = 180^{\circ} - C'$. Adopting keyword values of SELN and SELT for selenographic coordinates we may write

```
CRPIX1S = 2048.5,
CRPIX2S = 2048.5,
CDEL1S = 0.0562896,
```

Table 12. Summary of new coordinate keywords introduced in this paper; see also Table 3 for alternate types used in binary tables.

| Keyword | Type | Sect. | Use | Status | Comments |
|-------------|-----------|-------|---------------------|------------|--|
| LONPOLE a | floating | 2.2 | coordinate rotation | new | Longitude in the native coordinate system of the celestial system's north pole. Default: 0° if $\delta_0 \geq \theta_0$, 180° otherwise. |
| LATPOLE a | floating | 2.4 | coordinate rotation | new | Latitude in the native coordinate system of the celestial system's north pole, or equivalently, the latitude in the celestial coordinate system of the native system's north pole. Default: 90° , unless $(\theta_0, \delta_0, \phi_p - \phi_0) = (0, 0, \pm 90^\circ)$ in which case it has no default. |
| RADESYS a | character | 3.1 | frame of reference | new | Reference frame of equatorial and ecliptic coordinates; recognized values are given in Table 2. Default: FK4 if EQUINOX a < 1984.0, FK5 if ≥ 1984.0 , or ICRS if EQUINOX a is not given. |
| EQUINOX a | floating | 3.1 | coordinate epoch | new | Epoch of the mean equator and equinox in years; Besselian if RADESYS a is FK4 or FK4-NO-E, Julian if FK5; not applicable to ICRS or GAPPT. Default: EPOCH if given, else 1950.0 if RADESYS a is FK4 or FK4-NO-E, or 2000.0 if FK5. |
| EPOCH | floating | 3.1 | coordinate epoch | deprecated | Replaced by EQUINOX a . |
| MJD-OBS | floating | 3.1 | time of observation | new | Modified Julian Date (JD - 2 400 000.5) of observation. Default: DATE-OBS if given, else no default. |

CDELTS = 0.0562896,
CTYPE1S = 'SELN-AZP',
CTYPE2S = 'SELT-AZP',
PV2_1S = 202.64,
CRVAL1S = -0.23,
CRVAL2S = 5.89,
LONPOLES = 161.06,
WCSNAMES = 'SELENOGRAPHIC COORDINATES'.

We have used the letter S to denote the alternate coordinate system simply to demonstrate that there is no requirement to start with A. A WCSNAME a keyword, defined in Paper I, is used to identify the coordinate system. Note that selenographic coordinates are right-handed so that selenographic longitude increases towards the west on the celestial sphere as seen from the Earth and this is handled by setting CDELTS *positive*.

As an extension of this example, a FITS header with three coordinate systems might be constructed for an image of Saturn; a celestial grid for the background, a saturnographic system for the surface of the planet, and a third system for its rings. The rings might be described by a zenithal equidistant (ARC) projection with associated linear transformation matrix set to match the oblique viewing angle.

7.5. Realization

Calabretta (1995) has written, and made available under a GNU license, a package of routines, WCSLIB, which implements all projections and coordinate conversions defined here. It contains independent C and Fortran libraries.

The Fortran library includes a routine, PGSBOX, which is based on PGLOT and uses WCSLIB to draw general curvilinear coordinate axes. It was used to generate Fig. 36.

8. Summary

We have developed a flexible method for associating celestial coordinates with a FITS image and implemented it for all projections likely to be of use in astronomy. It should be a relatively simple matter to add new projections should the need ever arise.

The FITS-header keywords defined in this paper are summarized in Table 12 with the 3-letter projection codes listed in Table 13. The column labeled θ_0 gives the native latitude of the reference point in degrees ($\phi_0 = 0$ always) and the parameters associated with each projection are listed in the nomenclature of Sect. 5.

Acknowledgements. The authors would particularly like to thank Patrick Wallace (U.K. Starlink) for his helpful comments which included the text for some of the paragraphs of Sect. 3.1 and the suggestion of the zenithal polynomial projection. Also, Steve Allen (UCO/Lick Observatory) who provided valuable feedback and suggestions over the long period of this work's development. We are grateful for the assistance provided by Bob Hanisch (Space Telescope Science Institute) in bringing the manuscript to its final form. We also thank William Pence, Arnold Rots, and Lorella Angelini (NASA Goddard Space Flight Center) for contributing the text of Sect. 4.

The authors thank the following for comments and suggestions: Rick Balsano, David Berry, Emmanuel Bertin, Jeff Bloch, Peter Bunclark, Julian Daniels, Lindsey Davis, Rick Ebert, Douglas Finkbeiner, Immanuel Freedman, Brian Glendenning, Bill Gray, Dave Green, Mike Kesteven, Doug Mink, Jonathan McDowell, François Ochsenbein, Fred Patt, Tim Pearson, William Thompson, Doug Tody, Stephen Walton, and Don Wells.

Table 13. Summary of projection codes, default values of ϕ_0 and θ_0 , special properties, full name, and required parameters. Where a projection has a special property other than being conformal, equiareal, or equidistant a reference is given to the section where this is discussed.

| FITS Code | ϕ_0 | θ_0 | Special properties | Projection name | Projection parameters associated with <i>latitude</i> [†] axis <i>i</i> | | | | |
|-----------|----------|------------|------------------------|---------------------------------------|--|----------------|----------------|----------------|----------------|
| | | | | | PVi_0 <i>a</i> | PVi_1 <i>a</i> | PVi_2 <i>a</i> | PVi_3 <i>a</i> | PVi_4 <i>a</i> |
| AZP | 0° | 90° | Sect. 5.1.1 | Zenithal perspective | | μ | γ | | |
| SZP | 0° | 90° | Sect. 5.1.2 | Slant zenithal perspective | | μ | ϕ_c | θ_c | |
| TAN | 0° | 90° | Sect. 5.1.3 | Gnomonic | | | | | |
| STG | 0° | 90° | Sect. 5.1.4, Conformal | Stereographic | | | | | |
| SIN | 0° | 90° | Sect. 5.1.5 | Slant orthographic | | ξ | η | | |
| ARC | 0° | 90° | Equidistant | Zenithal equidistant | | | | | |
| ZPN | 0° | 90° | | Zenithal polynomial | P_0 | P_1 | P_2 | P_3 | $\dots P_{20}$ |
| ZEA | 0° | 90° | Equiareal | Zenithal equal-area | | | | | |
| AIR | 0° | 90° | Sect. 5.1.9 | Airy | | θ_b | | | |
| CYP | 0° | 0° | | Cylindrical perspective | | μ | λ | | |
| CEA | 0° | 0° | Equiareal | Cylindrical equal area | | λ | | | |
| CAR | 0° | 0° | Equidistant | Plate carrée | | | | | |
| MER | 0° | 0° | Conformal | Mercator | | | | | |
| SFL | 0° | 0° | Equiareal | Sanson-Flamsteed | | | | | |
| PAR | 0° | 0° | Equiareal | Parabolic | | | | | |
| MOL | 0° | 0° | Equiareal | Mollweide | | | | | |
| AIT | 0° | 0° | Equiareal | Hammer-Aitoff | | | | | |
| COP | 0° | θ_a | | Conic perspective | | θ_a | η | | |
| COE | 0° | θ_a | Equiareal | Conic equal-area | | θ_a | η | | |
| COD | 0° | θ_a | Equidistant | Conic equidistant | | θ_a | η | | |
| COO | 0° | θ_a | Conformal | Conic orthomorphic | | θ_a | η | | |
| BON | 0° | 0° | Equiareal | Bonne's equal area | | θ_1 | | | |
| PCO | 0° | 0° | | Polyconic | | | | | |
| TSC | 0° | 0° | Sect. 5.6.1 | Tangential Spherical Cube | | | | | |
| CSC | 0° | 0° | Sect. 5.6 | COBE Quadrilateralized Spherical Cube | | | | | |
| QSC | 0° | 0° | Sect. 5.6 | Quadrilateralized Spherical Cube | | | | | |

[†] Parameters PVi_0*a*, PVi_1*a*, and PVi_2*a* associated with *longitude* axis *i* implement user-specified values of (ϕ_0, θ_0) as discussed in Sect. 2.5, and PVi_3*a*, and PVi_4*a* encapsulate the values of LONPOLE*a* and LATPOLE*a* respectively, as discussed in Sect. 2.6.

Many others contributed indirectly via requests for clarification of particular points leading potentially to improvements in the wording or formalism.

Mark Calabretta would also like to thank the following for feedback on wcsLIB: Klaus Banse, David Barnes, David Berry, Wim Brouw, Lindsey Davis, Rick Ebert, Ken Ebisawa, Brian Glendenning, Neil Killeen, Thomas A. McGlynn, Doug Mink, Clive Page, Ray Plante, Keith A. Scollick, and Peter Teuben.

Coastline data for Fig. 36 are from the ‘‘CIA World DataBank II’’ map database, which is in the public domain. Dave Pape’s plain-text version was obtained from <http://www.evl.uic.edu/pape/data/WDB/> and this site also provides references to the original, highly compressed binary encodings.

The Australia Telescope is funded by the Commonwealth of Australia for operation as a National Facility managed by CSIRO.

The National Radio Astronomy Observatory is a facility of the (U.S.) National Science Foundation operated under cooperative agreement by Associated Universities, Inc.

Appendix A: Projection aliases

Table A.1 provides a list of aliases which have been used by cartographers for special cases of the projections described in Sect. 5.

Appendix B: Mathematical methods

B.1. Coordinate rotation with matrices

The coordinate rotations represented in Eqs. (2) or (5) may be represented by a matrix multiplication of a vector of direction cosines. The matrix and its inverse (which is simply the transpose) may be precomputed and applied repetitively to a variety of coordinates, improving performance. Thus, we have

$$\begin{pmatrix} l \\ m \\ n \end{pmatrix} = \begin{pmatrix} r_{11} & r_{12} & r_{13} \\ r_{21} & r_{22} & r_{23} \\ r_{31} & r_{32} & r_{33} \end{pmatrix} \begin{pmatrix} l' \\ m' \\ n' \end{pmatrix}, \quad (\text{B.1})$$

where

$$\begin{aligned} (l', m', n') &= (\cos \delta \cos \alpha, \cos \delta \sin \alpha, \sin \delta), \\ (l, m, n) &= (\cos \theta \cos \phi, \cos \theta \sin \phi, \sin \theta), \end{aligned}$$

Table A.1. Projection aliases.

| Name | Alias for | Name | Alias for |
|--------------------------------------|--|--|-------------------------------------|
| Gnomonic = Central | AZP with $\mu = 0$ | Miller | CAR with x scaled by $2/\pi$ |
| Near-sided perspective | AZP with $\mu = 1.35$ | Equirectangular | CAR with unequal scaling |
| Clarke's (first) | AZP with $\mu = 1.35$ | Cartesian | CAR |
| Clarke's (second) | AZP with $\mu = 1.65$ | = Equidistant cylindrical | |
| James' | AZP with $\mu = 1.367$ | Cassini | CAR transverse case |
| La Hire's | AZP with $\mu = 1.71$ | Transverse Mercator | MER transverse case |
| Approximate equidistant zenithal | AZP with $\mu = 1.7519$ | = Transverse cylindrical orthomorphic | |
| Approximate equal area zenithal | AZP with $\mu = 2.4142$ | Sinusoidal | SFL |
| Postel | ARC | = Global sinusoid (GLS) | |
| = Equidistant | | = Mercator equal-area | |
| = Globular | | = Mercator-Sanson | |
| Lambert azimuthal equivalent | ZEA | = Sanson's | |
| = Lambert azimuthal equal area | | Craster | PAR |
| = Lambert polar azimuthal | | Bartholomew's atlantis | MOL oblique case |
| = Lorgna | | Mollweide's homolographic | MOL |
| Gall's cylindrical | CYP with $\mu = 1, \lambda = \sqrt{2}/2$ | = Homolographic | |
| Cylindrical equal area | CYP with $\mu = \infty$ | = Homalographic | |
| Simple cylindrical | CYP with $\mu = 0, \lambda = 1$ | = Babinet | |
| = Central cylindrical | | = Elliptical | |
| = Cylindrical central perspective | | Hammer equal area | AIT |
| = Gall's stereographic | | = Aitoff | |
| Lambert's cylindrical | CYP with $\mu = \infty, \lambda = 1$ | = Aitov | |
| = Lambert's equal area | | Bartholomew's nordic | AIT oblique case |
| Behrmann equal area | CEA with $\lambda = 3/4$ | One-standard conic | Conic with $\theta_1 = \theta_2$ |
| Gall's orthographic | CEA with $\lambda = 1/2$ | = Tangent conic | |
| = Approximate Peter's | | Two-standard conic | Conic with $\theta_1 \neq \theta_2$ |
| Lambert's equal area | CEA with $\lambda = 1$ | = Secant conic | |
| | | Murdoch conic | similar to COD |
| | | Alber's | COE |
| | | = Alber's equal area | |
| | | Lambert equal area | COE with $\theta_2 = 90^\circ$ |
| | | Lambert conformal conic | for spherical Earth = COO |
| | | Werner's | BON with $\theta_1 = 90^\circ$ |

$$\begin{aligned}
r_{11} &= -\sin \alpha_p \sin \phi_p - \cos \alpha_p \cos \phi_p \sin \delta_p, \\
r_{12} &= \cos \alpha_p \sin \phi_p - \sin \alpha_p \cos \phi_p \sin \delta_p, \\
r_{13} &= \cos \phi_p \cos \delta_p, \\
r_{21} &= \sin \alpha_p \cos \phi_p - \cos \alpha_p \sin \phi_p \sin \delta_p, \\
r_{22} &= -\cos \alpha_p \cos \phi_p - \sin \alpha_p \sin \phi_p \sin \delta_p, \\
r_{23} &= \sin \phi_p \cos \delta_p, \\
r_{31} &= \cos \alpha_p \cos \delta_p, \\
r_{32} &= \sin \alpha_p \cos \delta_p, \\
r_{33} &= \sin \delta_p.
\end{aligned}$$

The inverse equation is

$$\begin{pmatrix} l' \\ m' \\ n' \end{pmatrix} = \begin{pmatrix} r_{11} & r_{21} & r_{31} \\ r_{12} & r_{22} & r_{32} \\ r_{13} & r_{23} & r_{33} \end{pmatrix} \begin{pmatrix} l \\ m \\ n \end{pmatrix}. \quad (\text{B.2})$$

B.2. Iterative solution

Iterative methods are required for the inversion of several of the projections described in this paper. One, Mollweide's, even requires solution of a transcendental equation for the forward equations. However, these do not give rise to any particular difficulties.

On the other hand, it sometimes happens that one pixel and one celestial coordinate element is known and it is required to find the others; this typically arises when plotting graticules on image displays. Although analytical solutions exist for a few special cases, iterative methods must be used in the general case. If, say, p_2 and α are known, one would compute pixel coordinate as a function of δ and determine the value which gave p_2 . The unknown pixel coordinate elements would be obtained in the process.

This prescription glosses over many complications, however. All bounded projections may give rise to discontinuities in the graph of p_2 versus δ (to continue the above example), for example where the meridian through α crosses the $\phi = \pm 180^\circ$ boundary in cylindrical, conic and other projections. Even worse, if the meridian traverses a pole represented as a finite line segment then p_2 may become multivalued at a particular value of δ . The derivative $\partial p_2 / \partial \delta$ will also usually be discontinuous at the point of discontinuity, and it should be remembered that some projections such as the quad-cubes may also have discontinuous derivatives at points within their boundaries.

We will not attempt to resolve these difficulties here but simply note that `wcsLIB` (Calabretta, 1995) implements a solution.

Appendix C: The slant orthographic projection

The slant orthographic or generalized SIN projection derives from the basic interferometer equation (e.g. Thompson et al. 1986). The phase term in the Fourier exponent is

$$\varphi = (\mathbf{e} - \mathbf{e}_0) \cdot \mathbf{B}, \quad (\text{C.1})$$

where \mathbf{e}_0 and \mathbf{e} are unit vectors pointing towards the field center and a point in the field, \mathbf{B} is the baseline vector, and we measure the phase φ in rotations so that we don't need to carry factors of 2π . We can write

$$\varphi = p_u u + p_v v + p_w w, \quad (\text{C.2})$$

where (u, v, w) are components of the baseline vector in a right-handed coordinate system with the w -axis pointing from the geocenter towards the source and the u -axis lying in the equatorial plane, and

$$\begin{aligned} p_u &= \cos \theta \sin \phi, \\ p_v &= -\cos \theta \cos \phi, \\ p_w &= \sin \theta - 1, \end{aligned} \quad (\text{C.3})$$

are the coordinates of $(\mathbf{e} - \mathbf{e}_0)$, where (ϕ, θ) are the longitude and latitude of \mathbf{e} in the spherical coordinate system with the pole towards \mathbf{e}_0 and origin of longitude towards negative v , as required by Fig. 3. Now, for a planar array we may write

$$n_u u + n_v v + n_w w = 0 \quad (\text{C.4})$$

where (n_u, n_v, n_w) are the direction cosines of the normal to the plane. Using this to eliminate w from Eq. (C.2) we have

$$\varphi = \left[p_u - \frac{n_u}{n_w} p_w \right] u + \left[p_v - \frac{n_v}{n_w} p_w \right] v. \quad (\text{C.5})$$

Being the Fourier conjugate variables, the quantities in brackets become the Cartesian coordinates, in radians, in the plane of the synthesized map. Writing

$$\begin{aligned} \xi &= n_u / n_w, \\ \eta &= n_v / n_w, \end{aligned} \quad (\text{C.6})$$

Eqs. (61) and (62) are then readily derived from Eqs. (C.3) and (C.5). For 12-hour synthesis by an east-west interferometer the baselines all lie in the Earth's equatorial plane whence $(\xi, \eta) = (0, \cot \delta_0)$, where δ_0 is the declination of the field center. For a

“snapshot” observation by an array such as the VLA, Cornwell & Perley (1992) give $(\xi, \eta) = (-\tan Z \sin \chi, \tan Z \cos \chi)$, where Z is the zenith angle and χ is the parallactic angle of the field center at the time of the observation.

In synthesizing a map a phase shift may be applied to the visibility data in order to translate the field center. If the shift applied is

$$\Delta \varphi = q_u u + q_v v + q_w w \quad (\text{C.7})$$

where (q_u, q_v, q_w) is constant then Eq. (C.2) becomes

$$\varphi = (p_u - q_u)u + (p_v - q_v)v + (p_w - q_w)w, \quad (\text{C.8})$$

whence Eq. (C.5) becomes

$$\begin{aligned} \varphi &= [(p_u - q_u) - \xi(p_w - q_w)]u \\ &\quad + [(p_v - q_v) - \eta(p_w - q_w)]v. \end{aligned} \quad (\text{C.9})$$

Equations (61) and (62) become

$$\begin{aligned} x &= \frac{180^\circ}{\pi} [\cos \theta \sin \phi + \xi(\sin \theta - 1)] - \frac{180^\circ}{\pi} [q_u - \xi q_w], \\ y &= -\frac{180^\circ}{\pi} [\cos \theta \cos \phi - \eta(\sin \theta - 1)] - \frac{180^\circ}{\pi} [q_v - \eta q_w], \end{aligned} \quad (\text{C.10})$$

from which on comparison with Eqs. (61) and (62) we see that the field center is shifted by

$$(\Delta x, \Delta y) = \frac{180^\circ}{\pi} (q_u - \xi q_w, q_v - \eta q_w). \quad (\text{C.11})$$

The shift is applied to the coordinate reference pixel.

References

- Atkinson, R. d'E. 1951, *MNRAS*, 111, 448
 Blaauw, A., Gum, C. S., Pawsey, J. L., & Westerhout, G. 1960, *MNRAS*, 121, 123
 Brouwer, W. N. 1971, Ph.D. Thesis, Sterrenwacht, Leiden
 Bunclark, P., & Rots, A. 1996, *Precise Re-definition of DATE-OBS Keyword Encompassing the Millennium*, located at http://www.cv.nrao.edu/fits/documents/standards/as_year2000.txt
 Calabretta, M. R. 1992, *Spherical Map Projections*, AIPS++ Memo No. 107, The AIPS++ Consortium, c/o National Radio Astronomy Observatory, Charlottesville, Virginia, Dec 15. <http://aips2.nrao.edu/docs/memos/107.ps>
 Calabretta, M. R. 1995, *wcsLIB*, version 2, located at <ftp://ftp.atnf.csiro.au/pub/software/wcslib/wcslib.tar.gz>
 Calabretta, M. R., et al. 2002, *Representations of distortions in FITS world coordinate systems*, A&A, in preparation
 Chan, F. K., & O'Neill, E. M. 1975, *Feasibility Study of a Quadrilateralized Spherical Cube Earth Data Base*, EPRF Technical Report 2 - 75 (CSC), Computer Sciences Corporation (Silver Springs, Maryland)
 Cornwell, T. J., & Perley, R. A. 1992, *A&A*, 261, 353
 Cotton, W. D., Tody, D., & Pence, W. D. 1995, *A&AS*, 113, 159
 Evenden, G. I. 1991, *Cartographic Projection Procedures for the UNIX Environment - A User's Manual*, Open-File Report 90-284, United States Department of the Interior Geological Survey. Available as `0F90-284.ps.gz` at <ftp://kai.er.usgs.gov/pub/PROJ.4/> with accompanying code and related documents. The documents are also cached at <http://www.cv.nrao.edu/fits/wcs/USGS/>

- Górski, K. M., & Hivon, E. F. 1999, HEALPix homepage, located at <http://www.eso.org/science/healpix>
- Geldzahler, B., & Schlesinger, B. M. 1997, A User's Guide for the Flexible Image Transport System (FITS), NASA/OSSA Office of Standards and Technology, Greenbelt, Maryland, version 4.0 (April 1997). Located via http://www.gsfc.nasa.gov/astro/fits/fits_home.html
- Greisen, E. W. 1983, Non-linear Coordinate Systems in AIPS, AIPS Memo No. 27, National Radio Astronomy Observatory, Charlottesville, Virginia. Revised January 1993, located at http://www.cv.nrao.edu/fits/wcs/as_aips27.ps.Z
- Greisen, E. W. 1986, Additional Non-linear Coordinates, AIPS Memo No. 46, National Radio Astronomy Observatory, Charlottesville, Virginia, May 20, available as `aips46.ps.Z` from <http://www.cv.nrao.edu/fits/wcs/>
- Greisen, E. W., Valdes, F. G., Calabretta, M. R., & Allen, S. L. 2002, Representations of spectral coordinates in FITS, A&A, in preparation
- Greisen, E. W., & Calabretta, M. R. 2002, A&A, 395, 1061 (Paper I)
- Greisen, E. W., & Harten, R. H. 1981, A&AS, 44, 371
- Hanisch, R. J., & Wells, D. C. 1988, World Coordinate Systems Representations Within the FITS Format, draft based on notes from a meeting sponsored by the National Aeronautics and Space Administration, Code EZ, held in Charlottesville, Virginia in January 1988, located at http://www.cv.nrao.edu/fits/wcs/as_wcs88.ps.Z
- Hanisch, R. J., Farris, A., Greisen, E. W., et al. 2001, A&A, 376, 359
- Hohenkerk, C. Y., Yallop, B. D., Smith, C. A., & Sinclair, A. T. 1992, Explanatory Supplement to the Astronomical Almanac, ed. P. K. Seidelmann, Chap. 3 (University Science Books, Mill Valley, California)
- IAU, 1998, Proceedings of the Twenty-Third General Assembly, Kyoto 1997, Transactions of the IAU, vol. XXIII-B
- Jones, M. H. 1993, Observatory, 113, 213
- Kellaway, G. P. 1946, Map Projections (Methuen & Co. Ltd., London, England)
- O'Neill, E. M., & Laubscher, R. E. 1976, Extended Studies of the Quadrilateralized Spherical Cube Earth Data Base, NEPRF Technical Report 3 – 76 (CSC) Computer Sciences Corporation (Silver Springs, Maryland)
- Schlegel, D. J., Finkbeiner, D. P., & Davis, M. 1998, ApJ, 500, 525
- Snyder, J. P. 1993, Flattening the Earth (University of Chicago Press, Chicago and London)
- Tegmark, M. 1996, ApJ, 470, L81
- Thompson, A. R., Moran, J. W., & Swenson, G. W. 1986, Interferometry and Synthesis in Radio Astronomy (J. Wiley, New York, USA)
- Thompson, W. 1999, Coordinate Systems for Solar Image Data (proposed). Located at <http://orpheus.nascom.nasa.gov/~thompson/papers/coordinates.ps>
- Wells, D. C., Greisen, E. W., & Harten, R. H. 1981, A&AS, 44, 363